

PANDORA: Design of a 2 DOF Scapulohumeral Device

A Thesis

Presented in Partial Fulfillment of the Requirements for the

Degree of Master of Science

with a

Major in Mechanical Engineering

in the

College of Graduate Studies

University of Idaho

by

Shawn T. Trimble

Major Professor: Joel C. Perry, Ph.D.

Committee Members: Eric T. Wolbrecht, Ph.D.; Edwin M. Odom, Ph.D.

Department Administrator: Steven W. Beyerlein, Ph.D.

December 2016

AUTHORIZATION TO SUBMIT THESIS

This thesis of Shawn Trimble, submitted for the degree of Master of Science with a Major in Mechanical Engineering and titled "PANDORA: Design of a 2 DOF Scapulohumeral Device," has been reviewed in final form. Permission, as indicated by the signatures and dates below, is now granted to submit final copies to the College of Graduate Studies for approval.

Major Professor: _____ Date: _____
Joel C. Perry, Ph.D.

Committee Members: _____ Date: _____
Eric T. Wolbrecht, Ph.D.

_____ Date: _____
Edwin M. Odom, Ph.D.

Department Administrator: _____ Date: _____
Steven W. Beyerlein, Ph.D.

ABSTRACT

This thesis describes the development and design of a two-DOF scapulohumeral device. The theory of employing clavicular motion to control scapulothoracic movement is explored and ultimately used as the principle concept of this research. The result is PANDORA, a dual four-bar mechanism that is independent of location via its unique ability to maintain a parallel relationship between its coupler and ground links. Furthermore, its overall rigidity allows it to serve as the base link for the project to which it is attached, BLUE SABINO. Thus PANDORA also serves to gravity balance the entirety of the exoskeleton. FEA simulations reveal PANDORA performs better than anticipated. This is due in part to the synergy of the component design. The topic of synergy and further aspects of the FEA simulation results are discussed followed by identification of potential future work. Finally, the need for additional testing and experimental verification is emphasized.

ACKNOWLEDGMENTS

First and foremost, I wish to thank my major professor Dr. Joel Perry for this incredible opportunity. Thank you for your guidance and for funding my research. Furthermore, thank you for taking a chance on someone unknown to you. It has been an honor to work on a project of this magnitude with such a noble purpose behind it.

Thank you Dr. Wolbrecht for all of the advice over the years. I'm not sure if you realize it, but you are a wonderful mentor. Thank you for helping fund my education through teaching assistantships, and thank you for always being willing to lend an ear.

Thank you Dr. Odom. I truly believe that without you I would not have attended graduate school. I've always admired the way your mind works, and appreciated your sage advice. I wouldn't trade my time with you as my senior design advisor for anything. Thank you.

Finally, I wish to express my gratitude toward the University of Idaho. I came here with hope, heart, and a theatre degree. The latter is not conducive to becoming an engineer. But it is because of this University that I've been able to change my lot in life. For that I am truly grateful.

DEDICATION

I dedicate this work to my wife and her parents. Thank you my dear for believing in me even when I didn't believe in myself. Thank you Patrick and Christi Pedrow, for your encouragement, patience, and support. But most of all, thank you for letting me live in your basement these last few years.

TABLE OF CONTENTS

Authorization to Submit Thesis	ii
Abstract	iii
Acknowledgments	iv
Dedication	v
Table of Contents	vi
List of Figures	ix
1. Introduction	1
1.1. Robotics	1
1.2. Rehabilitation Robotics	3
1.3. Blue Sabino	6
1.3.1. Evolution of BLUE SABINO	6
1.3.2. State-of-the-Art: Upper Limb Exoskeletons	9
1.3.3. BLUE SABINO: Objectives and Expected Outcomes	14
2. Background	15
2.1. Anatomy and Function of the Human Shoulder	15
2.1.1. Sternoclavicular Joint.....	16
2.1.2. Acromioclavicular Joint.....	16
2.1.3. Glenohumeral Joint	17
2.1.4. Scapulothoracic Joint	18
2.1.5. Scapulohumeral Rhythm	19
2.1.6. ROM of Common Shoulder Movements	20
2.1.7. Summary.....	21
2.2. Harmonic Drives	22
2.2.1. History of Harmonic Drives.....	22
2.2.2. Basic Operating Principles.....	23
2.2.3. The Wave Generator	24
2.2.4. The Flexible Spline	24
2.2.5. The Circular Spline.....	25
2.2.6. Summary.....	26

2.3. Principles of Four-Bar Linkages.....	27
2.3.1. Links	27
2.3.2. Joints.....	27
2.3.3. Gruebler’s Equation.....	28
2.3.4. Defining a Four-Bar Mechanism.....	29
2.3.5. Grashof Criteria	30
2.3.6. Kinematic Synthesis.....	31
2.3.7. Graphical Method.....	32
2.3.8. Analytical Method.....	34
2.3.9. Summary.....	36
2.4. Bearings.....	37
2.4.1. Deep Groove Ball Bearings	38
2.4.2. Tapered Roller Bearings	38
2.4.3. Internal Clearance	39
2.4.4. Preload	40
2.4.5. Summary.....	43
2.5. Gravity Equilibrium.....	43
2.5.1. Zero-Free-Length Spring	44
2.5.2. Basic Gravity Equilibrator.....	46
2.5.3. Achieving Equilibrium Using Normal Springs.....	47
2.5.4. Adjustment of Gravity Equilibrators	49
2.5.5. Summary.....	53
3. Design of a 2-DOF Scapulohumeral Rhythm Device	55
3.1. Design Considerations.....	55
3.1.1. Using Clavicular Motion to Model Scapulohumeral Rhythm	58
3.1.2. Parallelogram Four-Bars, Achieving Freedom in Joint Location.....	60
3.1.3. Finding the Perfect Balance.....	61
3.1.4. Bearing Selection	62
3.1.5. Proof of Concept: Wood Prototype	62
3.2. Transitioning from Proof of Concept to Final Design	66
3.2.1. Link Design	68
3.2.2. Elevation/Depression Sub-Assembly	69
3.2.3. Ground and Coupler Link Design.....	70

3.2.4. Protraction/Retraction Sub-Assembly.....	71
3.2.5. Pulley-Based Gravity Balancer.....	72
3.2.6. Actuation and Flexible Shaft Coupling.....	73
3.2.7. The Final Design: PANDORA.....	77
4. Results.....	81
4.1. Material Selection and Link Design.....	81
4.2. Elevation/Depression Sub-Assembly Verification.....	82
4.3. FEA of Ground and Coupler Link.....	83
4.4. Ground and Coupler Link Sub-Assembly Simulation	84
4.5. Motor Mount, Driven Link, and Driven Shaft Analysis	84
5. Discussion	87
5.1. Future Work.....	89
5.2. Concluding Remarks	91
References	92

LIST OF FIGURES

FIGURE 1.1. THE EXO-UL1 AND EXO-UL3.....	7
FIGURE 1.2. THE EXO-UL7	8
FIGURE 1.3. 3-D MODEL OF THE EXO-UL8	9
FIGURE 1.4. MGA EXOSKELETON	10
FIGURE 1.5. INTELLIARM SYSTEM.....	11
FIGURE 1.6. THE ARMIN III	12
FIGURE 1.7. MEDARM SYSTEM.....	13
FIGURE 1.8. THE HARMONY	13
FIGURE 2.1. THE SHOULDER COMPLEX	15
FIGURE 2.2. STERNOCLAVICULAR JOINT	16
FIGURE 2.3. THE ACROMIOCLAVICULAR JOINT	17
FIGURE 2.4. THE GLENOHUMERAL JOINT	18
FIGURE 2.5. THE PRIMARY MOTIONS OF THE SCAPULA	19
FIGURE 2.6. SCAPULAR MOVEMENT	20
FIGURE 2.7. TYPES OF SHOULDER MOVEMENT	21
FIGURE 2.8 THE THREE COMPONENTS THAT CONSTITUTE A HARMONIC DRIVE	23
FIGURE 2.9. TWO PIECE CONSTRUCTION OF THE WAVE GENERATOR	24
FIGURE 2.10. THE FLEXIBLE SPLINE	25
FIGURE 2.11. THE MOTION OF A HARMONIC DRIVE	25
FIGURE 2.12. THE CIRCULAR SPLINE	26
FIGURE 2.13. THE THREE COMMON FORMS OF LINKS	27
FIGURE 2.14. EXAMPLES OF TYPICAL ONE DOF JOINTS	28
FIGURE 2.15. EXAMPLES OF MULTIPLE DOF JOINTS	28
FIGURE 2.16. SKELETON DIAGRAM OF A FOUR-BAR MECHANISM.....	30
FIGURE 2.17. THE FOUR GRASHOF MECHANISMS.....	31
FIGURE 2.18. EXAMPLE OF THE RELATIVE POLE METHOD	33
FIGURE 2.19. THE RELATIVE POLE METHOD USED TO DETERMINE ONE POSSIBLE SOLUTION	34
FIGURE 2.20. FOUR-BAR MECHANISM TO ILLUSTRATE THE CONCEPT OF FREUDENSTEIN'S EQUATION	35
FIGURE 2.21. EXPLODED VIEW OF A BALL BEARING.....	38
FIGURE 2.22. DIAGRAM OF ROLLER CENTERLINES	39
FIGURE 2.23. ILLUSTRATION OF RADIAL CLEARANCE IN A BALL BEARING.....	40
FIGURE 2.24. EFFECT OF PRELOADING ON THE FATIGUE LIFE OF TWO DIFFERENT BEARINGS.....	41
FIGURE 2.25. POSITION PRELOADING.....	42
FIGURE 2.26. THE MECHANE	44
FIGURE 2.27. EXTENSION SPRING AND FORCE LENGTH CHARACTERISTICS	45

FIGURE 2.28. LACOSTE METHOD FOR CREATING A ZERO-FREE-LENGTH SPRING	45
FIGURE 2.29. BASIC GRAVITY EQUILIBRATOR	47
FIGURE 2.30. EMULATION OF A ZERO-FREE-LENGTH SPRING.....	48
FIGURE 2.31. BASIC GRAVITY EQUILIBRATOR USING A ZERO-FREE-LENGTH SPRING	49
FIGURE 2.32. SIMULTANEOUS DISPLACEMENT METHOD	50
FIGURE 2.33. VIRTUAL SPRING METHOD	50
FIGURE 2.34. STORAGE SPRING METHOD	51
FIGURE 2.35. K-TYPE METHOD.....	52
FIGURE 3.1. DIAGRAM OF THE LOWER AND UPPER BOUNDS OF CLAVICLE LENGTH.....	59
FIGURE 3.2. ILLUSTRATION OF HOW A PARALLELOGRAM FOUR-BAR MAINTAINS PARALLELISM	61
FIGURE 3.3. SOLID MODEL PROTOTYPE	63
FIGURE 3.4. ILLUSTRATION OF THE AXES OF ROTATION FOR ALL JOINTS	64
FIGURE 3.5. SOLIDWORKS MODEL AND PHYSICAL MODEL OF THE PROOF OF CONCEPT PROTOTYPE	65
FIGURE 3.6. ILLUSTRATION OF POSITIONS USED FOR MOMENT AND FORCE METRICS	66
FIGURE 3.7. MOMENTS AND FORCE DERIVED FROM THE EXO-UL8 SOLID MODEL	67
FIGURE 3.8. RENDERS OF DIFFERENT LINK VIEWS	69
FIGURE 3.9. ILLUSTRATION OF THE ELEVATION/DEPRESSION SUB-ASSEMBLY	70
FIGURE 3.10. GROUND LINK	71
FIGURE 3.11. ILLUSTRATION OF PROTRACTION/RETRACTION ASSEMBLY	72
FIGURE 3.12. SECTION VIEW OF ENTIRE BALANCING MECHANISM	73
FIGURE 3.13. SOLID MODEL USED TO DETERMINE MOMENT OF INERTIA FOR THE EXO-UL8	74
FIGURE 3.14. ILLUSTRATION OF THE THREE TYPES OF MISALIGNMENT	77
FIGURE 3.15. ISOMETRIC VIEW OF PANDORA	78
FIGURE 3.16. SIDE VIEW OF PANDORA ILLUSTRATING PARALLEL MOVEMENT	78
FIGURE 3.17. PROPOSED CONCEPT FOR WIDTH ADJUSTMENT.....	79
FIGURE 3.18. REAR VIEW HIGHLIGHTING THE IMPORTANCE OF WIDTH ADJUSTMENT	79
FIGURE 3.19. FRONT VIEW OF PANDORA	80
FIGURE 4.1. FEA ANALYSIS OF THE LINK DESIGN	82
FIGURE 4.2. ELEVATION/DEPRESSION SUBASSEMBLY ANALYSIS	83
FIGURE 4.3. RESULTS OF FEA ANALYSIS ON THE COUPLER LINK	83
FIGURE 4.4. FEA SIMULATION OF THE GROUND/COUPLER LINK ASSEMBLY	84
FIGURE 4.5. MOTOR MOUNT, DRIVEN LINK, AND DRIVE SHAFT FOR PROTRACTION/RETRACTION	85
FIGURE 4.6. LOCATIONS OF MOTOR MOUNT, DRIVEN LINK, AND DRIVE SHAFT	85

1. INTRODUCTION

1.1. ROBOTICS

The world of robotics is vast with a long and storied history. There is much speculation as to who invented the first robot or what the first robot was. This can primarily be attributed to the fact that the very definition of “robotics” is a highly contentious matter. At one end of the argument is the belief that the term robot can only be applied to a mechanism that looks and behaves like a human. The other side of the debate would state that robots are devices used for repetitive tasks, such as industrial robots. Regardless of which viewpoint is adopted, the concepts that led to modern robotics date back several millennia.

The initial inspirations that evolved into modern robotics can be seen sprinkled throughout history. As early as 3000 years ago, human-controlled statues were created and used by Egyptians [1]. In 800 B.C. autonomous mobile robots were described in Homer’s Iliad [2]. Ctesibus of Alexandria created a “water-clock” in 270 B.C. which many consider one of the original robots [3]. The first century saw mechanical animals that could be actuated through the use of water, steam, or air [2]. As technology progressed, the sixteenth through eighteenth centuries developed clockwork-based dolls that could write, draw, and even play the piano [1], [2]. Though the early manifestations of robots were really just clever mechanical devices, they did pave the way for the emergence of more sophisticated robots in the twentieth century.

The term “robot” and the inception of the modern robotic era began in the 1920s. Karel Capek wrote a play titled *Rossum’s Universal Robots* in 1921. The plot line involved the creation of futuristic humanoid workers that were ultimately used as inexpensive laborers. However, Karel needed a name for the humanoids. As the story goes, he turned to his brother Josef for inspiration. Thus it was Josef that coined the word “robot”. Until then, robots had been referred to as “automatons” [3]. Therefore, the Capek brothers are rightly attributed to initiating public interest in robotics through their imaginative stories. However, if the Capek brothers were the sparks that started the robotics fire of the 20th century, then it was Isaac Asimov who fanned the flames.

Isaac Asimov (1920-1992) was primarily a science fiction writer (he also wrote in the genre of nonfiction) who made a substantial impact to the early evolution of modern robotics. From 1940-1958 Asimov wrote a series of robot inspired short stories. Of these, the *Foundation Trilogy* is considered his most famous work [3]. During this time, Asimov created what has come to be known as the “Three Laws of Robotics”. They first appeared together and fully formed in *Runaround* circa 1942. The “Three Laws of Robotics” are as follows: First Law: a robot may not injure a human being, or, through inaction, allow a human being to come to harm, unless this would violate a higher order law. Second Law: a robot must obey the orders given to it by human beings, except where such orders would conflict with a higher order law. Third law: a robot must protect its own existence, as long as such protection does not conflict with a higher order law. The ingenious work of Asimov captivated the imagination of scientists and engineers alike, inspiring them to innovate, create, and ultimately transition the field of robotics from science fiction into reality.

Post-World War II, the US economy was bolstered through an industrial push and massive advances in technology. The breakthroughs in technology (e.g. solid state electronics) were crucial to robotics. Prior to this, robots were simply clever mechanical devices as previously described. But with the advent of transistors, servos, digital logic, etc., these clever devices evolved into modern robots. Mechanisms that could be programmed, act autonomously, or even be teleoperated. The first significant example of a modern robot was the Unimate, an industrial robot used for unloading high temperature parts from a die casting machine. It was employed in 1961 by the General Motors plant in Trenton, New Jersey.

Since the Unimate, the world of robotics has grown exponentially. Presently, the use of robots has expanded to include areas such as space exploration, nuclear applications, military and law enforcement, and research laboratories. The capabilities of modern robots are diverse. Ranging from the simplest tasks such as vacuuming floors, to complex actions like artificial intelligence. The advantages that robots provide have resulted in their incorporation into the medical field as well. Surgical robots like the da Vinci, Zeus, and Robodoc systems provide accuracy and repeatability in surgery not attainable by human hands [4]. This feature, combined with the added benefit of small incisions, has made operations like gall bladder and

appendix removal easier to perform with faster recovery time for patients. Since the introduction of surgical robots into the medical domain, their use has extended into other subdivisions. Robots are used to administer medication to older patients, or comfort to lonely ones [5]. Their potential benefits have also been realized in the scope of rehabilitation. Robots are particularly well suited for repetitive tasks and data acquisition, two features that are extremely valuable in rehabilitation. Robots and their role in therapy is the focus of this thesis. Therefore the discussion that follows is confined exclusively to this purpose.

1.2. REHABILITATION ROBOTICS

One of the chief concerns in rehabilitation robotics is post-stroke therapy. Each year more than 800,000 people will suffer a stroke in the United States alone. This statistic is even greater in other countries like Japan [6], [7]. Even more alarming than this, the risk of stroke doubles every decade past the age of 55. In America, a disproportionate amount of the population (i.e. “baby boomers”) is age 65 and greater. Thus rehabilitation is a necessity. Other neurological disorders only exacerbate this fact. For example, every year in the United States multiple sclerosis, Parkinson’s disease, and spinal cord injuries add 350,000, 500,000, and 250,000 new cases respectively to the already staggering number of patients in need [6].

The demand for therapy exceeds the number of clinicians available to provide it. It is for this reason that rehabilitation robotics is an important topic of research. Not only can robots help to meet the growing need for therapy, but they also provide the capability of repetition that can’t be matched by therapists. In a 45-minute session a robot can help a patient move their arm 800-1000 times. A therapist can only perform 60-80 movements in the same time interval [8]. Not only is the population of therapists to patients inadequate, but the nature of the work can be problematic as well. There are times when two therapists may be needed to help a patient balance and walk. The potential for the therapist to be injured while helping a patient is also a concern. However, this is not to say that therapists can or should be replaced. They offer a level of care that robots simply can’t provide. What this information does imply is the need to incorporate robots to help load level the demand of an ever growing demographic [9].

Rehabilitation robotics truly began in the early 1960s. Prior to this, devices did exist that served to facilitate those who had lost mobility in a limb, or who had lost a limb entirely. The latter is known as a prosthetic, or a device that is intended to replace a lost limb and its function. The former is known as an orthotic, or a device that is worn to help correct impairment of movement and restore partial functionality to a deficient limb [10]. An example of a relatively modern orthotic was the “foot operated feeder” invented in 1936. It was a simple wheel chair attachment that supported a weakened arm. Operated with a foot pedal, the support enabled elbow flexion/extension thereby allowing the patients to feed themselves with the affected arm. Parallel to the advent of the feeder, the body operated Bowden arm became a popular prosthetic at the end of World War II. Used to replace amputated upper limbs, the Bowden arm is still in use today as its design is simple and gives the user kinesthetic feedback [11]. Although these mechanisms are useful, they are not generally included in the field of rehabilitation robotics. The demarcation lies in the use of technology and the ability to actuate the orthotics and prosthetics by means other than the user’s own body.

The first recognized upper limb rehabilitation robot was the CASE manipulator. Built in the early 1960s, the CASE manipulator was a powered orthotic with four degrees of freedom (DOF) [11]. It was driven through the use of myoelectric signals. The CASE manipulator led to the creation of the Rancho “Golden” arm in 1969. A seven DOF manipulator designed as a robotic arm replacement. The patient operated the manipulator with a set of tongue switches, joint by joint as a crude form of end effector control [10]–[12].

The application of rehabilitation robotics expanded in the 1970s. The first workstation robots were created to rehabilitate patients by performing activities of daily living (ADL). Unlike the joint-to-joint manipulators, the workstation robots used a command-type interface. At the same time the Spartacus was being developed in France. Designed for people with high level spinal cord injuries and children with cerebral palsy, the Spartacus was a manipulator that could be controlled with a joystick for pick and place type tasks [12].

Mobile manipulator applications became the focus of rehabilitation robotics in the 1980s. Building on the previous work of the Spartacus, the MANUS was a wheelchair-mounted manipulator controlled by joystick. A similar device called the

Powered Reacher was developed at this time and was capable of telescoping, thus allowing the user more freedom in its application. Another product of the 1980s was the advent of autonomous navigation for electric wheelchairs. However, it was also during this period that rehabilitation robotics started to recognize the importance of therapy-based devices. The mid 1980s saw the emergence of the first programmable, force-controlled mechanisms. The RTX manipulator was one such device that was equipped with a touch sensitive end effector [10], [12]. By moving to different locations in space, patients with weakened upper extremities could touch the end effector at each position. Reaction times were logged by the RTX and compared against earlier sessions. Thus the effectiveness of the therapy could be quantified.

The progress of the 1980s helped to propel therapy based robotics in the 1990s. The MIT-MANUS, MIME, and SEAT were all advanced force control mechanisms focused on upper extremity rehabilitation. The MIT-MANUS in particular has been very successful both commercially and in research settings. This success is due not only to the metrics these systems provide to the therapist, but also in its ability to reduce motor impairments [13]. The accomplishments of the MIT-MANUS and other therapy-based devices of the 1990s are directly responsible for the continued evolution and advancement of the field of rehabilitation robotics.

The 2000s ushered in a new era of therapy based robots. Although workstations, mobile manipulators, and end effector based robots are still being developed, upper limb exoskeletons have emerged as the new trend in technology. Upper limb exoskeletons are not new however. They have been around since the 1960s but have had limited success. It wasn't until the turn of the century that material science and computer software could accommodate the technological demands needed to produce such complex mechanisms.

An upper limb exoskeleton can be considered an orthosis. But unlike an end effector based orthosis where the patient aligns to the end effector; the joint axes of the exoskeleton align with those of the patient. The main advantage of an exoskeleton is in the data it provides to the therapist, and the precise motion control it is capable of. There have been several upper-limb exoskeletons produced since 2005 that have furthered the development of these devices. Most notable is the ARMin line of exoskeletons that have several versions available. Many exoskeletons have been created that incorporate different forms of actuation (e.g. hydraulic,

electric, pneumatic) and control (e.g. impedance, myoelectric) [14]. However there still exists a need to improve upon current designs. The medical community still knows little about the processes behind neurological damage, neural plasticity, specific muscle recruitment, etc. Continued refinement of exoskeleton design, actuation, control, and data acquisition could lead to new insights in these areas and a better understanding of how to apply appropriate effective therapy.

1.3. BLUE SABINO

BLUE SABINO is a collaborative project funded by the NSF and involves the University of Idaho, UCLA, Tecalia-Germany, and St. Luke's Rehabilitation Institute. BLUE SABINO (BiLateral-Upper extremity Exoskeleton for Simultaneous Assessment of Biomechanical and Neuromuscular Output) is a venture that aims to break new ground in exoskeleton research, and vastly expand the current understanding of the mechanisms behind motor impairment. The research that ultimately led to this project began in 1998 with Dr. Jacob Rosen. What follows is a brief history and evolution that preceded BLUE SABINO, a look at current exoskeletons and their abilities, and an in-depth discussion of the motivations and expected outcomes of the BLUE SABINO project.

1.3.1. Evolution of BLUE SABINO

In 1998, Dr. Jacob Rosen developed a one degree of freedom (DOF) apparatus (EXO-UL1) to test the feasibility of a myosignal-driven exoskeleton [15], [16]. The device consisted of two joints, one at the shoulder, and one at the elbow. The shoulder joint was fixed at specific angles ranging from 0° to 180° while the elbow joint was left free to rotate from 0° to 145° (Fig. 1.1). Surface electromyography (SEMG) electrodes were placed on the patient's triceps and biceps brachii. An external load applied to the system was manipulated through the human-machine interface (HMI), a simple handle attached to the forearm link. Two load cells were used, one to measure the actual shear force due to the applied load, and one to measure the shear force felt by the operator. The difference in forces was due to the use of a small actuator at the elbow. The actuator supplied most of the torque required to lift the external load, resulting in a minimal effort from the patient.

The purpose of the apparatus was to test the Hill-based muscle model [16]. The SEMG provided neuromuscular feedback that in combination with the joint kinematics could be passed into the myoprocessor (Hill-based muscle model) to predict muscle moments at the elbow joint. The predicted moments could then be integrated with the measured moments supplied by the aforementioned load cells. The feedback loop provided by the load cells was used to alleviate inaccuracies due to the myoprocessor and nonlinear dynamics associated with the system itself. Experimental testing of the device showed that myosignal command signals significantly improved mechanical gain and maintained control of the system better than other control algorithms based on position or contact forces. Therefore the concept of myosignal-controlled exoskeletons had been proven feasible.

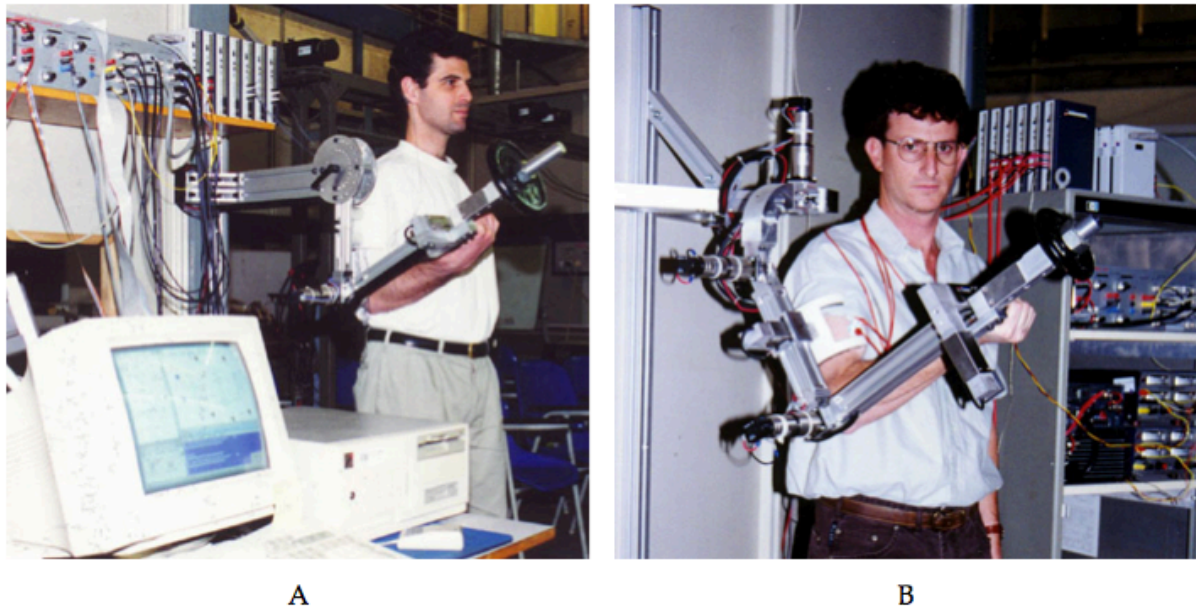


Figure 1.1. (A) Dr. Rosen testing the EXO-UL1 prototype. (B) The EXO-UL3 prototype. Expanding on the work of its predecessor, the EXO-UL1, this exoskeleton had three DOF and an additional HMI at the upper arm [15].

The EXO-UL3 was a three-link, three-joint device that expanded on the previous work of the EXO-UL1. However, the EXO-UL3 had three DOFs and an additional HMI by way of a cuff placed around the upper arm (Fig. 1.1). Similar to its predecessor, the device used myosignal control with load cell feedback. The purpose of this prototype was to further prove the validity of a myosignal driven exoskeleton. The EXO-UL3 was the last “simple” exoskeleton before Dr. Rosen applied the myosignal-based approach to a seven DOF exoskeleton design.

The EXO-UL7 (also known as the CADEN-7) was a seven-DOF, myosignal controlled upper-limb exoskeleton designed by Dr. Joel Perry in fulfillment of his Ph.D. dissertation under the guidance of Dr. Rosen in 2007 [17]. The EXO-UL7 was cable actuated, giving it a unique advantage in power to weight ratio. Unlike similar serial chain robots that have to carry the weight of their actuators, the EXO-UL7 carried only the weight of the cables, links, and pulleys. This resulted in a low-weight, low-inertia design (Fig. 1.2). With a focus on anthropometry, the EXO-UL7 allowed the user full range of motion (ROM) to accomplish typical ADLs. Another feature that set it apart from similar exoskeletons of the time was its HMI. Rather than having fully enclosed cuffs at the upper and lower arms, the EXO-UL7 used a semicircular arrangement. For impaired users, this feature provided easier donning and doffing of the device. Due to its dexterous design, the EXO-UL7 was versatile. As such, it was applicable to rehabilitation, diagnostics, human power amplification (orthotic), and more.

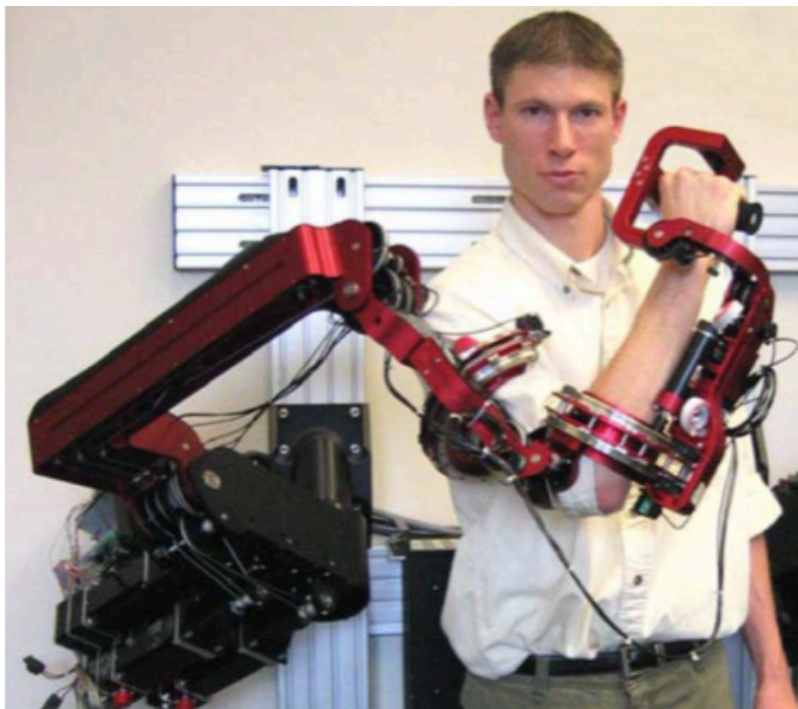


Figure 1.2. The EXO-UL7. The actuators are mounted to the wall unit, allowing for lightweight, low-inertia links. The semicircular design of the upper and lower arm HMIs allows for easier donning and doffing of the exoskeleton for impaired users [17].

After the success of the EXO-UL7 the EXO-UL8 followed. Designed and built by the Bionics Lab at UCLA, the EXO-UL8 utilizes harmonic drives (Sec. 2.2) as its actuators. The addition of harmonic drives allows for higher positional accuracy,

while eliminating cable routing, pulley reductions, and cable terminations that can prematurely fail. The physical design in terms of joint axis locations, workspace, and singularity placement in the EXO-UL8 (Fig. 1.3) are identical to those of the EXO-UL7.

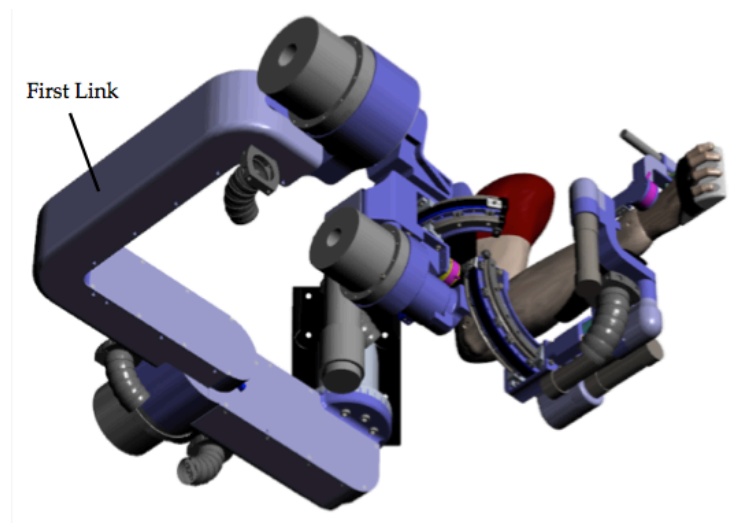


Figure 1.3. 3-D model of the EXO-UL8. Cable actuation has been replaced by harmonic drives. The overall weight of the exoskeleton is considerably greater than that of the EXO-UL7.

No longer driven by cables, the EXO-UL8 weighs considerably more than its predecessor. However, it retains the original HMIs, wall mount design, and seven DOFs with an additional DOF at the hand for grasping. The first link, pictured in (Fig. 1.2), differs from the EXO-UL7 in that it's modular. The EXO-UL7 link was machined from a single piece of aluminum, resulting in high machining cost. The EXO-UL8 maintains the original link shape and orientation, but is assembled with three pieces. It is the most recent design in the evolution of the BLUE SABINO project. Like the EXO-UL8, the BLUE SABINO will build upon the successes of its predecessors, and offer improvements through innovative design and control algorithms. Further discussion of these improvements can be found in (Sec. 3.1).

1.3.2. State-of-the-Art: Upper Limb Exoskeletons

Though the current trend in upper limb exoskeletons have provided several multiple-DOF systems, few of them account for full shoulder mobility [10], [11], [14], [17]–[19]. The shoulder joint described in (Sec. 2.1), consists of five DOFs, but many designs account for only three. The articulations of the scapulothoracic joint in concert with the sternoclavicular joint are often neglected to simplify design.

However, these articulations are vital to achieving full ROM of the shoulder, thus there have been recent exoskeletons developed to accommodate this movement. One of the core objectives of BLUE SABINO is the addition of a two-DOF scapulohumeral mechanism (Ch. 3). Another fundamental goal is the duality of the device, the ability to serve both as a rehabilitation tool, but also as an instrument for acquiring data critical to understanding the underlying mechanisms of impairment. Therefore, the following discussion is focused on current devices that share one or both of these two central design themes.

The first system to consider is the MGA exoskeleton. Built in 2005, the MGA is a six-DOF upper-limb exoskeleton capable of both rehabilitation and data acquisition. Driven by a combination of admittance and impedance control, the MGA has the ability to guide patients through prescribed motions and provide haptic feedback (resistive force) during virtual simulations. The MGA models the glenohumeral joint (Sec. 2.1.3) as a ball and socket, with three actuated DOFs. A fourth DOF is placed behind the patient in line with the sternoclavicular joint (Fig. 1.4), which allows for elevation/depression of the shoulder girdle [20], [21]. A fifth actuated DOF is positioned at the elbow, while a sixth passive DOF (a handle) is placed at the hand to allow for forearm pronation/supination. The addition of the joint for sternoclavicular motion allows for increased glenohumeral mobility and stability, but ultimately fails to provide full ROM due to protraction/retraction of the shoulder not being accounted for.

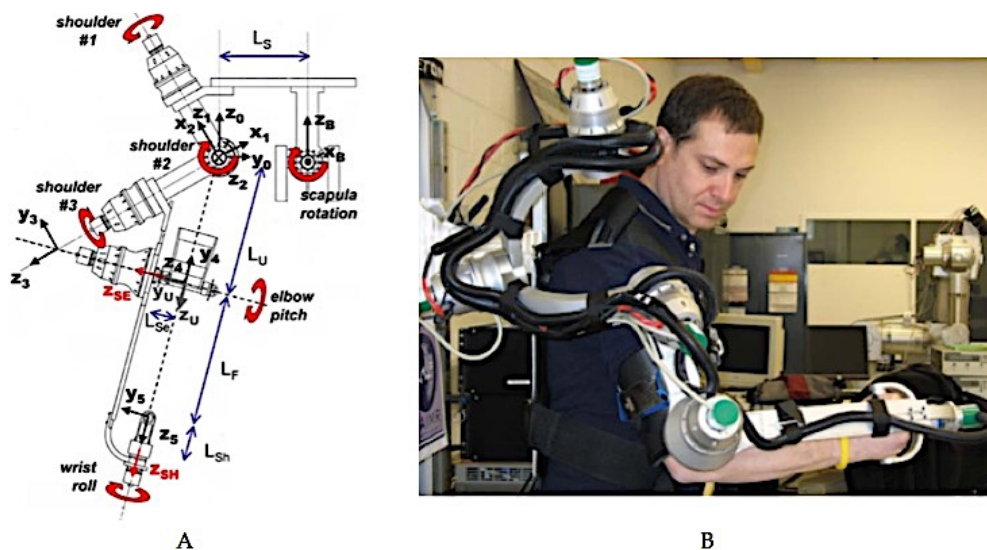


Figure 1.4. (A) Diagram of the MGA exoskeleton. The revolute joint labeled "scapula rotation" is responsible for elevation/depression of the shoulder. (B) The actual MGA in use [20].

The IntelliArm is a six-DOF exoskeleton specifically designed for both rehabilitation and diagnosis. Operated by position control when guiding patient movement and impedance control when patient guided; one of its main objectives is identifying abnormal muscle synergies, or neural deficits that result in a loss of coordination between muscle groups. Abnormal synergies affect the kinematics of voluntary movement through mechanisms like spasticity, an involuntary muscle contraction often seen in post stroke patients [19]. The IntelliArm uses three joints to account for shoulder elevation/depression. Two passive prismatic joints (Sec. 2.3.2) allow for natural alignment of the glenohumeral joint as the arm moves, while a third actuated prismatic joint is responsible for the elevation/depression of the shoulder girdle (Fig. 1.5). Noteworthy, the glenohumeral joint is actuated at one axis only, to perform flexion/extension. As can be seen in (Fig. 1.5), additional DOFs are provided at the elbow and wrist. However, due to the unique combination of active and passive joints, the ROM of the patient is greatly reduced, thereby limiting the capabilities of the device and overall effectiveness of the therapy.

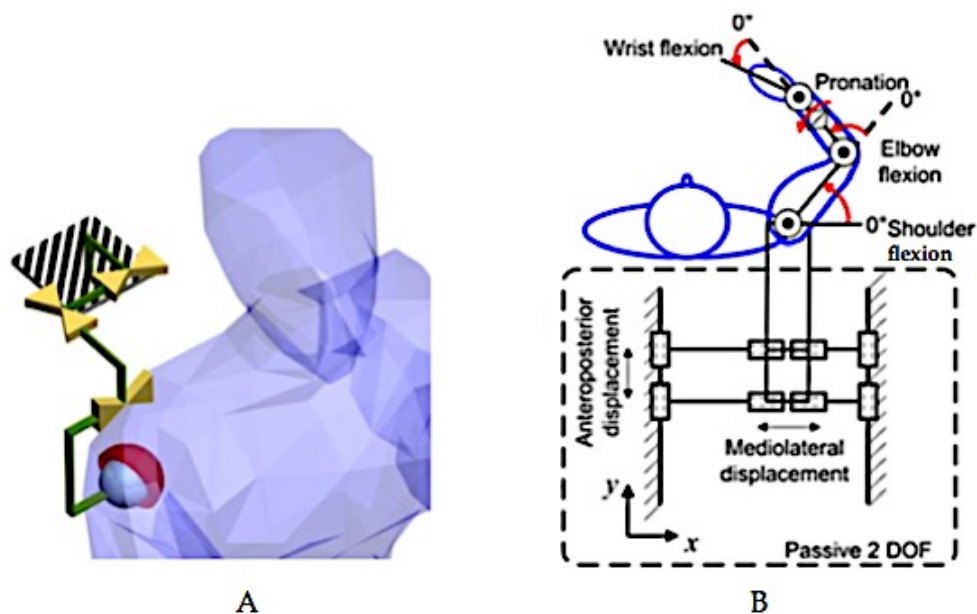


Figure 1.5. (A) Diagram of the three prismatic joints that allow for shoulder elevation/depression [21]. (B) Diagram of the overall IntelliArm system [19].

The ARMin III is a six-DOF exoskeleton with one DOF dedicated solely to shoulder elevation/depression. Unlike the previous devices, the ARMin III uses only position sensors to operate, thus it is used exclusively for rehabilitation. Elevation and depression of the shoulder is accomplished by linear actuation that

effectively lifts and lowers the entire exoskeleton (Fig. 1.6). The ARMin III is considerably heavier than comparable devices but operates similarly to the MGA, through a combination of admittance and impedance control. Like the aforementioned systems, protraction/retraction of the shoulder is excluded. However, near full range of motion is accomplished in the workspace due to the four DOFs at the shoulder, and the added DOF at both the elbow and wrist [14], [21], [22]. Furthermore, the ARMin III is the only exoskeleton of those discussed here that is commercially available (as the ArmeoPower). The other systems exist in research settings only.

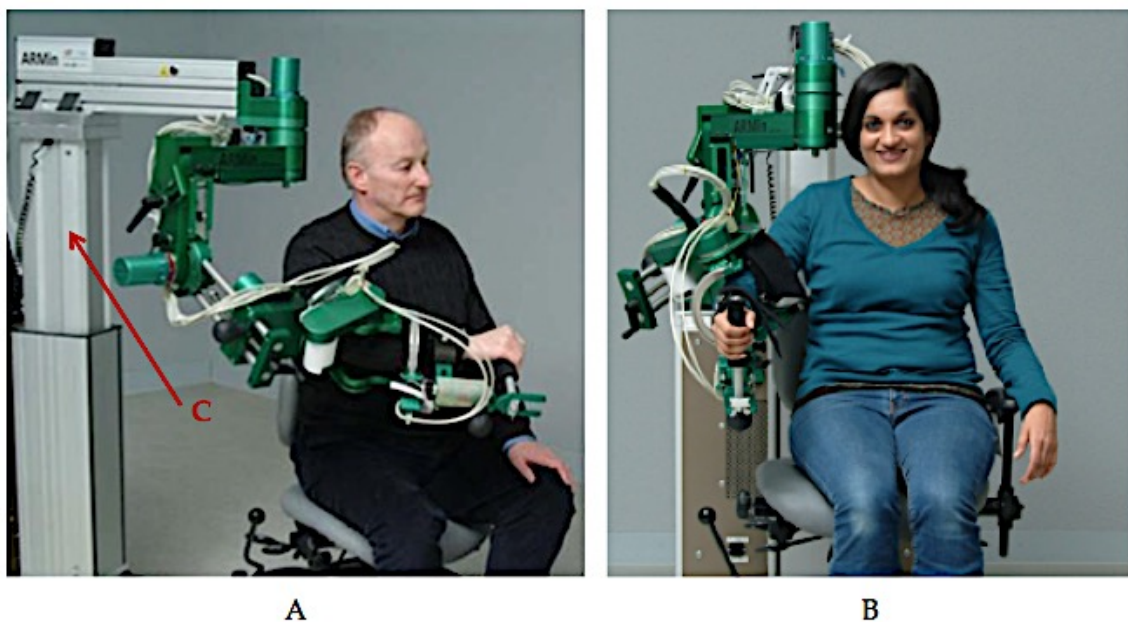


Figure 1.6. (A) The ARMin III, arrow (C) identifies the linear actuator responsible for shoulder elevation/depression [21]. (B) Front view of the ARMin III with a healthy patient [23].

The MEDARM is a six-DOF exoskeleton that claims to be the first rehabilitation robot to fully account for shoulder movement [24]. Two dedicated DOFs are aligned with the sternoclavicular joint, while the glenohumeral joint is supplied with the typical three DOFs (Fig. 1.7). Therefore, the entirety of shoulder girdle motion is accommodated. Though the control scheme is not specified, the system is cable driven like that of the EXO-UL7. The sixth DOF is found at the elbow joint, thus the MEDARM is focused toward shoulder/elbow rehabilitation and does not include protocol for the wrist or hand. The MEDARM is a large device, and as a result is platform-based. Due to the weight of the mechanism, gravity compensation (Sec. 2.5) has been incorporated into the design as well.

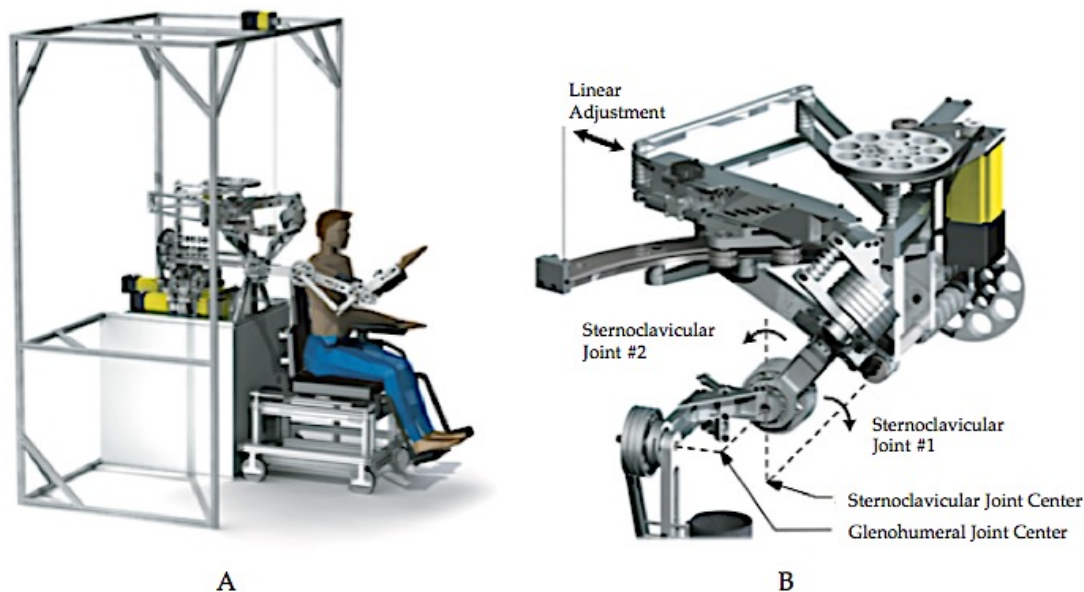


Figure 1.7. (A) 3D Model of the overall MEDARM system. (B) The two DOF shoulder mechanism responsible for elevation/depression and protraction/retraction of the shoulder joint. The curved track approximates the protraction/retraction while the elevation/depression is simply a revolute joint. As can be seen in the figure, the actuation is driven by electric motors and timing belts. The linear adjustment mechanism accommodates for size differences in patients [24].

The HARMONY is a dual upper-limb exoskeleton developed for rehabilitation by the University of Texas at Austin. Like the MEDARM, the HARMONY proposes a novel solution to the shoulder mobility problem [25], [26]. Scapulohumeral rhythm is accounted for by way of a parallelogram mechanism positioned behind the patient (Fig. 1.8).

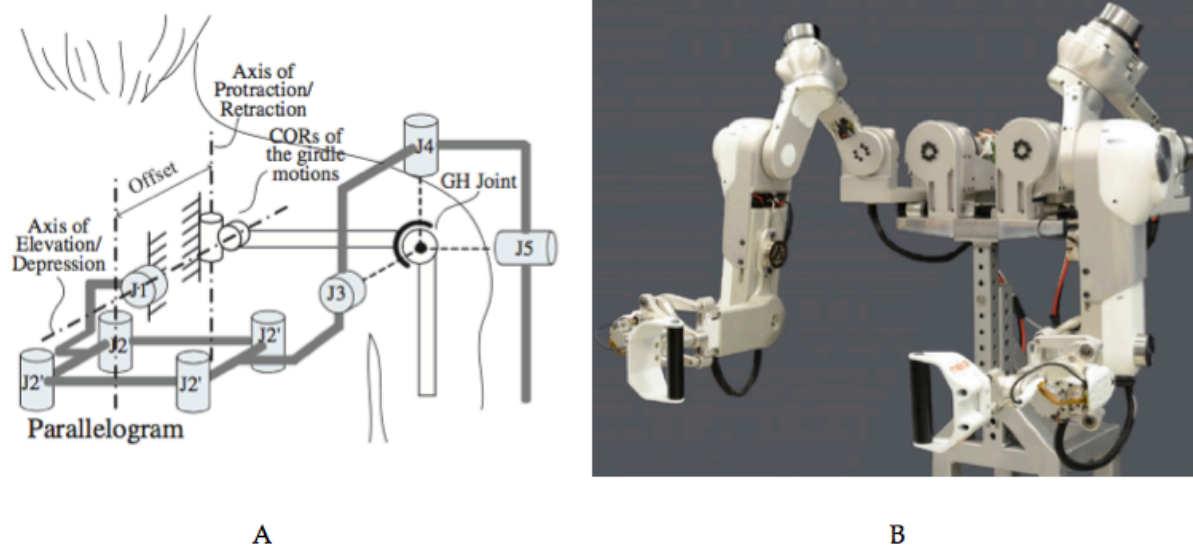


Figure 1.8. (A) Diagram of the five DOF shoulder mechanism [26]. (B) The HARMONY dual upper limb exoskeleton [25].

The parallelogram (Fig. 1.8) serves to provide protraction/retraction of the joint while a single revolute joint permits elevation/depression. Motion of the glenohumeral joint is accomplished through three DOFs placed at the shoulder, while an additional DOF is added at the elbow and hand. The device is driven through a combination of torque compensation and impedance control. Although the HARMONY is designed for therapy purposes, the exoskeleton could be adapted and someday used as a diagnostic tool as well.

1.3.3. BLUE SABINO: Objectives and Expected Outcomes

BLUE SABINO is a device that aims to be uniquely beneficial to the field of rehabilitation robotics. Like the systems reviewed in (Sec. 1.3.2), the addition of scapulohumeral rhythm compensation is a chief concern in the design process. A total of 28 DOF combined with electroencephalogram (EEG) and electromyography (EMG) will produce an instrument unlike any that have come before it. Full shoulder, elbow, wrist, and finger actuation combined with six-axis force/torque sensors at each HMI will provide unparalleled data acquisition capabilities. Standard metrics like force, torque, velocity, and acceleration will be quantifiable, but the BLUE SABINO project also aims to explore “intent”. The intent to move, detectable through brainwaves can be measured with EEG. The resulting motion at the muscular level can be recorded with SEMG sensors, potentially leading to new understanding of the neuromotor pathway and the underlying mechanisms that contribute to motor impairment.

Upon considering the potential capabilities of BLUE SABINO, the duality of its function becomes apparent. As an instrument, BLUE SABINO can provide important assessments of patients, insight into the inner workings of motor impairment, evaluation of therapy protocols, identification of abnormal synergies, etc. In turn this work can potentially lead to better brain-machine interfaces and improved neuroprosthetics. As a rehabilitation tool, BLUE SABINO can perform task-oriented training through both real and virtual objects. However the accuracy and repeatability of these attributes is ultimately dependent upon its design. As such, the remainder of this document is dedicated to the development of a two-DOF scapulohumeral shoulder mechanism and its integration into the overall architecture that is BLUE SABINO.

2. BACKGROUND

2.1. ANATOMY AND FUNCTION OF THE HUMAN SHOULDER

The shoulder complex is the most mobile joint in the human body. However, due to its vast range of motion, the shoulder is inherently unstable. The complex consists of three main bones: the clavicle, humerus, and scapula. Of these, only the clavicle is connected to the rest of the axiskeleton via the sternum. The remainder of the shoulder is supported purely through the close interrelations of muscles, ligaments, and tendons. These connections form four joints that each possesses three DOFs: the sternoclavicular, acromioclavicular, glenohumeral, and scapulothoracic joints. The overall structure of the shoulder complex is illustrated in (Fig. 2.1).

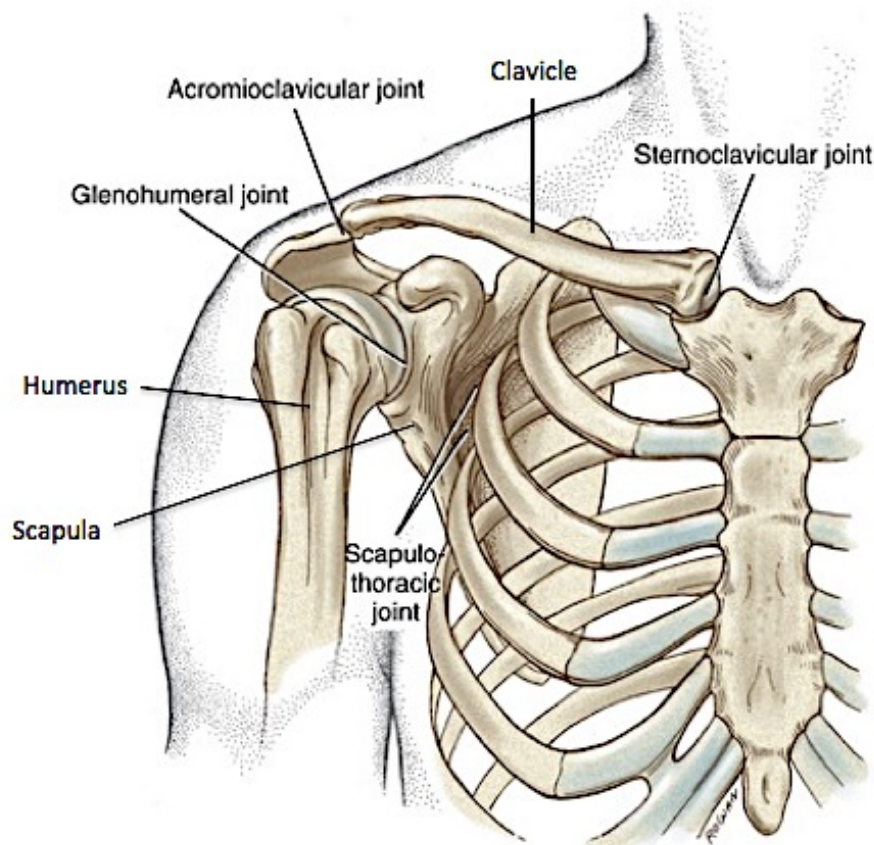


Figure 2.1. The shoulder complex. The shoulder is comprised of three bones: the clavicle, humerus, and scapula. Four joints form the entire shoulder girdle: sternoclavicular, acromioclavicular, glenohumeral, and the scapulothoracic joints [27].

2.1.1. Sternoclavicular Joint

The sternoclavicular joint (SC) is formed by the connection between the clavicle and manubrium of the sternum (Fig. 2.2). It is often described as a synovial saddle joint whose main function is elevation/depression and protraction/retraction of the arm. However, the SC joint does allow for rotation about the longitudinal axis of the clavicle, which is critical during arm abduction, flexion, and extension. The range of rotation is more limited than the aforementioned actions. Currently, it is estimated between 25° and 55° for external rotation and less than 10° for internal rotation [28]. Regardless of the precise ROM of the SC joint, it is well known that its function is intimately linked to the other joints of the shoulder.

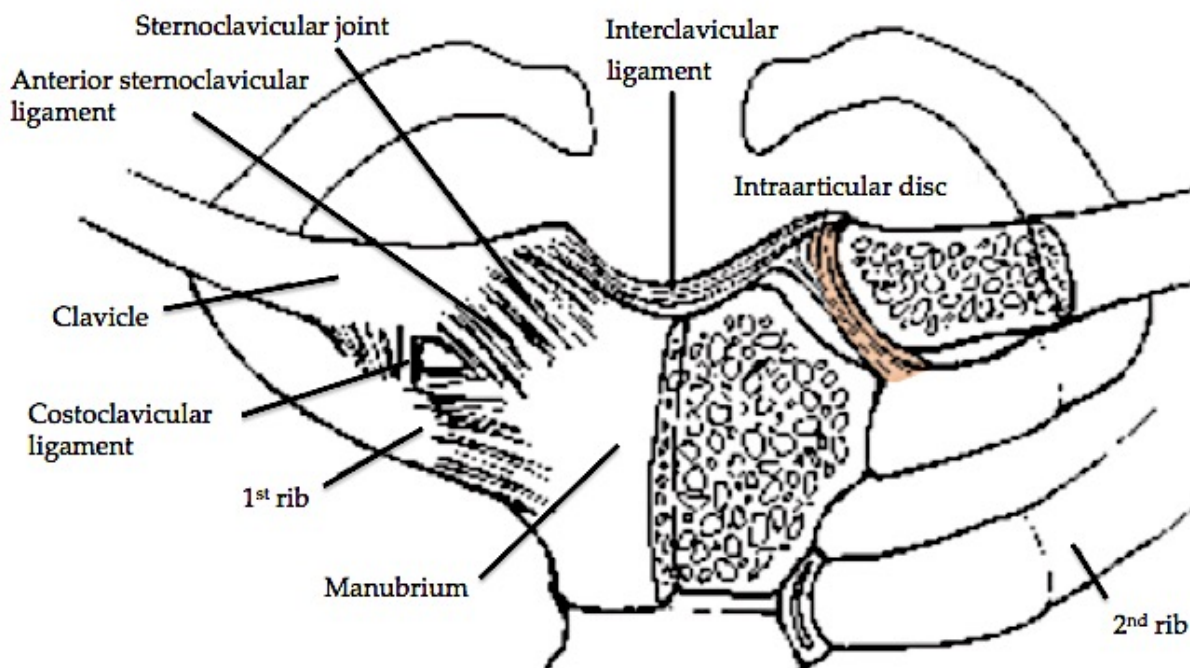


Figure 2.2. Sternoclavicular joint location and accompanying musculoskeletal structure [28].

2.1.2. Acromioclavicular Joint

The acromioclavicular joint (AC) is located at the top of the shoulder and is formed by the union of the acromion process and the clavicle (Fig. 2.3). The acromion is part of the scapula and forms the highest point of the shoulder. Considered a “gliding” joint, the AC is also synovial and its main function is the translation of motion. Specifically, the AC joint is responsible for much of the

scapular motion relative to the clavicle. One noteworthy feature of the AC joint is the extracapsular coracoclavicular ligament. It serves as critical joint support and is considered by many to be the primary suspensory ligament for the entire shoulder [28].

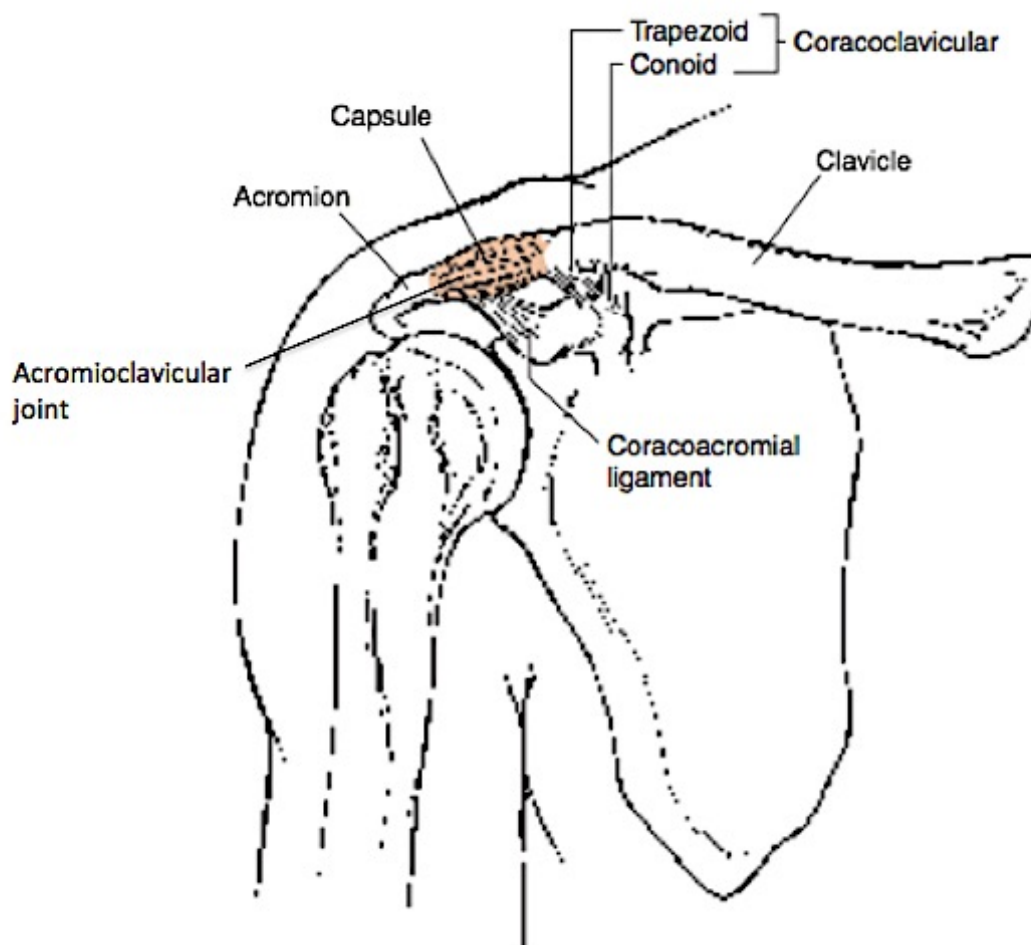


Figure 2.3. The acromioclavicular joint and supporting musculoskeletal system [28].

2.1.3. Glenohumeral Joint

The glenohumeral joint (GH) is a synovial ball and socket joint formed by the head of the humerus and the glenoid fossa of the scapula. Commonly, the GH joint is referred to as the “shoulder”. However, this characterization is misleading due to its simplification of the complex motion of the shoulder. As can be seen, shoulder motion is obtained through the intricate interactions of the four joints that form the entire shoulder complex. At the junction of the humerus and glenoid fossa the articular surfaces are not truly spherical but actually oval, with the surface area of

the humeral head being three to four times larger than that of the glenoid fossa [29]. The shallow nature of the glenoid fossa is what affords the GH joint its three DOFs and remarkable ROM, but is also the cause of its intrinsic instability. Primarily the superior, middle, and inferior glenohumeral ligaments support the function of the GH joint, in conjunction with the coracohumeral ligament. The anatomical placement of these ligaments and the joint location are represented in (Fig. 2.4).

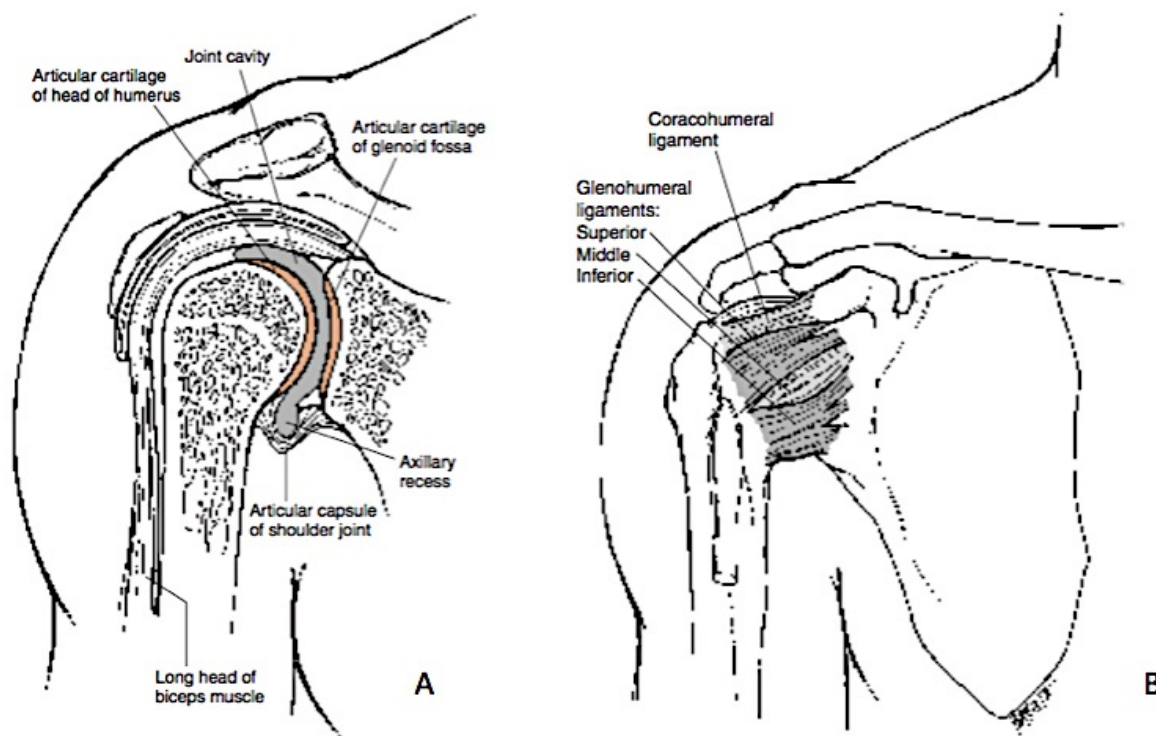


Figure 2.4. (A) The glenohumeral joint and associated structures. (B) The supporting ligaments that stabilize the glenohumeral joint [28].

2.1.4. Scapulothoracic Joint

The term “scapulothoracic joint” (ST) is actually a misnomer. The movement of the scapula relative to the thorax (ribcage) is accomplished by the subscapularis and serratus anterior. These muscles lie between the thorax and scapula and glide past one another during scapular motion. The space occupied by these muscles, specifically between the concave anterior surface of the scapula and the posterolateral surface of the thorax is what defines the scapulothoracic joint [29]. Scapular movement is the product of articulations by the SC and AC joints. As a result the SC joint is capable of three DOF, primarily translation and rotation (Fig. 2.5).

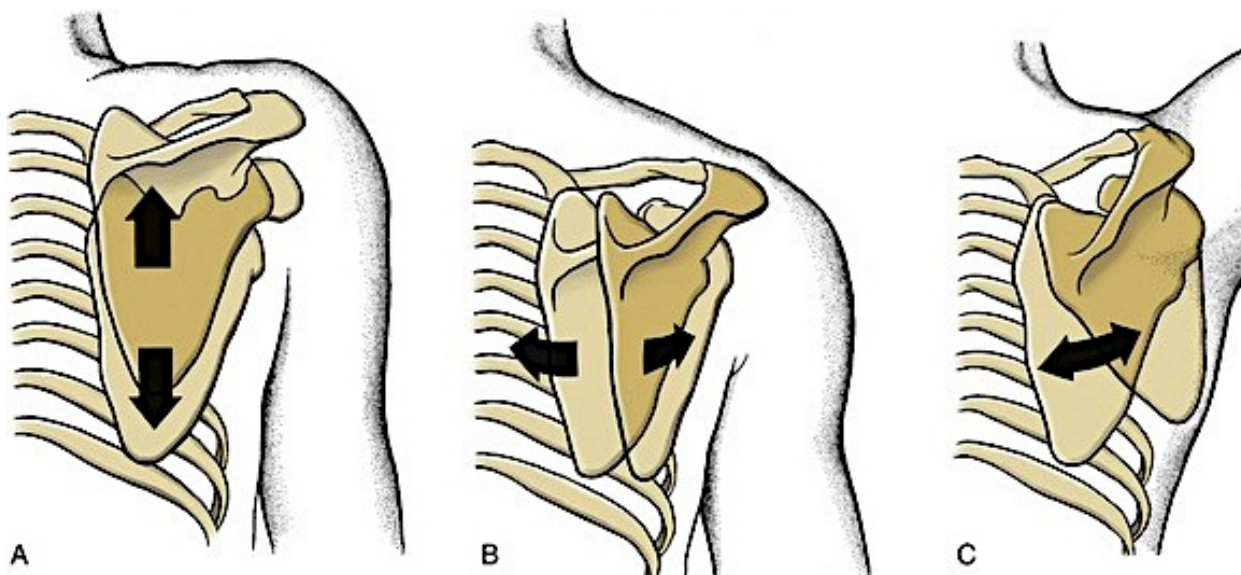


Figure 2.5. The primary motions of the scapula. (A) Elevation and depression. (B) Protraction and retraction. (C) Abduction and adduction [27].

2.1.5. Scapulohumeral Rhythm

The primary role of the ST joint is to facilitate and increase the ROM of the GH joint. Because the motion of the scapula and GH joint are so intrinsically linked, their relationship has been given the name “Scapulohumeral Rhythm” (SR) [30]. Or in other words, how the scapula moves in relation to the humerus. Classifying the specific motion and mechanisms that define it has been a challenge over the last few decades. Part of the difficulty lies in the nonlinear nature of the rhythm. During the first 30° of arm abduction (where 0° is defined as the arm resting at one’s side) the scapula hardly participates. The ratio is 4.3:1, with the convention of glenohumeral to scapulothoracic movement [31]. After initial abduction the ratio begins to decrease. It is at this point the scapula becomes an active participant in the overall motion of the shoulder complex.

Ultimately the scapula has two axes of rotation during arm abduction. From 30° to 100° of abduction the scapula rotates about the root of the scapular spine. This rotation allows the arm to abduct by simultaneously causing the SC joint to rotate (Fig. 2.6). After 100° of abduction, the center of rotation shifts to the AC joint (Fig. 2.6). This is due to the costoclavicular ligament becoming taut (Fig. 2.2), effectively stopping the rotation of the SC joint. When the AC joint becomes the center of rotation, the root of the scapular spine no longer rotates but translates

laterally instead. Near full abduction, the trapezoid ligament becomes taut rendering the AC joint immobile. At this interval the clavicle and scapula once again move together. The clavicle rotates about its longitudinal axis allowing for the last portion of abduction [29]. The ratio of the glenohumeral to scapulothoracic movement from 30° abduction and on is generally accepted to be 2:1 by Inman et al. [30]. However, other published reports place it at 1.25:1, 1.35:1, and 2.34:1 [29].

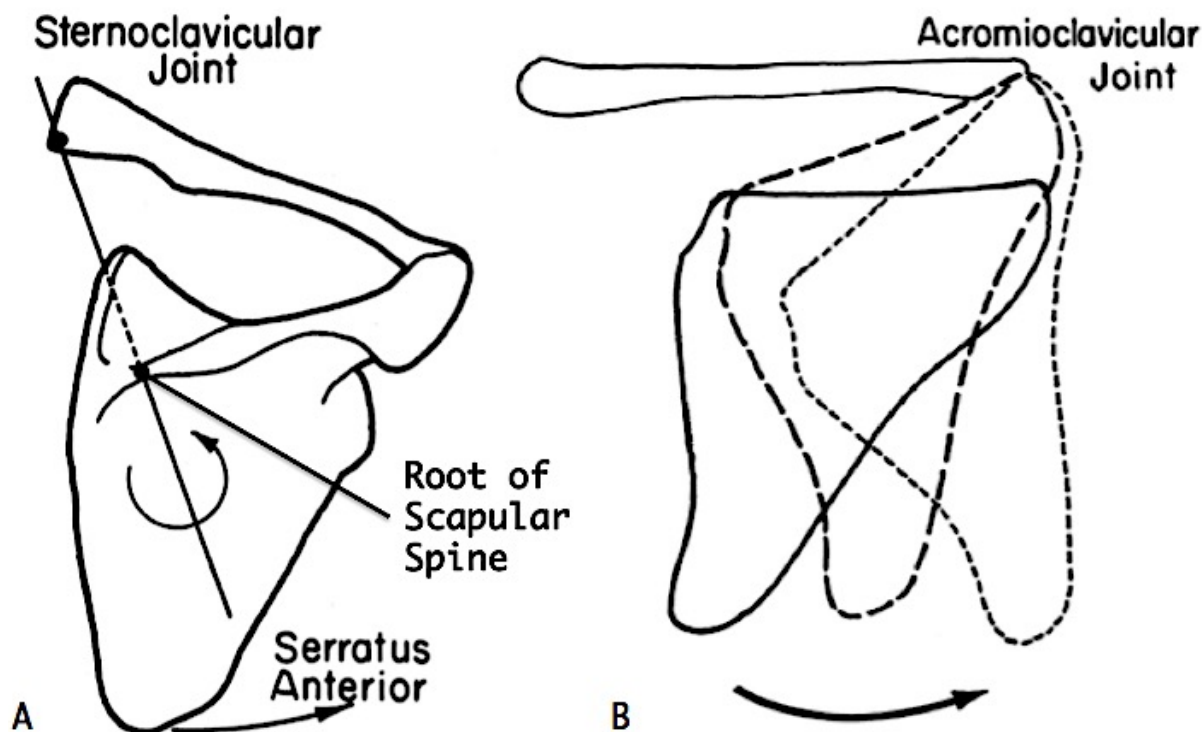


Figure 2.6. (A) After 30° of abduction the scapula rotates about the root of the spine. (B) After 100° of abduction the acromioclavicular joint becomes the center of rotation and the root of the spine moves laterally outward [29].

2.1.6. ROM of Common Shoulder Movements

The human shoulder has an astonishing ROM and a number of well-specified movements. The nomenclature that follows will be used throughout this document to describe the specific type of motion under discussion. This is done as clarification for the reader and to provide consistency throughout the body of this text. As previously explained the shoulder complex consists of four joints that work in concert with one another. The overall movement of the structure is simplified by designating specific monikers to each distinct motion. The abovementioned monikers and the ROM associated with each are illustrated in (Fig. 2.7).

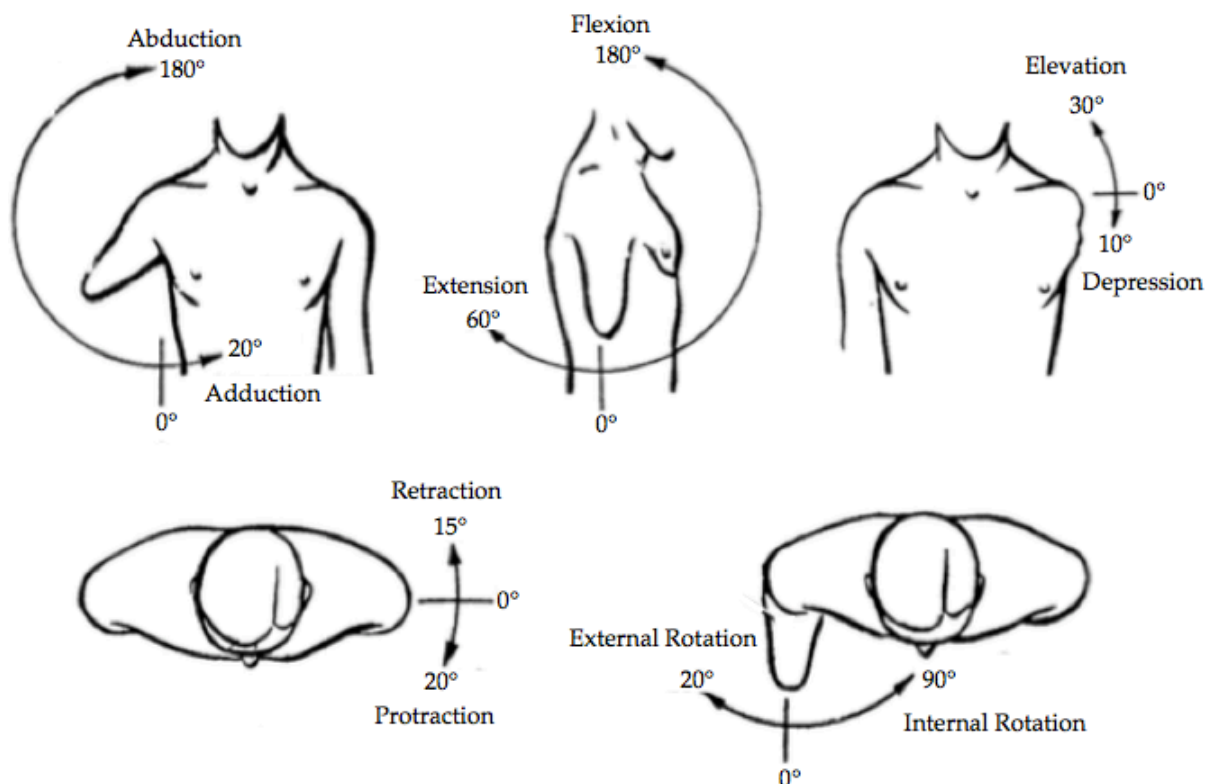


Figure 2.7. Types of shoulder movement and the corresponding ROM for each [32],[33]–[35].

2.1.7. Summary

The shoulder is the most mobile joint in the human body. It is this mobility however that causes the shoulder to be inherently unstable. While many people associate the “shoulder” with only the glenohumeral joint, it is actually comprised of four joints that form the shoulder complex. The sternoclavicular, acromioclavicular, glenohumeral, and scapulothoracic joints are intrinsically linked, and it is through their concerted effort that shoulder movement is achieved.

The scapulothoracic joint is actually a misnomer; it is not truly a joint. The “joint” consists of the space between the scapula and thorax. Its motion is a function of the subscapularis and serratus anterior as they glide past one another. The primary purpose of the ST joint is to facilitate in the ROM of the GH joint. However, the precise motion of the scapula and how it relates to GH motion is complex and the mechanisms behind it are hard to quantify.

Scapulohumeral rhythm is a term used to describe the movement of the scapula relative to the humerus. It has been found to be a nonlinear relationship, with very little movement occurring during the first 30° of arm abduction. From 30°

to 100° of abduction the scapula rotates about its spinal root. Though published values differ, the generally accepted ratio for glenohumeral to scapular movement is 2:1 provided by Inman et al. [30] through their definitive work in the 1940's. Past 100° the AC joint becomes the center of rotation until nearly the end of abduction; upon which the scapula and clavicle move together to complete the full ROM.

Lastly, it is important that shoulder movements and their corresponding ROM have distinct names and limits. There are interchangeable terms for many of the movements performed by the shoulder complex. It is for this reason that care has been taken to clearly define these movements and their respective ROM to provide clarity and consistency for the reader (Fig. 2.7).

2.2. HARMONIC DRIVES

Harmonic drives are a common choice for actuation in industrial robotics, aerospace, machine tooling, and many other forms of motion control. Their popularity is a result of their unique structure and consequent capabilities. Lauded for their high positioning accuracy, precision, repeatability, zero backlash, and high power to weight ratio; harmonic drives offer distinctive advantages over traditional gearing. In fields like aerospace and rehabilitation robotics, size and weight are two primary concerns during the design phase. Harmonic drives provide a practical solution to these demands while also offering increased design flexibility where other more traditional solutions may not.

2.2.1. History of Harmonic Drives

Clarence Walton Musser (1909-1998) first received a patent for “strain wave gearing” in 1957. Though Musser is credited with the patent, the main concept used in his design was previously known. A Russian engineer A.I. Moskvitin had claimed the idea in a patent dating back to 1944 [36]. In 1958, Harmonic Drive Division was born in Beverly Massachusetts and strain wave gearing became synonymous with the words “Harmonic Drive”. Initially, harmonic drives were manufactured for use in aircraft and defense applications [37]. It wasn't until the 1970s that the application of harmonic drives were expanded to include the fields of industrial robotics, aerospace, and machine tools. The first space application was in 1971 when harmonic drives were used for the Lunar Roving Vehicle on the Apollo 15 mission.

Since then, the versatility and reliability of harmonic drives has resulted in their implementation in the auto industry, surgical robots, silicon wafer processing machines, industrial motion control and more [36].

2.2.2. Basic Operating Principles

Harmonic drives are unique in their construction and function. The primary concept behind the harmonic drive is utilization of the elasticity of metal. A harmonic drive is composed of three parts: the wave generator, flexible spline, and circular spline (Fig. 2.8).

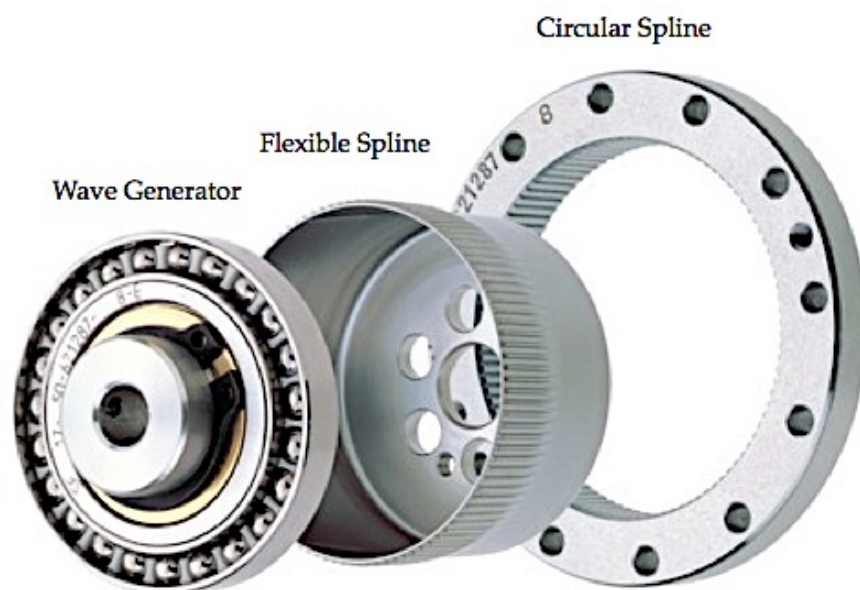


Figure 2.8 The three components that constitute a harmonic drive [38].

The wave generator is not circular but in fact slightly elliptical. As the wave generator rotates, the major axis of the generator forces the flexible spline to elastically deform. Having two less teeth than the circular spline, the flexible spline moves one tooth for every 180° the wave generator rotates [39]. It is this relationship between the components that allow for high gear reductions within a single staging. Furthermore, because the generator is elliptical, multiple teeth at both ends of the ellipse share the transmitted load. This feature is but one of many that makes harmonic drives advantageous over traditional gearing. The components and their functions are discussed in greater detail in the following sections.

2.2.3. The Wave Generator

The wave generator serves as the input to the harmonic drive and is mounted to the motor shaft. To enact rotation, a specially designed thin-raced ball bearing is pressed onto an elliptical hub (Fig. 2.9). Like the flexible spline, the ball bearing deforms about the hub as it rotates. The interaction of the hub, ball bearing, and flexible spline is the source of the generator's name. Mussel explained the theory of the motion as, "A continuous deflection wave generated in a flexible spline element achieves high mechanical leverage between concentric parts" [36].

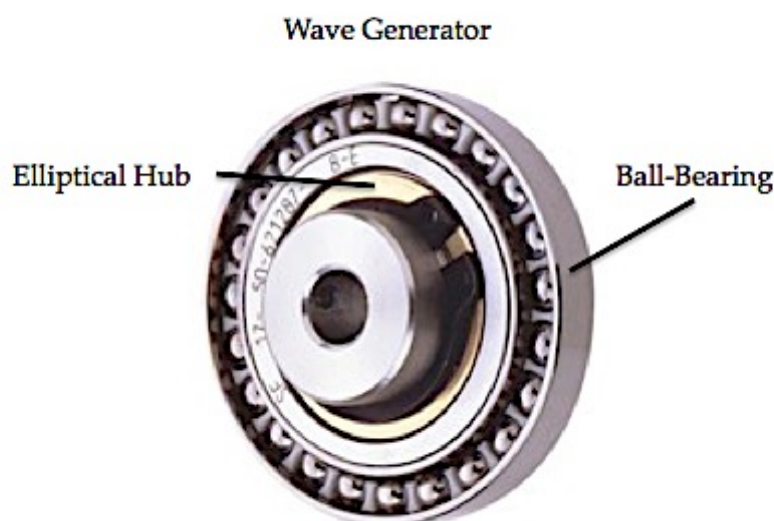


Figure 2.9. Two piece construction of the wave generator. The thin raced ball bearing is pressed onto the elliptical hub [38].

2.2.4. The Flexible Spline

The flexible spline serves as the intermediary between the wave generator and the circular spline. It is a thin cylindrical cup with external teeth on the open end. It also serves as the output to the harmonic drive, thus the other end is thicker, rigid, and attached to the output flange (Fig. 2.10). The generator is inserted into the open end of the cup upon which the spline conforms to its elliptical shape. There are two less teeth on the flexible spline than its circular counterpart. As the generator rotates clockwise, the flexible gear rotates counterclockwise. Every 180° of rotation results in the gear advancing one tooth in relation to the circular spline, subsequently two teeth are skipped for every full revolution of the generator (Fig. 2.11).



Figure 2.10. The flexible spline, including location of the attachment point for the output flange [38].

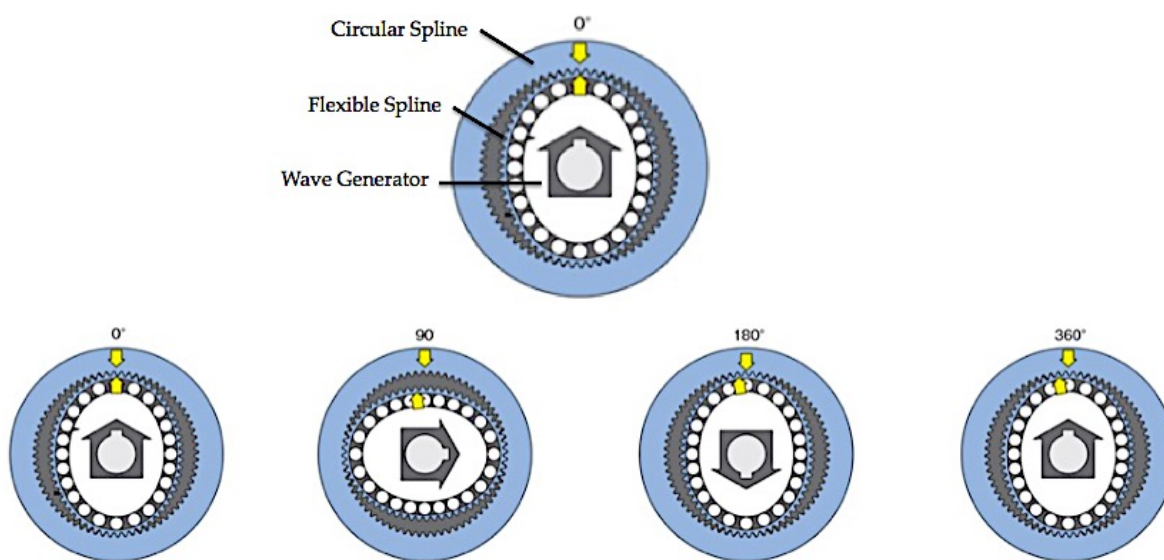


Figure 2.11. An exaggerated diagram, showing the motion of a harmonic drive. As the wave generator rotates clockwise, the flexible spline rotates counterclockwise. These dynamics allow the flexible spline to skip two teeth in relation to the circular spline for each full revolution [38].

2.2.5. The Circular Spline

The circular spline is rigid and the only stationary member of the harmonic drive (Fig. 2.12). It has two more internal teeth than the flexible spline and is fixed to the gear housing. As the generator rotates, the circular spline engages the flexible gear on the two opposing ends of the ellipse across the major axis. Since the meshing of the teeth is almost purely radial there is little friction loss or wear. The contacting

regions of the gears have multiple tooth engagement which distribute the load, allowing the teeth to transmit torques nearly proportional to their static strength [36].

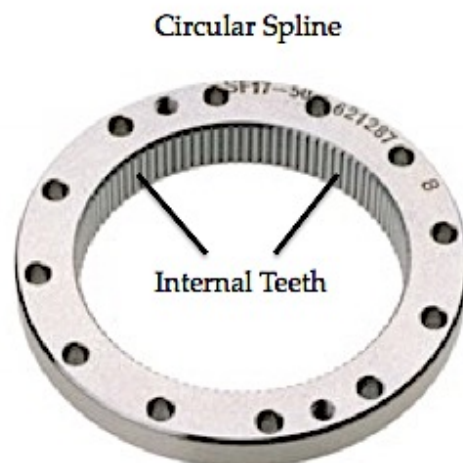


Figure 2.12. The circular spline is mounted to the gear housing, making it the only stationary component of a harmonic drive [38].

2.2.6. Summary

Strain wave gearing or “harmonic drives”, were first realized by Clarence Walton Mueller in 1957. Originally produced for aircraft and defense applications, harmonic drives found their way into the aerospace industry. In 1971 harmonic drives were used on the Lunar Roving Vehicle during the Apollo 15 mission. Since then harmonic drives have become a staple in precision motion applications such as robotics and machine tooling.

Harmonic drives are comprised of three main components: the wave generator, flexible spline, and circular spline. The wave generator is elliptical, and as it rotates clockwise, the flexible spline rotates counterclockwise. Because the flexible spline has two fewer teeth than the circular spline, it is able to advance two teeth per revolution. The circular spline is stationary and mounted to the gear housing. Due to the elliptical wave generator, the flexible and circular splines mesh at opposing sides of the major axis. The unique design and operation of harmonic drives affords many beneficial characteristics. A few of these benefits are high positional accuracy, efficiency, lightweight, high gear reductions, zero backlash, and compactness. These features make harmonic drives an ideal solution in many high-precision motion applications.

2.3. PRINCIPLES OF FOUR-BAR LINKAGES

Linkages and the mechanisms they form are fundamental in the field of engineering. One of the most common linkage assemblies in use is the four-bar mechanism. They are found in thousands of applications ranging from vise-grips to actuating buckets on heavy machinery [40]. They are relatively simple in construction and well defined in theory, which is why they are a popular choice in many applications. They do however have limitations. Four-bars are constrained to one DOF. As such, more complex movements may require the addition of links, resulting in five and six-bar configurations. The following sections describe the components and theory behind the design and operation of four-bar linkages.

2.3.1. Links

The term link is used to describe a rigid body with at least two nodes or attachment points. The most common links are binary, ternary, and quaternary: possessing two, three, and four nodes respectively (Fig. 2.13).

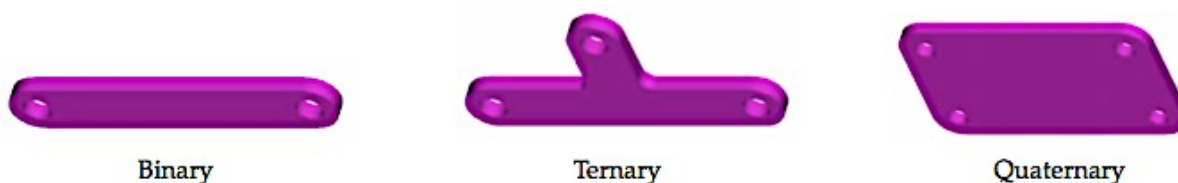


Figure 2.13. The three common forms of links [40].

When joints combine two or more links, the result is a linkage. Linkages can form open and closed loops which are known as kinematic chains [41]. If the chains formed by these linkages have one link fixed but allow mobility in the surrounding links, it is defined as a mechanism [41]. If no mobility exists, it is defined as a structure.

2.3.2. Joints

Joints are the connections between links that allow for relative motion of one link to the other. One to three DOFs can be achieved per joint depending upon the type used. Typical one-DOF joints are revolute (purely rotational), prismatic (sliding), and helix (threads on a screw) (Fig. 2.14).

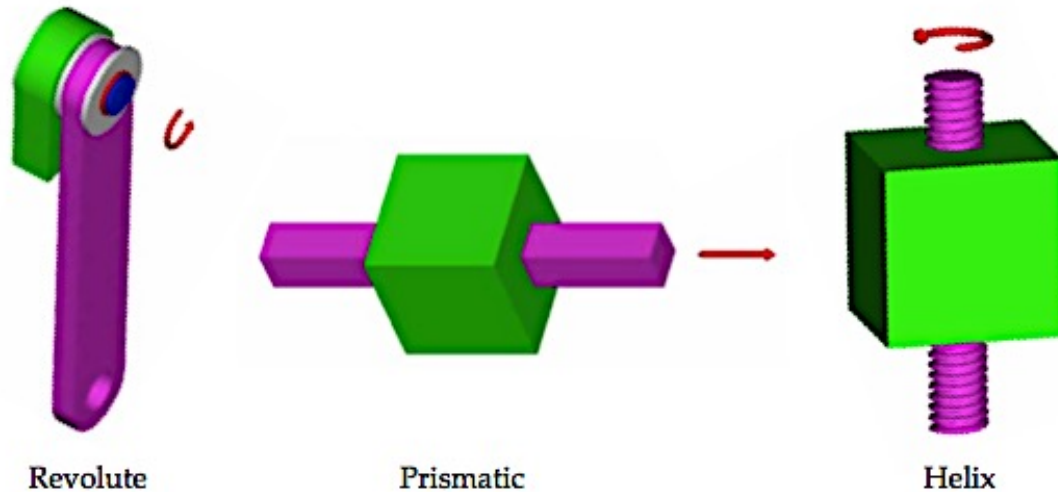


Figure 2.14. Examples of typical one DOF joints [40].

Common multiple-DOF joints include the cylindrical, spherical, and planar joints. The cylindrical joint is an example of a two-DOF joint that accommodates both sliding and rotation. Spherical joints can rotate about all three axes and are therefore capable of three DOFs. The planar joint like the abovementioned spherical joint permits three DOFs. However, two DOFs are sliding while the third is rotation (Fig. 2.15)

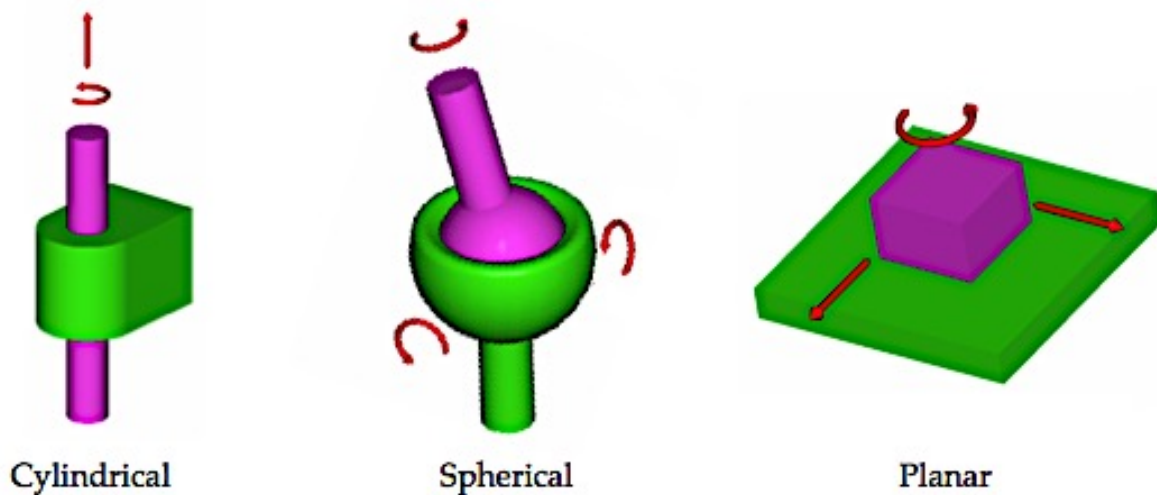


Figure 2.15. Examples of multiple DOF joints [40].

2.3.3. Gruebler's Equation

When analyzing a configuration of linkages, the DOF of the system may not be obvious. However, there is a systematic process to determine the DOF of a system by using the type of connections in combination with Gruebler's equation.

First, a clear demarcation must be made between *lower* and *higher* pairs of joints as these distinctions directly affect the use of Gruebler's equation. Lower pairs are joints that permit motion between a fixed surface and moving surface through constant direct contact. All of the joints shown in (Fig. 2.14) are examples of lower pair joints. Higher pair joints allow movement through contact at certain points or line segments (e.g. cam and follower, gears) [41]–[44]. By identifying the types of joints in use, Gruebler's equation may be employed:

$$F = 3(n - 1) - 2j - h \quad (1)$$

where F is the total DOF, n is the total number of links including the ground link, j is the number of lower pairs, and h is the number of higher pairs. If Gruebler's equation is applied to a planar four-bar linkage:

$$F = 3(4 - 1) - 2(4) - 0 \Rightarrow F = 1$$

therefore Gruebler's equation correctly states the total DOF is one. Although Gruebler's equation is applicable to most situations, exceptions do exist. For example, a three-piece linkage comprised entirely of sliding joints; or three links consisting of one sliding joint, revolute joint, and helix joint (e.g. a fly press) [42]. The total DOFs in either scenario will not be correctly quantified by Gruebler's equation.

2.3.4. Defining a Four-Bar Mechanism

In the simplest sense, a four-bar mechanism is merely the combination of four links that are connected by four pinned or revolute joints. However, the four-bar linkage as Natesan states, "derives its renown from the fact that the members of a three bar linkage are incapable of relative motion and a linkage composed of more than four bars has indeterminate motion with a single input" [43].

The four-bar as the name implies, consists of four main parts. The *ground* or *frame* link is the fixed link of the chain; it remains stationary relative to the other links. The *crank* or *rocker* is the link that serves as the input to the chain. If the link is

allowed to fully rotate, it is referred to as a crank. If however the rotation of the link is limited and serves an oscillatory function, it is known as a rocker. The *follower* is connected to the other end of the ground link; its motion is dependent on the crank. Finally the *coupler* link is the output of the chain and also the link that closes the loop by coupling the crank and follower (Fig. 2.16).

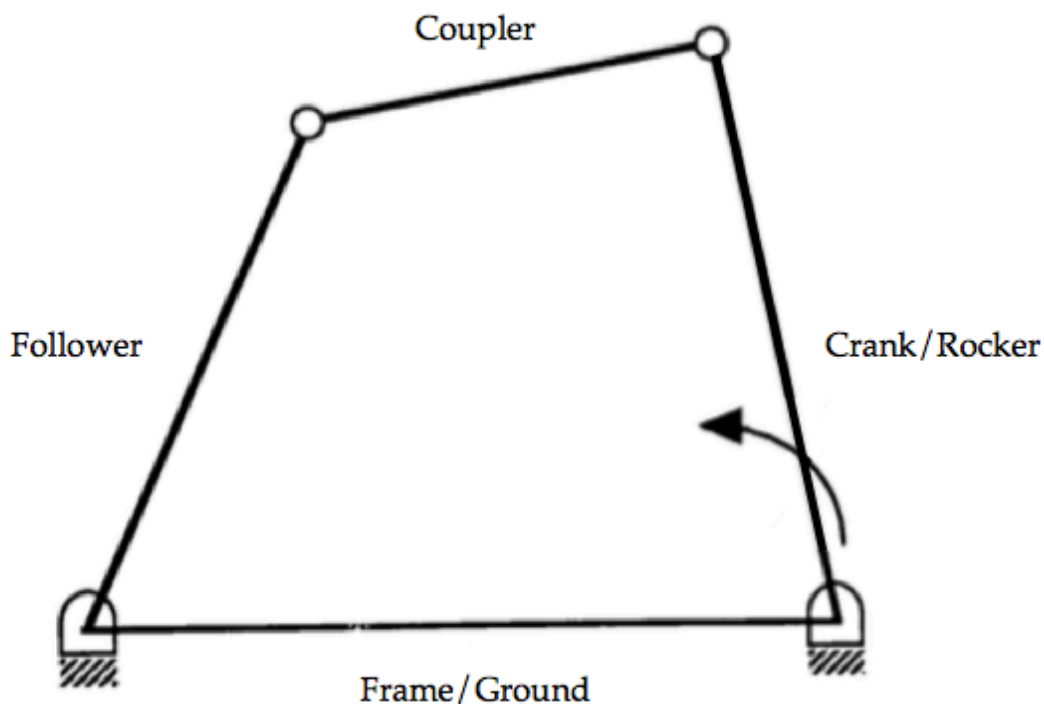


Figure 2.16. Skeleton diagram of a four-bar mechanism with the individual links identified [43].

2.3.5. Grashof Criteria

The motion of a typical four-bar mechanism can be anticipated by applying Grashof's criteria. The criteria states, "The sum of the shortest (S) and longest (L) links of a planar four-bar linkage cannot be greater than the sum of the remaining two links (P, Q) if there is to be continuous relative motion between two links" [40]. Therefore, only four types of four-bar mechanisms exist that obey Grashof's criteria: crank-rocker, drag link, double-rocker, and crossover-position/change point. These types are defined by the aforementioned criteria and by which link in the chain is shortest (Fig. 2.17). Like Gruebler's equation, exceptions do exist. The defining characteristic of a Non-Grashof mechanism is the inability for any of its links to rotate 360° . Non-Grashof mechanisms include double-rockers of the second kind and triple-rockers [43].

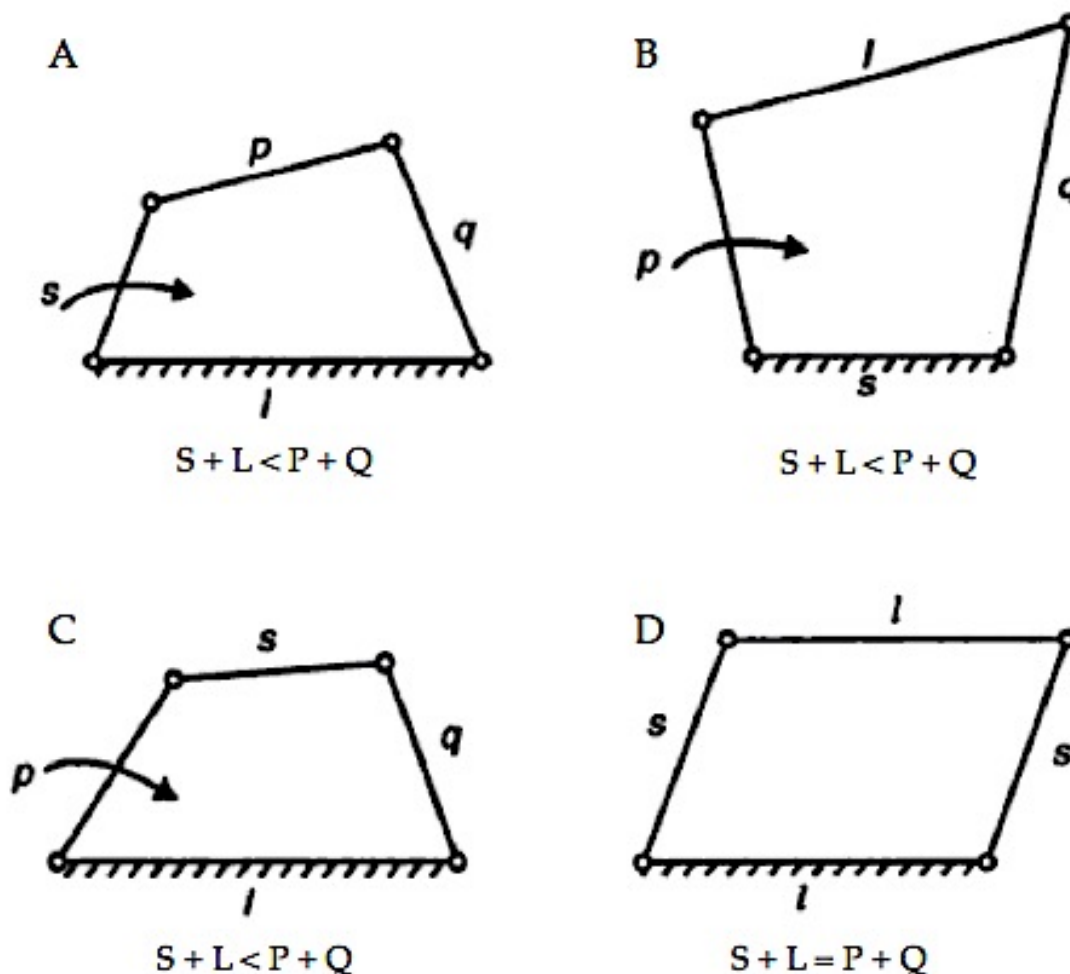


Figure 2.17. The four Grashof mechanisms. (A) Crank-rocker—a function of the crank being the shortest link. (B) Drag link—the ground link is the shortest link. (C) Double-rocker—the coupler is the shortest link. (D) Crossover-position—the mechanism is a parallelogram [45].

2.3.6. Kinematic Synthesis

Many times in design a particular motion is desired and the mechanism to perform it must be created. The process of creating a mechanism given a prescribed movement is known as *kinematic synthesis*. There are three main categories that comprise kinematic synthesis: type, number, and dimensional. Determining the means to accomplish a task is what defines *type synthesis*. Deciding what types of mechanisms are required (e.g. gears, cams, links) are the goals in this phase of kinematic synthesis. Answering questions such as how many links and DOFs are needed is the function of *number synthesis*. Pioneered by Gruebler (Sec. 2.3.3) number synthesis is sometimes grouped with type synthesis as a subcategory. Lastly, *dimensional synthesis* focuses on the link lengths and starting point of the

mechanism in question. Together, the abovementioned concepts form the basis of kinematic synthesis.

Like the three forms of synthesis previously discussed, there exists three main *tasks* that kinematic synthesis aims to accomplish: function, path, and motion generation [40]–[43], [46]. As the name implies, *function generation* dictates that the output motion of the mechanism be a function of the input motion. If the task is instead to have a point on the coupler trace a distinct route, it is known as *path generation*. Lastly, if the task is to move a rigid body such as a link through a series of specified positions, it is called *motion generation*. Often times motion generation is easier to accommodate in design than function or path generation.

2.3.7. Graphical Method

Before computers, the graphical method was one of the most effective ways to design mechanisms through the approach of kinematic synthesis. There are numerous graphical methods available to the engineer. Though not as accurate as analytical methods, graphical solutions are relatively quick and easy to perform with results that are acceptable in accuracy. A brief discussion of graphical methods is presented here, for a more detailed explanation see [41], [42], [45].

A common graphical method is the *three-position synthesis* approach. Consider a four-bar mechanism. In (Fig. 2.18) the input crank (link A) is rotated through three positions. Likewise, the follower (link B) is placed in three desired output positions. The goal is to determine the length and starting angle (ϕ) of the follower. The scenario described utilizes function generation (output as a function of input) to define the requirements of the mechanism. A popular approach to solving this problem is the relative pole method.

In the relative pole method, lines drawn from the centers of rotation at both the crank and follower are extended until intersection (Fig. 2.18). The intersection point (R_1 and R_2) is known as a relative pole, a center of rotation relative to both the crank and follower. In the case of three-point synthesis, it is necessary to identify two such poles. A second pair of lines can be extended from the relative center (preserving angle) to intersect the tip of the crank (length is chosen by designer), allowing the other line of the pair to simultaneously identify the tip of the follower

and the angle (ϕ) of its starting position (Fig. 2.19). It can be seen that there is in fact an infinite number of solutions along the lines of the poles. This fact only remains true if the intersection of the lines and link tips are observed. If this relationship is maintained, an infinite number of solutions can be achieved along the pole lines by simply adjusting the link lengths. The example shown here considered three arbitrary positions of the crank and follower. In practice, precise points are used for the output as a function of the input. The most widely used technique to determine these points while reducing structural error (error between calculated output vs. actual output) is Chebyshev spacing.

The graphical form of Chebyshev spacing is achieved through the use of a circle and polygon. Increasing the number of points increases the accuracy, but also the difficulty in calculating the points. Typically, three to six points are used. In this discussion three points are considered. First, an interval for the motion of the link must be established. Next, a circle with a diameter equal to the range of the interval is drawn. The center of the circle should correspond to the center of the interval. A polygon is then inscribed within the circle. The number of sides is determined by simply multiplying the desired number of points by two. Lastly, the vertices of the polygon are projected onto the x-axis thereby distinguishing the precision points (Fig. 2.18). It's important to note that these points should be considered a first approximation. Optimization by iteration is often required to refine the expected output of the linkage when employing the graphical method.

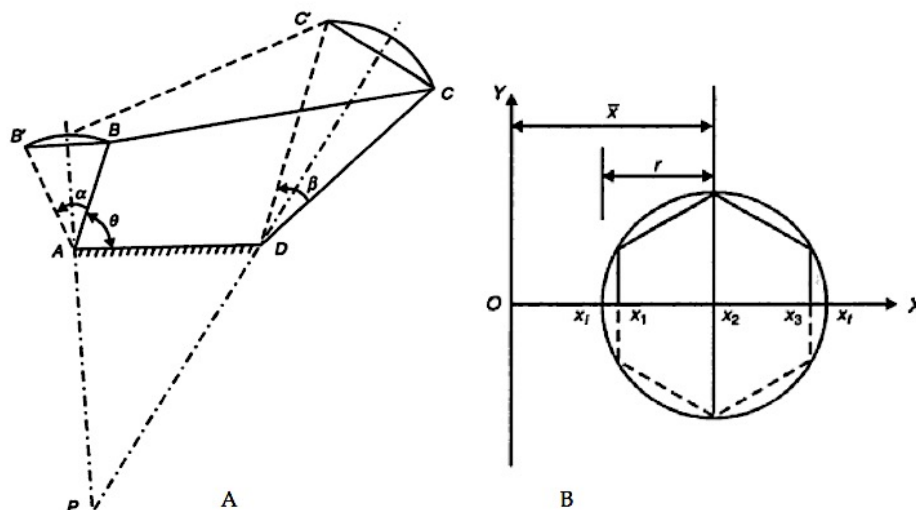


Figure 2.18. (A) Example of the relative pole method. (B) Example of a graphical approach to finding three precision points using Chebyshev spacing [45].

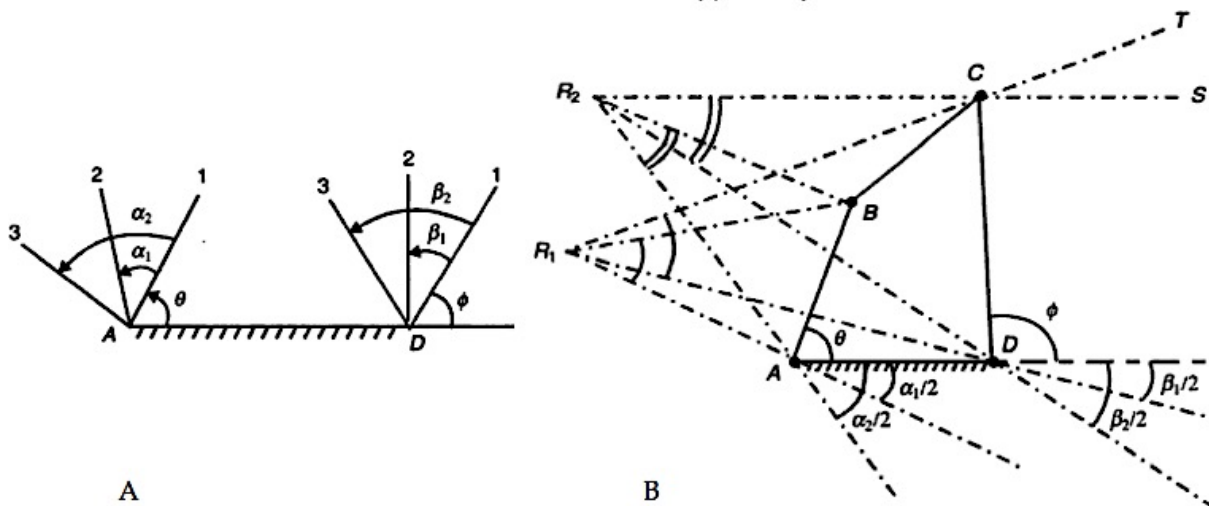


Figure 2.19. (A) Three known positions of the crank and follower. (B) The relative pole method used to determine one possible solution [45].

2.3.8. Analytical Method

The analytical approach produces the most accurate results but involves solving multiple sets of equations. Today this does not present the same challenges it did prior to the age of computers. Software programs like MATLAB have made such tasks easy to perform, thus the graphical method is quickly becoming obsolete. However, like the previous method, identification of precision points is a prerequisite to employing the analytical method. Similarly, an interval must be specified. However, the spacing is determined by the following equation:

$$x_j = \frac{1}{2}(x_i + x_f) - \frac{1}{2}(x_f - x_i) \cos \frac{\pi(2j - 1)}{2n}, \quad j = 1, 2, \dots, n \quad (2)$$

where j is the number of the precision point, n is the total number of points, x_i is the initial value of the interval, and x_f is the final value of the interval. The analytical approach to finding the Chebyshev spacing can be time saving and less prone to mathematical error when combined with a capable software program. Although three points have been the subject of this discussion, as previously mentioned it is not uncommon to include more points to increase accuracy. The analytical method can be less cumbersome in this situation than the process described to obtain the graphical representation.

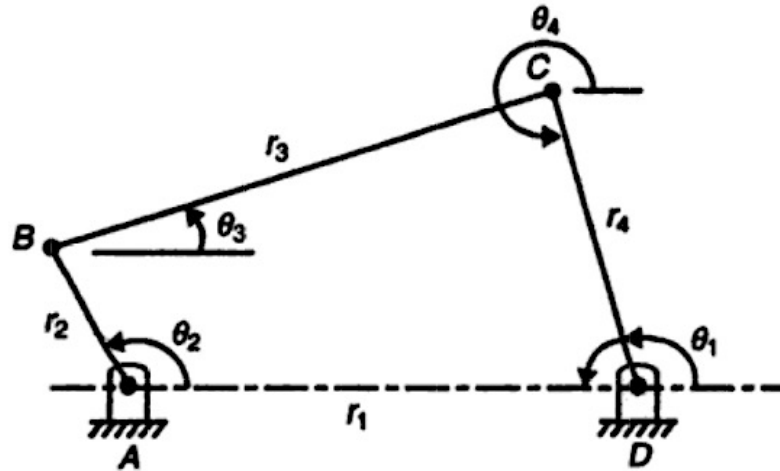


Figure 2.20. Four-bar mechanism to illustrate the concept of Freudenstein's equation [42].

The following is an example of one of the many available analytical methods. Note that the angles and links represented below are illustrated in (Fig. 2.20) above. The method highlighted here centers around Freudenstein's equation, Eq. (3):

$$K_1 \cos \theta_2 + K_2 \cos \theta_4 + K_3 = \cos (\theta_2 - \theta_4) \quad (3)$$

$$K_1 = \frac{r_1}{r_4} \quad (4)$$

$$K_2 = \frac{r_1}{r_2} \quad (5)$$

$$K_3 = \frac{r_3^2 - r_1^2 - r_2^2 - r_4^2}{2r_2 r_4} \quad (6)$$

where r_1 through r_4 are the individual link lengths. It can be seen that with three points provided by the use of Chebyshev spacing, three values for θ_2 and θ_4 are also known. Therefore Freudenstein's equation can be written three times in terms of the different theta values. Three equations and three unknowns allow for the solution of each individual K value. Setting r_1 equal to one, the link lengths can also be obtained [41], [42], [45], [47]. Changing the length of r_1 merely results in the rest of the link

lengths scaling accordingly. The combination of Chebyshev spacing and the Freudenstein equation result in an accurate and expedient (with the aid of software) solution to the function generation problem.

2.3.9. Summary

The four-bar mechanism is one of the most common and versatile linkages in use today. They can be found everywhere from vise-grips to buckets on heavy machinery. Although they are widely used, they do have their limitations. If a complex movement is needed, often time's links must be added (five and six bar mechanisms) to accommodate for the complexity of the task.

Four-bar mechanisms are simply a configuration of links and joints. Though there are many types of joints, they ultimately fall into two categories: lower and higher pairs (Sec. 2.3.3.) A planar four-bar mechanism employs the use of revolute joints. To determine the DOF of the output, Gruebler's equation can be used (Sec. 2.3.3). The motion of a four-bar mechanism can also be predicted through the use of Grashof's criteria (Sec. 2.3.5).

When a particular motion is desired and a device needs to be designed to perform it, the process is known as kinematic synthesis. Three categories form the first role of kinematic synthesis: type, number, and dimensional synthesis. The second function of synthesis is task related. The output of a mechanism can be defined by its task: function, path, or motion generation. Through application of synthesis and identification of task, graphical or analytical methods can be applied to determine the necessary configuration of the mechanism.

Regardless of the method used, precision points should be identified as a first approximation for a solution. This can be accomplished through the use of Chebyshev spacing either graphically or analytically. Link lengths and starting positions can be found graphically by identifying relative poles, a center of rotation relative to both the crank and follower (Sec. 2.3.7). Similarly, the same lengths and starting positions may be found through an analytical approach. By implementing Chebyshev spacing with the Freudenstein equation, accurate solutions can be found readily (Sec. 2.3.8). Before computers became common, the graphical method was the quickest way to solve linkage problems. With today's technology, the analytical method is actually faster and produces more accurate results.

2.4. BEARINGS

A bearing is a device that allows for relative motion between two objects. More importantly, the role of a bearing is to increase the efficiency of the movement through the reduction of friction. The earliest known bearing that illustrates this concept dates back to 3200 B.C., where wheels on carts were used to transport large stones in Mesopotamia. Other examples of early bearing technology can be found in Egypt, the Indus Valley, and China [48]. Centuries later the first bearing that used rolling elements (balls and rollers) was designed by Leonardo da Vinci [49], [50]. It wasn't until the industrial revolution however that advances in technology produced the modern form of the bearing and its resulting widespread use.

Bearings are capable of two types of motion, rotary or linear, which are achieved through contact and non-contact bearing types. Contact bearings like the name implies, operate through the mechanical contact of its elements. Rolling element bearings (e.g. balls or rollers) and flexure bearings (e.g. door hinge) are two forms of contact bearings used for rotary motion. Sliding bearings (e.g. dresser drawer) are a form of contact bearing that permits linear movement. Contact bearings are the most commonly used of the two types available.

Non-contact bearings allow for relative motion between two objects without the moving elements of the bearing contacting each other. This is achieved through the use of fluids or magnetic fields. The major advantage to these types of bearings is the lack of wear and fatigue experienced in contact bearings. Non-contact bearings are also quieter in operation and higher in mechanical efficiency due to extremely low friction between components. Magnetic bearings have the added benefit of being able to operate in a vacuum, however magnetic and fluid bearings are much more costly than their contacting counterparts.

Though there are many types of bearings in both the contact and non-contact variety, only two types are discussed here. This is done in part for the sake of brevity, but is also a direct effect of the application involved (Sec. 3.1). Therefore the following sections focus on the features, functions, and other design considerations applicable to bearing selection. The two subjects of interest are deep groove ball bearings and tapered roller bearings. For more information on other types of bearings see [40], [51]–[53].

2.4.1. Deep Groove Ball Bearings

Deep groove ball bearings are the most widely used bearing type available. This is due to the simplicity in design, low cost, and versatile nature of the bearing itself. They perform well at high speeds, operate quietly, can handle combined loading, and require minimal maintenance [54]. Deep groove ball bearings consist of four main parts: the inner and outer races, balls, and the cage or separator (Fig. 2.21). They come pre-lubricated with the option to offer protection from external elements like dirt and debris through the use of seals or shields.

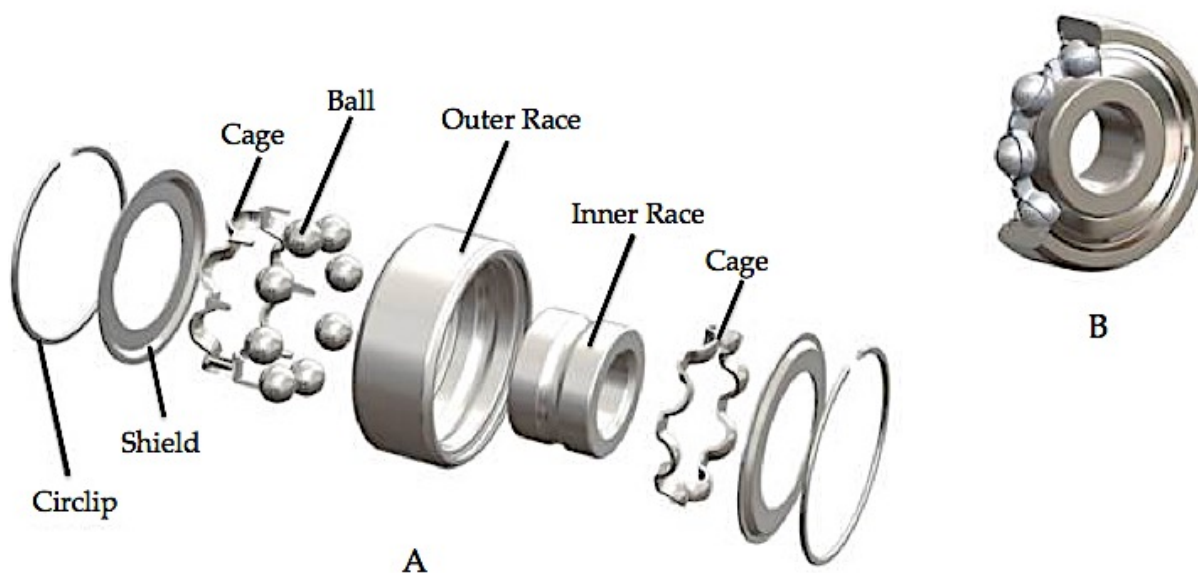


Figure 2.21. (A) Exploded view of a ball bearing, including shields and retaining circlips. (B) Section view of the ball bearing assembly [55].

2.4.2. Tapered Roller Bearings

Henry Timken invented tapered roller bearings in 1898. They were designed to address the complexity of heavy machinery design, specifically railroad axle bearing supports. Since their inception, they've become a popular choice in agriculture, mining, and construction equipment. Tapered bearings also consist of four main parts: the cup (outer race), cone (inner race), rollers, and cages. Like ball bearings, tapered bearings can also be outfitted with shields and seals. What makes tapered bearings unique is their contact angle. The cup, cone, and rollers form a "tapered" or conical assembly. Lines drawn from the center of the rollers to the centerline of the bearing all converge at a singular point (Fig. 2.22). This feature in combination with the larger surface area of the rollers is what allows tapered

bearings to have a much higher load capacity (and cost) than ball bearings of the same dimension. However, due to the contact angle, every radial load experienced by the bearing also results in an axial load. Therefore tapered bearings are usually used in pairs, which allow for radial, axial, and moment loading to be supported.

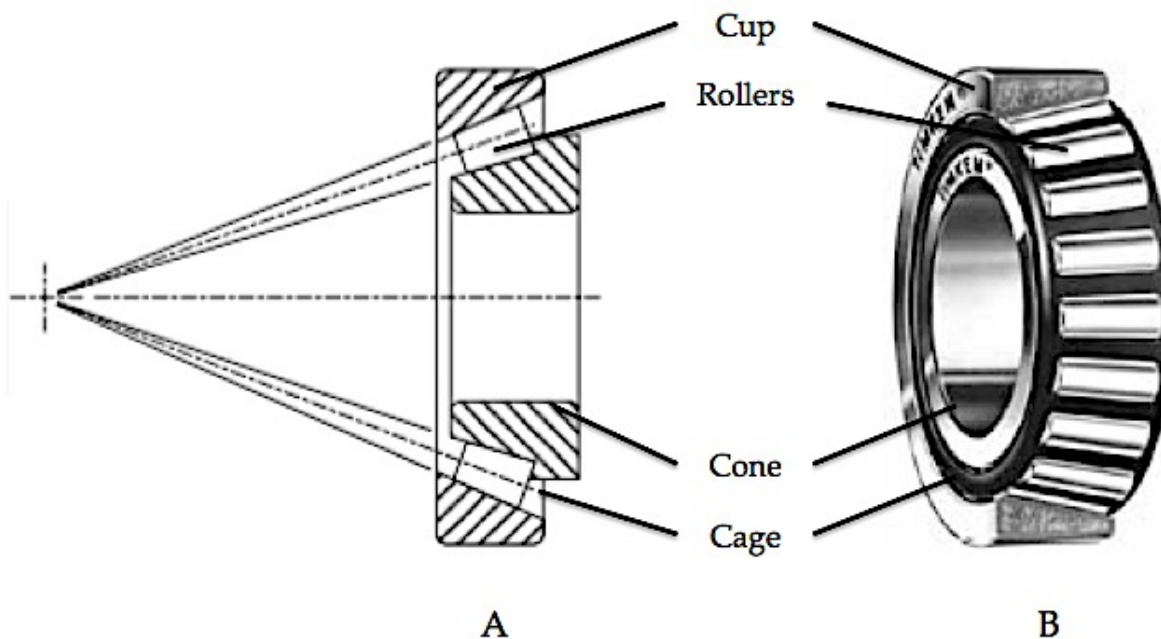


Figure 2.22. (A) Diagram of roller centerlines converging at a singular point on the bearing axis [40]. (B) Section view of a tapered bearing assembly [56].

2.4.3. Internal Clearance

The space between rollers or balls and their races either radially or axially are known as internal clearances (Fig. 2.23). These clearances can be increased or decreased based on the “fit” provided by the manufacturer. Some fits are identified by descriptions such as loose, normal, and tight. Precision bearings are classified by ABEC ratings odd numbered from one to thirteen. In this system one is the lowest tolerance fit while thirteen is the highest tolerance fit. Typically, higher tolerances produce more efficient bearings with greater speed capabilities.

Internal clearance is an important factor to consider in the selection of bearings. Depending on the application, internal clearance can be a benefit or a detriment. In some cases endplay caused by excessive clearance may be inconsequential to the overall performance of the device. Perhaps radial clearance is needed due to thermal expansion effects at normal operating temperatures. If

precise rotation and positional accuracy are required, radial or axial clearance may need to be at a minimum or effectively zero. It should be noted that axial clearance is a function of radial clearance and is often five to ten times greater than the radial clearance. When little to no play is a requirement for the application, or protection from impact is a concern, the common practice is to preload the bearings.

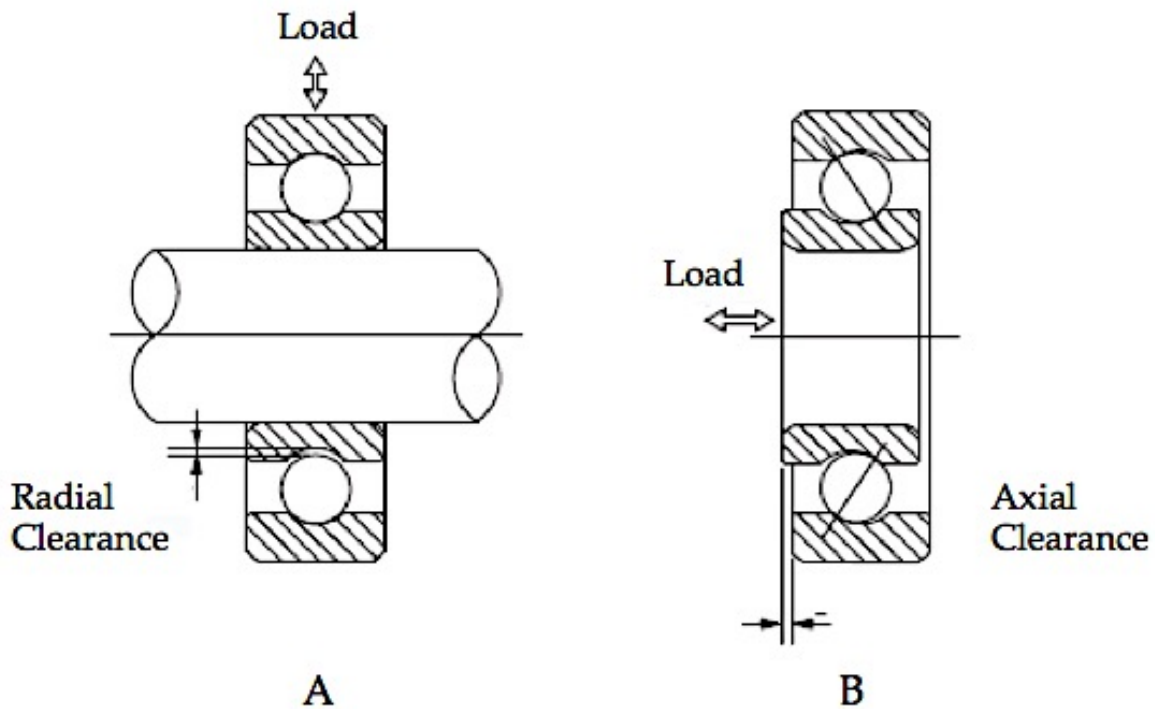


Figure 2.23. (A) Illustration of radial clearance in a ball bearing. (B) Illustration of axial clearance in a ball bearing. The same principles shown here for ball bearings apply to roller bearings [53].

2.4.4. Preload

The application of a preload to bearings offers many advantages. The stiffness of the bearing is improved, vibration and noise reduced, fatigue life increased, and damage due to shock or impact is lessened. Typically a slightly negative preload is desired for optimal bearing performance. The term negative in this situation means the balls or rollers and their respective races are in compressive contact. The compressive force is enough that the rolling elements elastically deform. This effectively reduces skidding of the rolling elements and enables more of the elements to share the load experienced by the bearing. Caution must be taken in how much preload is applied. The force applied by preloading is synonymous with the axial displacement of the inner race relative to the outer race. Small

displacements can result in very large forces on the components of the bearing. It is for this reason that care must be taken to avoid excessive negative preload, which can result in premature bearing damage and diminished fatigue life. However the converse of this situation is also true. Insufficient preload (positive) is defined by excessive clearance of the bearing components. This condition can also lead to decreased fatigue life due to fretting and vibration (Fig. 2.24).

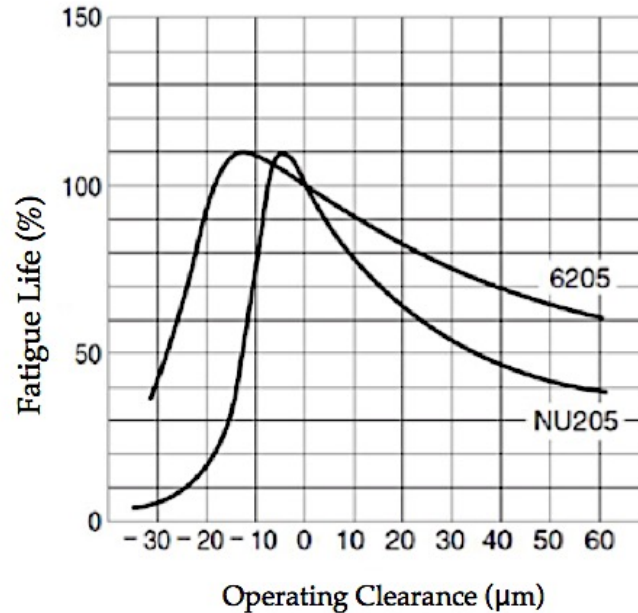


Figure 2.24. Effect of preloading on the fatigue life of two different bearings [57].

Preload is accomplished by two methods: *position* and *constant pressure* preload. Position preload is also known as solid preload. The outer races of two bearings are fixed at a certain distance while the inner races are axially displaced (Fig. 2.25). Precisely machined spacers dictate the amount of displacement. Often times additional shims are needed to adjust the spacing to its final dimension. The inner races are then held in place by a nut or other fastener. The advantage of this method is the high rigidity it imparts to the bearings. Usually the design is straightforward and the setup uses minimum space. One drawback to this design is the effect of thermal expansion. Since the locations of the bearings are fixed, thermal expansion can affect the force of the preload due to variations in temperature between inner and outer races. Therefore use of the position method is typically reserved for lower RPM applications.

A subcategory of the position method is the use of duplex bearings. Duplex bearings are precision ground bearings that come in pairs from the manufacturer. These bearings are placed next to each other and clamped or forced together by a nut or other fastener. Like the previously mentioned example, the outer races are held captive while the inner races are displaced by the clamping mechanism. However, spacers are not used as the precision ground inner races serve as the spacers. Tightening the nut until the inner races are securely clamped together fixes the preload. Though duplex bearings are a convenient choice they are also more expensive than standard bearings. An additional drawback due to their matched design is that if one fails both must be replaced.

The second method for preloading is known as constant pressure or spring preloading. Instead of using a spacer to fix axial displacement, a spring is used to apply a force to one of the races (Fig. 2.25). The resulting displacement due to the spring determines the amount of preload. This method is more forgiving than the position method as the precision-machined spacers are absent from the design. The use of springs (Belleville, spring washers, coil springs, etc.) also accommodates thermal expansion. Therefore the constant pressure method is well suited for higher speed applications. However, the constant pressure method does not perform well against impacts or higher torque applications. The space required to house the springs can also be a detriment in circumstances where room to operate is minimal.

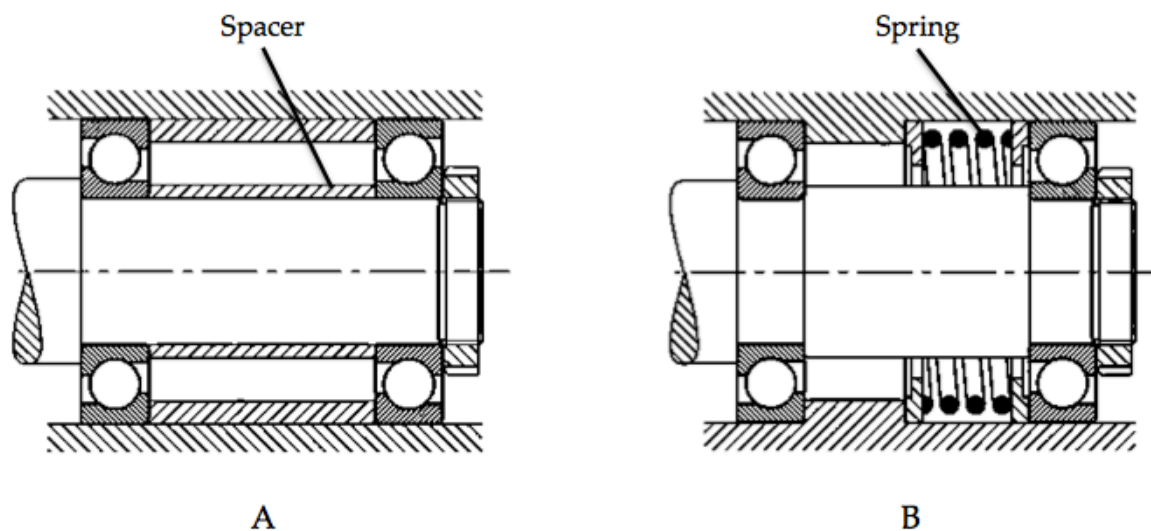


Figure 2.25. (A) Position preloading using machined spacers to dictate axial displacement of inner race. (B) Constant pressure preloading utilizing a spring to dictate axial displacement of outer race [52].

2.4.5. Summary

Bearings allow for relative motion between two moving objects. The first known use of bearings occurred in Mesopotamia in 3200 B.C. But it was the industrial revolution and the technological advances therein that produced the modern form of the bearing. Bearings are only capable of two motions, rotary and linear. Although many varieties of bearings exist, two categories, contact and non-contact bearing types encompass all of them.

This document discusses two types of contact bearings, deep groove ball bearings and tapered roller bearings. Both types can be used in pairs to support radial, axial, and moment loading. Deep groove ball bearings are the most common bearings used, are simple in design, and low in cost. Tapered roller bearings form a conical line of action from the center of the rollers to the axis of rotation of the bearing. This allows tapered bearings to support much larger loads than similar sized ball bearings. However, with increased load capacity comes increased cost.

Reducing vibration, noise, and improving fatigue life can all be accomplished by preloading bearings. Two main methods are used for preloading, position and constant pressure preloading. The position method utilizes precision ground spacers and fixes the location of both the inner and outer races. This provides improved rigidity, longer fatigue life, protection from impact or shock loading, and greatly reduced rotational position error. Due to the fixed positions, thermal expansion can be a problem if not properly accounted for, making position preloading ideal for lower-speed high-torque applications. Constant pressure preloading uses springs in place of spacers and is more forgiving of misalignments and thermal expansion. The use of springs often requires more space than the position method. The constant pressure method is less rigid and less tolerant to shock loading as well, making it ideal for lower-load higher-speed applications.

2.5. GRAVITY EQUILIBRIUM

The concept of statically balancing a mechanism against gravity is not new. One of the oldest examples is from ancient Greece (Fig. 2.26). A device called the *mechane* was used to “fly in” or transport actors to center stage from behind set scenery [58]. The *mechane* operated on the principle of a counterweight. The idea is simple; a mass at the end of a rotating beam is balanced by a counterweight at the

opposing end of the beam. Therefore no matter what position the mass assumes spatially, the potential energy is transferred to the counterweight and vice versa resulting in a state of constant potential energy. Though this method is simple in design and execution, one of the disadvantages to using it is the space needed for it to function and the inertia added to the system. This is especially problematic in fields like rehabilitation robotics where overall mass of the system is purposely kept to a minimum.

Another method to achieve static equilibrium is through the use of springs. In 1932 LaCoste created a zero-length spring to be used in a gravity meter [59]. The meter was so sensitive it was often used to find oil, as the instrument could measure the local gravity change due to underground oil fields. A second example that used zero-length springs can be found in the 1935 Anglepoise 1227 lamp (Fig. 2.26) designed by George Carwardine [58], [60]. The concept of using springs to statically balance mechanisms is an attractive option due to the low inertial effects of the springs and the minor space they occupy. It is for these reasons that the remaining discussion on gravity equilibrium will be confined to their use.

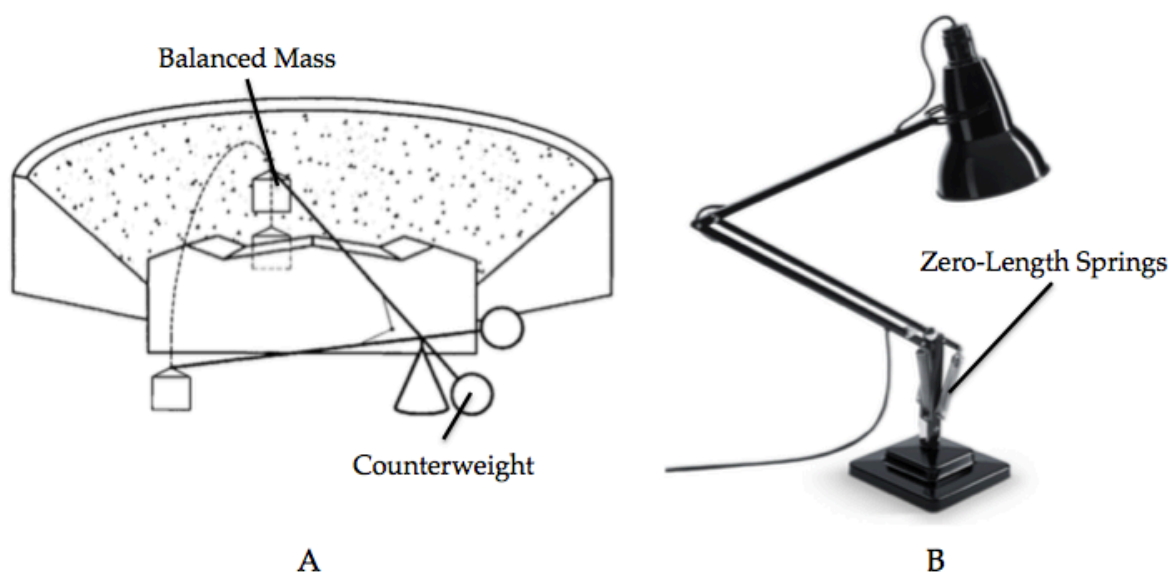


Figure 2.26. (A) The mechane, an example of statically balancing a mass by using a counterweight [58]. (B) The Anglepoise lamp, statically balanced by zero-length springs [60].

2.5.1. Zero-Free-Length Spring

Theoretically, if a force vs. length line were constructed for a zero-free-length spring it would cross at the origin. Physically this means that the spring would exert zero force if it had zero-free-length. This situation is impossible due to the fact that

no physical spring can actually contract to zero-free-length, at some point the coils touch and the spring can no longer shorten. However, the force-length relationship previously described *is* possible. If when winding a helical spring an additional twist is introduced into the wire it will effectively result in extra tension within the spring. The three scenarios illustrated in (Fig. 2.27) show the effects of this technique and their resulting force vs. length characteristics. Note the demarcation of L_0 (initial or resting length of the spring) and ℓ_0 (free length of the spring). The use of F_0 is to define the initial tension in the spring, or the force that is necessary to first initiate separation of the coils.

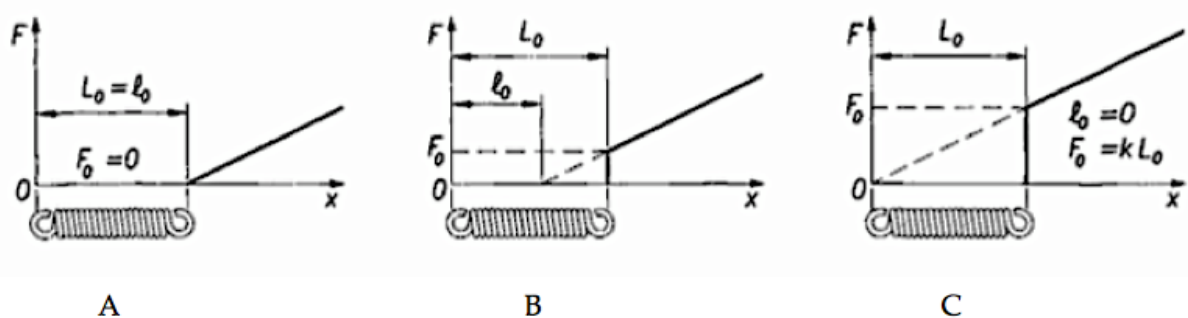


Figure 2.27. (A) Extension spring with no initial tension, thus initial length and free length are equal and the force-length line is far from the origin. (B) Extension spring with some initial tension, free length becomes less than the initial length and the force-length line moves closer to the origin. (C) Extension spring with sufficient tension so that the free length is zero and the force-length line intersects the origin. Therefore this case exemplifies the zero-free-length spring concept [58].

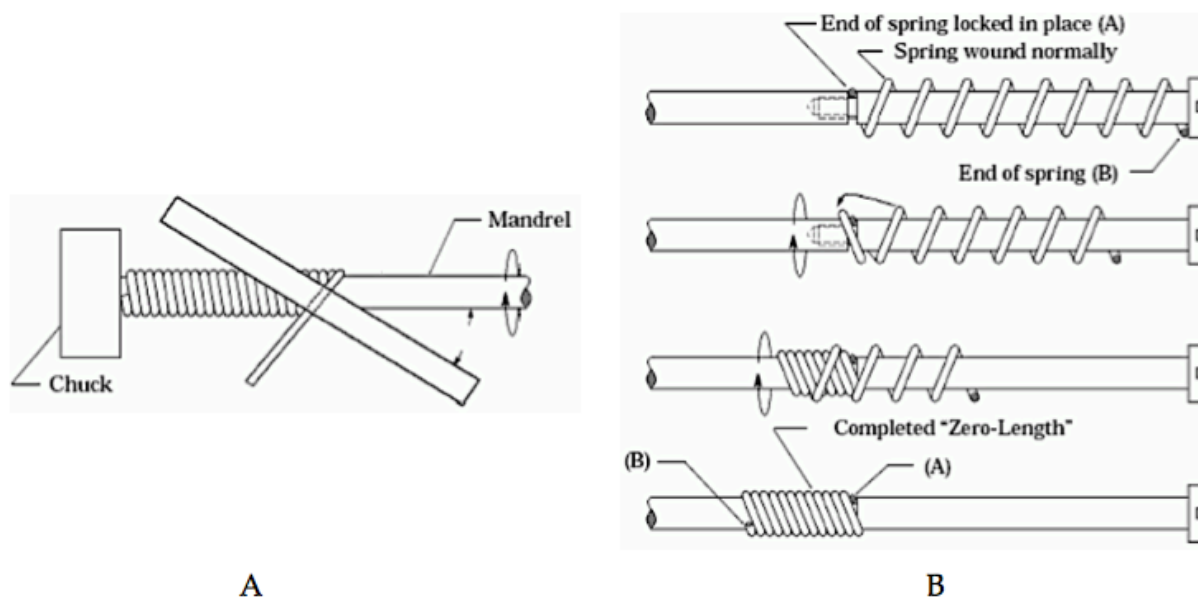


Figure 2.28. (A) LaCoste method for creating a zero-free-length spring, introducing a twist in the wire as it is coiled. (B) Alternative method that is known as "turning the spring inside out" [59].

It can be clearly seen in (Fig. 2.27) how the concept of a zero-free-length spring can be realized through the introduction of pre-tension during the coiling process. LaCoste developed his own method to accomplish this task (Fig. 2.28). In his first attempts, the coils of the springs pressed so hard against each other that the spring was actually a “negative length” spring. This presents no problem however, as a piece of straight wire can be added to the spring to precisely adjust it to a zero-free-length state [59]. Through the use of a zero-free-length spring, exact gravity equilibrium can be achieved. LaCoste utilized this feature to construct his gravity meter mentioned previously.

2.5.2. Basic Gravity Equilibrator

The fundamental or “basic” gravity equilibrator is a mechanism constructed of a rotating beam with a mass at the end that is balanced by a zero-free-length spring (Fig. 2.29). An important point to consider is the quasi-static nature of the system. That is to say, in order for equilibrium to exist, the total potential energy of the system U_p must equal the sum of the spring (U_s) and mass (U_m) potential energy [61], [62]. The mathematical representation of this fact is shown below:

$$U_p = U_m + U_s \quad (7)$$

$$U_m = mgl\cos(\varphi) \quad (8)$$

$$U_s = \frac{1}{2}k(a^2 + r^2 - 2ar\cos(\varphi)) \quad (9)$$

where m is the mass, g is gravity, l is the length of the pivot arm, φ is the rotation angle, a is the vertical distance between the pivot and the spring attachment, r is the distance between the pivot and the spring attachment on the pivot arm, and k is the spring constant. For equilibrium, the potential energy must be at a local minimum:

$$\frac{\partial U_p}{\partial \varphi} = -mgl\sin(\varphi) + akrs\sin(\varphi) = 0 \quad (10)$$

Therefore from the result of differentiation, it can be seen that equilibrium is independent of φ , thus static balance is achieved at any position provided the following relationship holds:

$$mgl = akr \quad (11)$$

Careful observation of this last equation shows that by varying a , k , r , or l , different masses can be statically balanced. This point is further discussed in (Sec. 2.5.4).

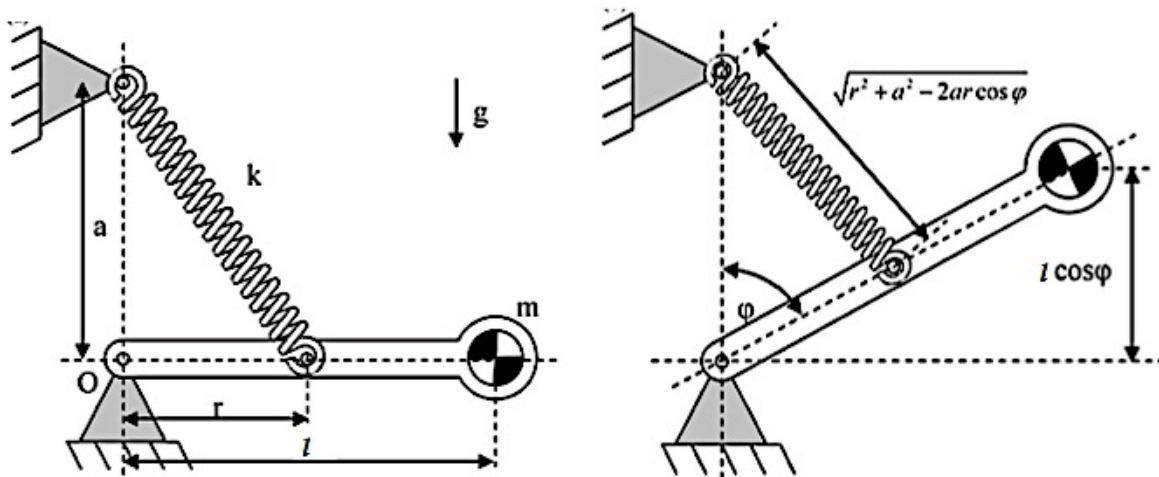


Figure 2.29. Basic gravity equilibrator in perfect static balance through the use of a zero-free-length spring. In this arrangement the total potential energy is constant and the parameters of a , r , k , and l determine the mass that can be balanced [61].

2.5.3. Achieving Equilibrium Using Normal Springs

Thus far the discussion of static equilibrium has only involved zero-free-length springs. Zero-free-length springs are not readily available to purchase, and manufacturing them independently is time consuming and doesn't always yield good results. An alternative approach is through the use of "normal" springs, or in other words, standard helical extension springs that can be purchased off the shelf. By modifying the application of the spring, zero-free-length spring behavior can be emulated through the use of normal springs. One such application is through the use of a pulley and string arrangement whereby the string starts accumulating force as it leaves the pulley. The free length of the spring is considered to be "stored" behind the pulley. Yet another option is to use a guiding element to direct the force of the spring while storing the free length behind the guide (Fig. 2.30).

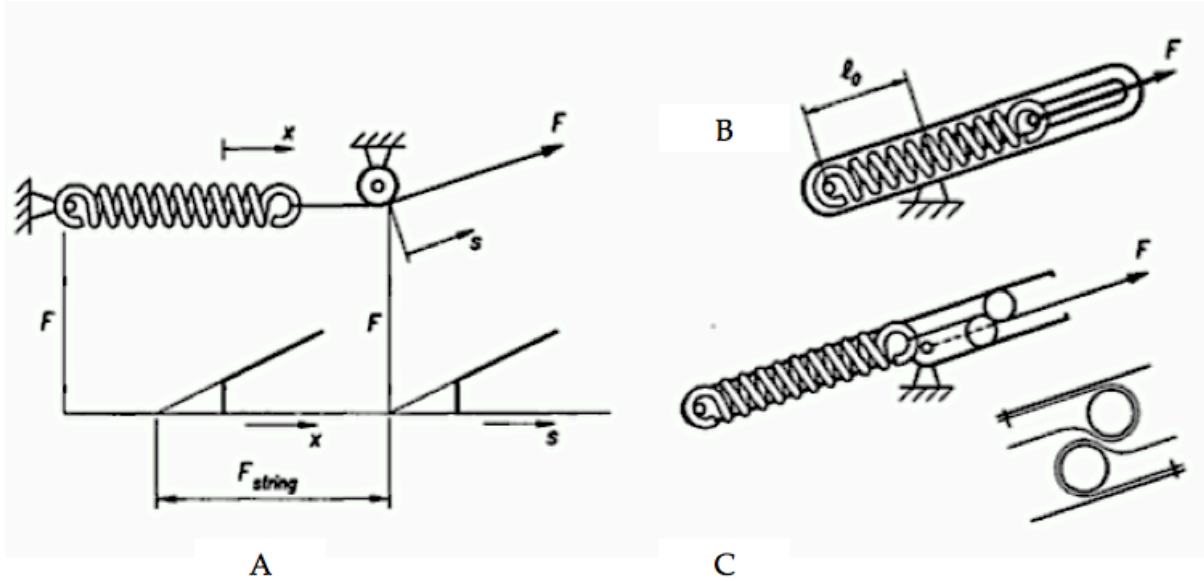


Figure 2.30. Emulation of a zero-free-length spring. (A) Pulley and string arrangement. (B) Guiding arrangement where the free length of the spring is stored behind the pivot. (C) Free length of the spring is stored behind the pivot and guided by a roller configuration [58].

The pulley and string arrangement shown in (Fig. 2.30) is a convenient solution using normal springs. The other two options illustrated typically operate with more friction loss due to the guides and are less stable than the pulley configuration. However, use of a single pulley introduces error due to the wrapping of the string about the pulley itself. To counteract this effect, an additional pulley can be used which effectively cancels the error introduced by a singular pulley.

The efficacy of the pulley and string arrangements shown in (Fig. 2.31) is based on the principle that they are an equivalent replacement for a zero-free-length spring. Thus perfect balance can be achieved using normal springs. Notably, the amount of string wrapped around the pulleys remains constant throughout the operation of the device. The only variable that changes during movement is the string length between points A and P shown in (Fig. 2.31). Thus the spring elongation is equal to the distance between points A and P. Consequently; it is critical to select the proper string length to obtain perfect balance:

$$L_s = a + r + 2\pi R - \ell_0 \quad (12)$$

where L_s is the required string length, R is the radius of the pulley, and ℓ_0 is the non-zero free length of the normal spring.

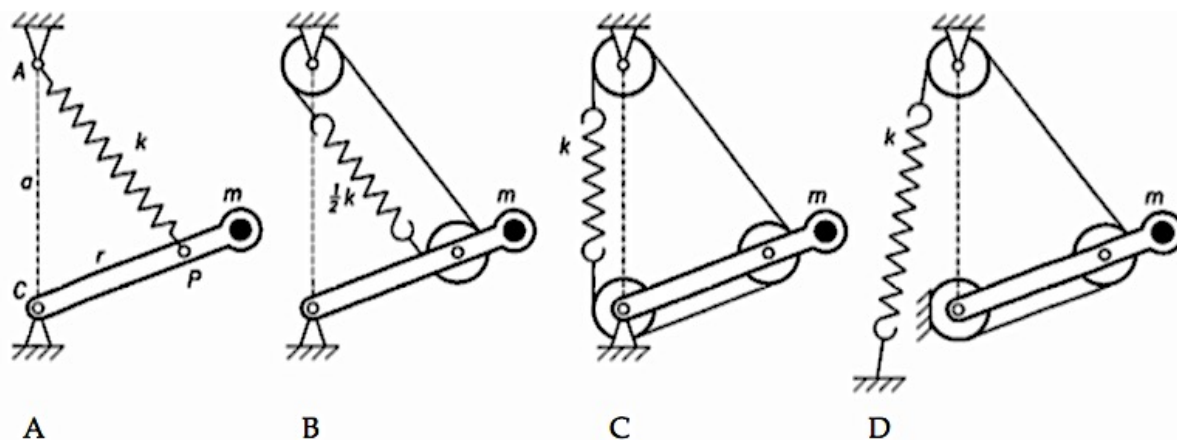


Figure 2.31. (A) Basic gravity equilibrator using a zero-free-length spring. (B) Two-pulley arrangement. (C) Three-pulley arrangement. (D) Three-pulley arrangement with spring fixed to ground. Illustration (D) is the most forgiving of the arrangements in regards to spring length [58].

2.5.4. Adjustment of Gravity Equilibrators

The ability to adjust gravity equilibrators in an efficient way is pinnacle when a system is subjected to varying payloads. Generally adjustment requires a change in spring stiffness that involves external energy applied to the system. Since the nature of static equilibrium is to maintain constant potential energy (i.e. maintain its position without the aid of external energy) it follows that an energy-free (i.e. the total energy of the system is unchanged) method of adjustment should be developed. There are in fact several such methods that have been established, four of which will be briefly discussed in the remainder of this section.

The first energy-free adjustment approach to review is known as the *simultaneous displacement* method [63]. As mentioned in (Sec. 2.5.2), the variables a , r , k , and l can all be varied to accommodate for a change in payload. By simultaneously displacing the a and r locations, the spring length remains unaffected while the product (ar) is modified. The difference in ar effectively adjusts for the change in load. The general process is illustrated in (Fig.2.32). Note the use of a two-pulley arrangement to emulate the function of a zero-free-length spring. The handle H is used to adjust the length of r , which by way of link CD simultaneously adjusts length a . As the handle H is adjusted, point A slides along its track while point C is repositioned. This ensures that the spring length remains unaltered, allowing only the distances a and r to be modified. Once the new desired location is reached, points P and Q serve to “lock” the mechanism in place and normal operation can proceed.

The advantage to the virtual spring approach is apparent in its application to the length of a . Similar to the simultaneous displacement method, the length of a is manipulated to adapt to a changing payload. The difference in the methods lies in the execution. Here a is changed due to the repositioning of connection points A and C (Fig. 2.33). This action is accomplished through the use of a pantograph, a four-bar mechanism (Sec. 2.3) that when adjusted changes not only the length of a but also the length of the virtual spring due to the relocation of the two substitute springs. Like the simultaneous displacement method, the points A and C must be “locked” into place once correctly positioned.

A third method of adjustment is known as spring-to-spring or *storage spring* balancing. The main principle in this method is the concept of trading energy between two springs. Thus one spring stores energy when a payload is decreased, and likewise shares energy when it is increased [65]. A simple illustration of this concept can be seen in (Fig. 2.34). The spring that spans the parallelogram is the storage spring. Therefore when the payload is increased the storage spring gives energy to the primary spring by way of adjusting the length of a . In the example shown in (Fig. 2.34) this requires that a gets longer which in turn decreases the length of the storage spring thereby providing more energy to the primary spring. This adjustment method like the ones previously described requires that a connection point (point B) can be repositioned. Once the system is rebalanced, point B is locked in place and normal operation can commence.

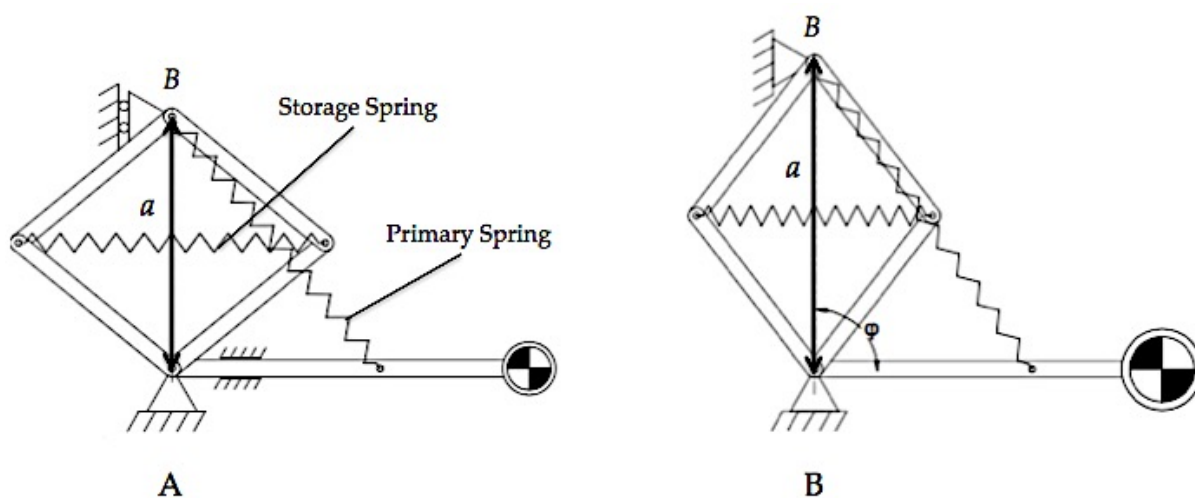


Figure 2.34. (A) Original configuration of a parallelogram in static equilibrium. (B) New configuration adjusted to account for a larger payload. The length of a must increase to allow for the storage spring to impart energy to the primary spring [65].

The final approach to energy-free adjustment involves manipulation of the spring constant and is therefore known as the K-type method [61]. Unlike the previously mentioned techniques, adjustment is possible without having to reposition connection points. Thus this approach has the potential to be the most compact and user-friendly of the four methods explored. The basis of K-type adjustment involves controlling the number of “active” coils in the spring. The effect of active coils in relation to the spring constant is expressed mathematically as:

$$K_s = \frac{Gd^4}{8nD^3} \quad (13)$$

where K_s is the spring constant, G is the shear modulus of the spring material, d is the wire diameter, n is the number of active coils, and D is the mean diameter of the spring. By using Eq. (11) in combination with Eq. (13) it can be seen that solving for n is straightforward. Thus the K-type method presents a direct means for adjusting mechanisms to changing payloads.

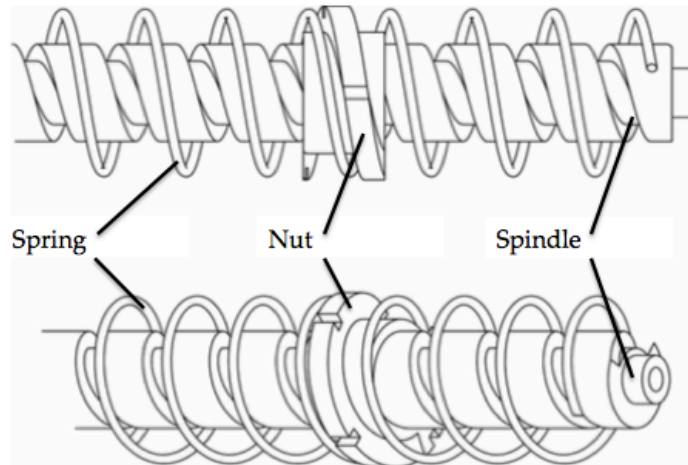


Figure 2.35. Prototype for adjusting number of active coils using the K-type method [61]. A specially designed spindle is placed inside the spring that allows a nut to traverse the coils. The position of the nut dictates the number of active coils.

Many options are available to isolate/captivate coils of a spring. The device shown in (Fig. 2.35) is a prototype currently being developed [61]. A spindle is carefully machined so that its pitch matches the spring in which it is inserted. A specially designed nut is placed on the spindle giving it the ability to traverse the

spring between its coils. The position of the nut determines the number of coils that are active. In this way, greater payloads can be balanced by moving the nut down the spindle, and lesser loads by moving up. It follows then that the range of payloads tolerated by the mechanism is determined by the spring used. That is to say that the capacity of the load is a function of the original spring constant and the number of coils it possesses.

2.5.5. Summary

The concept of gravity compensation dates back to ancient Greece when a device known as the mechane was used to fly in actors from behind stage scenery. This form of gravity compensation uses a counterweight to achieve equilibrium. The focus of this section has been on the use of spring-based mechanisms. One of the first devices that achieved static equilibrium through the use of springs was the gravity meter created in 1932 by LaCoste. LaCoste utilized a zero-free-length spring, which was critical to the success of his invention.

Creating a true zero-free-length spring is an impossible endeavor, as no physical spring can actually contract to a zero length. However, zero-free-length spring behavior can be achieved by introducing pretension into a spring when coiling it (Fig. 2.28). LaCoste and others have been successful in developing techniques to achieve this end. Yet the difficulty with using zero-free-length springs in design is that they are not readily available for purchase. It is for this reason that methods have been developed to effectively emulate zero-free-length springs through the use of normal springs.

A number of systems have been created that successfully mimic the behavior of zero-free-length springs by way of using normal springs (Sec. 2.5.3). One of the more prominent methods is through the implementation of pulley and string arrangements. It has been found that more than one pulley is necessary to eliminate wrapping error introduced by the pulley itself. Of the pulley arrangements devised, a three-pulley system with a spring fixed to an external anchor point allows for the most freedom in spring length (Fig. 2.31).

An important concern in the design of energy-free systems is the ability to adjust the system to accommodate changing payloads. Though several methods exist, this document explores the use of four main types: simultaneous

displacement, virtual spring, storage spring, and K-type methods. The K-type approach is the only one of the four that achieves adjustment without modification to the a and/or r parameters. This feature makes the K-type method an attractive option due to its low space requirements and ease of execution. It can be further stated that the K-type method seems especially well suited for a pulley and string arrangement.

3. DESIGN OF A 2-DOF SCAPULOHUMERAL RHYTHM DEVICE

One of the principal challenges in exoskeleton design is anthropomorphic alignment of joint axes. Exoskeletons are fundamentally orthotics, external devices aimed at rehabilitation, strength augmentation, impairment assessment, etc. However the efficacy of these tasks is diminished if the robot and user are misaligned. Issues ranging from unwanted forces exerted on the patient or instrument, to corrupted data resulting from inaccurate positioning can occur simply due to poor alignment. As a response to this concern, current exoskeleton designs are beginning to incorporate features that either accommodate slight misalignments, or attempt to eliminate them entirely.

A central goal of BLUE SABINO is the addition of a device to provide scapulothoracic motion. Full glenohumeral ROM cannot be achieved by a shoulder modeled simply as a ball and socket. Furthermore, natural movement of the shoulder girdle and subsequent quality of rehabilitation are intrinsically linked to the functional capabilities of the device itself. Hence, the inclusion of a mechanism that contributes to the full ROM of the shoulder complex is not only critical for therapy-based performance, but also significant data acquisition. What follows is the design, verification, and discussion of a novel two-DOF shoulder mechanism aimed at precisely this purpose.

3.1. DESIGN CONSIDERATIONS

Every journey begins with a first step, a platitude that summarizes the start of the design process well. Identifying constraints is one approach at taking the first “step”. Since BLUE SABINO is a result of years of prior research and discovery, there are several natural constraints that present themselves immediately. For instance, the EXO-UL8 is heavy with large links and actuators. This results in significant inertia, problematic when combined with acceleration. Sudden starts and stops are hard to accomplish if the mass intends to keep moving. This can potentially lead to unwanted dynamics such as overshoot. A large mass that is driven with a strong motor becomes a safety concern when combined with human interaction. These are but a few reasons that logically lead to the first constraint: BLUE SABINO must be lighter than its predecessors.

The second constraint is an extension of the first, if the new exoskeleton is lighter, then it follows that the actuators should be smaller. The largest actuators on the EXO-UL8 (SHA-32) have a mass of 6.2 Kg [38]. To put this in perspective, the entire mass of a 95th percentile male arm is 6 Kg [66]. Consequently, it is evident that the current actuators are too large. Furthermore, these actuators are capable of a peak torque of 433 N-m. Though other designs vary in weight and size, lighter systems like the EXO-UL7 and HARMONY report peak torques of 30 N-m at the shoulder [17], [25]. More robust models like the MGA and MEDARM report peak torques of 137 N-m and 91 N-m respectively [20], [24]. The BLUE SABINO is projected to be comparable to the MGA or MEDARM, thus a similar torque range is a logical assumption.

Rigidity is the third item of concern within the design criteria. The tip of the end effector will be approximately one meter from the base link. A small deflection at the base link results in a large deflection at the end effector. The scapulohumeral device will serve as the base link, a topic discussed in (Sec. 3.2), further highlighting the need for rigidity. It's important to recognize that rigidity is a function of component geometry and the modulus of elasticity associated with the material used to create it. Thus attention must be paid to both of these aspects. As such, rigidity is to be tightly controlled within the confines of this design.

Determination of a meaningful metric for defining a rigidity constraint within the design was challenging. Eventually, a maximum deflection of two millimeters at the end effector due to deformation of the scapulohumeral device was deemed an appropriate constraint. This value was arrived at in the following manner; first, a total deflection of ten millimeters at the end effector was imposed for the entire exoskeleton. The magnitude of which is a combination of the exoskeleton and 95th percentile male arm weight. Additionally, a 2.5 Kg mass clutched in the patient's hand is included to serve as a working payload during ADLs. Finally, the entirety of the system is subjected to the maximum design acceleration (Sec. 3.2.6). Including all of these factors provides a conservative "worst-case" loading condition as BLUE SABINO will weigh less than the EXO-UL8. By applying these criteria, the maximum allowable deflection for each sub-assembly can be determined (Ch. 4), providing confidence in the design.

Since the scapulohumeral device will serve as the base link, it will contribute the greatest deviation of any component in the serial chain toward the end effector. Thereby it follows that the device should be the most rigid component. It was determined that no more than 20% of the ten-millimeter allowance should be allotted to this one device alone. Consequently, the two-millimeter constraint was imposed. This restriction primarily focuses on the sub-assemblies rather than the individual components that comprise them. This is due in part to the synergy between components (Ch. 5) and the location of attachment between the scapulohumeral device and the rest of the exoskeleton. Therefore an emphasis on strength is applied to individual components (Ch. 4) while a focus on rigidity is applied to sub-assemblies.

With the exception of rigidity, the aforementioned criteria pertain to BLUE SABINO as a whole. That being said, the focus now turns toward the scapulohumeral device itself, new territory that is accompanied by a host of unknowns. The first of which is identifying the motion to emulate, scapular or clavicular? As discussed in (Sec. 2.1.5), scapulohumeral rhythm is extremely complex, without definitive agreement upon the exact ratio of glenohumeral to scapular motion. Consequently, the notion of modeling its movement is difficult at best. Alternatively, the motion of the clavicle relative to the glenohumeral joint is better understood and more straightforward with respect to modeling. Furthermore, the clavicle represents the only attachment of the shoulder girdle to the axiskeleton, resulting in a natural reference point. It is for these reasons that the clavicle and its motion form the basis of the design that is developed here.

In summary, several design constraints have been presented here. BLUE SABINO is the successor to the EXO-UL8, and as such will borrow much of its mechanical design. However, several key constraints have been identified. First, a reduction in structure and actuator mass has been deemed necessary. Secondly, a focus on rigidity has been implemented with a maximum deflection of two millimeters at the end effector established. Lastly, the design of the scapulohumeral mechanism must not compromise the aforementioned constraints. Moreover, a clavicular approach has been selected as the input to the design. The sections that follow implement these constraints and discuss the development of the scapulohumeral device in its entirety.

3.1.1. Using Clavicular Motion to Model Scapulohumeral Rhythm

As previously discussed, the driving input to the design of the scapulohumeral device is based upon clavicular motion. Scapular motion is hard to quantify, however its importance to glenohumeral motion is well understood. Since the scapulothoracic joint is not an actual joint (Sec. 2.1.4), it follows that the motion of other joints can induce its motion. When considering the shoulder complex it becomes apparent that it is a kinematic chain. Thus, if one link in the chain is perturbed then the other links are consequently affected. It is this synergy of the joints that can be capitalized upon.

Spatially, scapulohumeral rhythm assists the shoulder in elevation, depression, protraction, and retraction. It's important to understand that the human shoulder has redundancy built into its natural design. Each of the four joints is capable of three DOFs, even though the total motion of the shoulder can be emulated by five total DOFs. Three dedicated DOFs already exist for BLUE SABINO to account for glenohumeral motion. Therefore by the addition of this two-DOF device and a control algorithm capable of synchronizing clavicle and glenohumeral motion, total ROM is achievable. This assumption comes with the caveat that the clavicle can be used as the basis to the previously described movements.

The clavicle attaches to the acromioclavicular joint at its distal end, and is anchored to the axiskeleton via its proximal end at the manubrium. If a mechanical link possessing the same length as a given clavicle is externally placed at the same location, then presumably it would move along the same arcs as the clavicle. This of course implies that the centers of rotation are aligned and that the link is capable of two-DOF movement (e.g. a u-joint). The opposing end of the link could be attached to a spherical joint and the result would be a five-DOF shoulder, capable of full ROM. But is it really that simple? What happens if one user is a tall male and another user is a short female? How is proper alignment achieved? Where is the device placed in relation to the patient? How do the rotations affect the links downstream of the device? These are but a few of the questions that immediately surface when considering the abovementioned situation.

First, consider the issue of a fixed link length. Surely the link needs to be adjustable, right? Actually, careful consideration of clavicle length among varying populations reveals that this is not necessary. For instance, the lower bound of the

human clavicle is about 119 mm. This bound encompasses the 5th percentile female. The upper bound is about 152 mm, which represents the 95th percentile male [34]. At first glance this appears to be a significant difference in length. However, it's not when compared to the ROM of the clavicle in respect to the glenohumeral joint.

As discussed in (Sec. 2.1.6) the largest ROM experienced by the shoulder in regards to elevation/depression or protraction/retraction is approximately 30°. However, this ROM is due to the contribution of all the shoulder joints combined. Additionally, full ROM of the shoulder is generally not required to perform most ADLs, nor possible due to the impairment of the user. Therefore, often times total glenohumeral motion does not exceed 120° in flexion or abduction [17]. In this range the clavicle is only required to elevate 6° and protract/retract 15° [33], [35]. Thus it is assumed that most of the operation of this device will see a maximum angular displacement of 15° or less in any given direction. The point of this assumption harkens back to the original question, can a fixed link length be used? Given the conditions previously described, it can be seen in (Fig. 3.1) that a fixed length is in fact suitable for this application. Not only can full ROM be achieved for the entire span of clavicle lengths, the curve travelled is nearly identical for all cases. Even at the extremes of the motion the curves are in close agreement. Therefore, a fixed link length is appropriate.

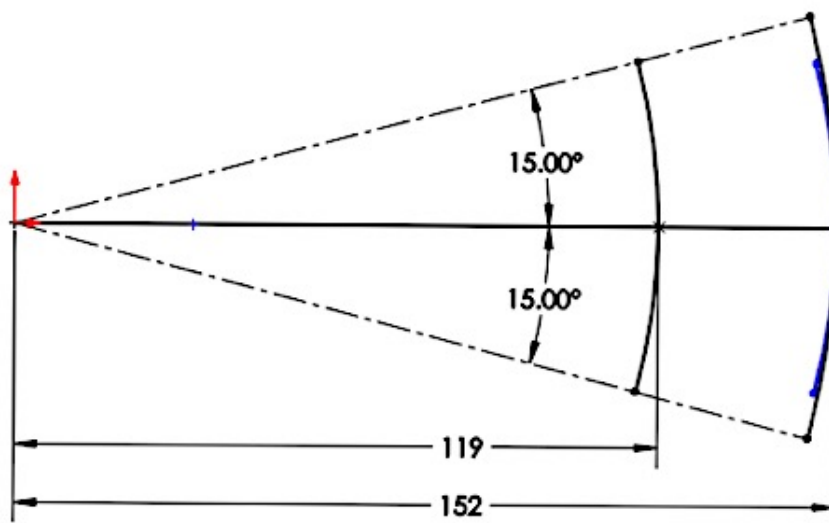


Figure 3.1. Diagram of the lower and upper bounds of clavicle length. The blue arc represents the lower bound arc projected onto the upper bound arc to illustrate similarity of curvature.

The concept of using the clavicle to approximate scapulohumeral rhythm has been used in several of the devices mentioned in (Sec. 1.3.2). The HARMONY, MGA, and MEDARM all use a clavicle-based approach to supplying another DOF at the shoulder. In the case of the MEDARM and HARMONY robots, both elevation/depression and protraction/retraction have been accounted for. All of these exoskeletons have adjustable link lengths; they also require proper alignment of the robot to the patient.

3.1.2. Parallelogram Four-Bars, Achieving Freedom in Joint Location

A limitation of exoskeleton design lies in joint placement. Typically, robot joints are intended to align with those of the person to whom it is attached. But what if a motion could be achieved remotely? This concept is the motivation behind the integration of a dual four-bar mechanism to achieve scapulohumeral rhythm. Simply put, a parallelogram is a special kind of four-bar device. As stated in (Sec. 2.3.5) a parallelogram is a Grashof mechanism, but it has a unique feature. The coupler link remains parallel to the ground link throughout its prescribed rotation (Fig.).

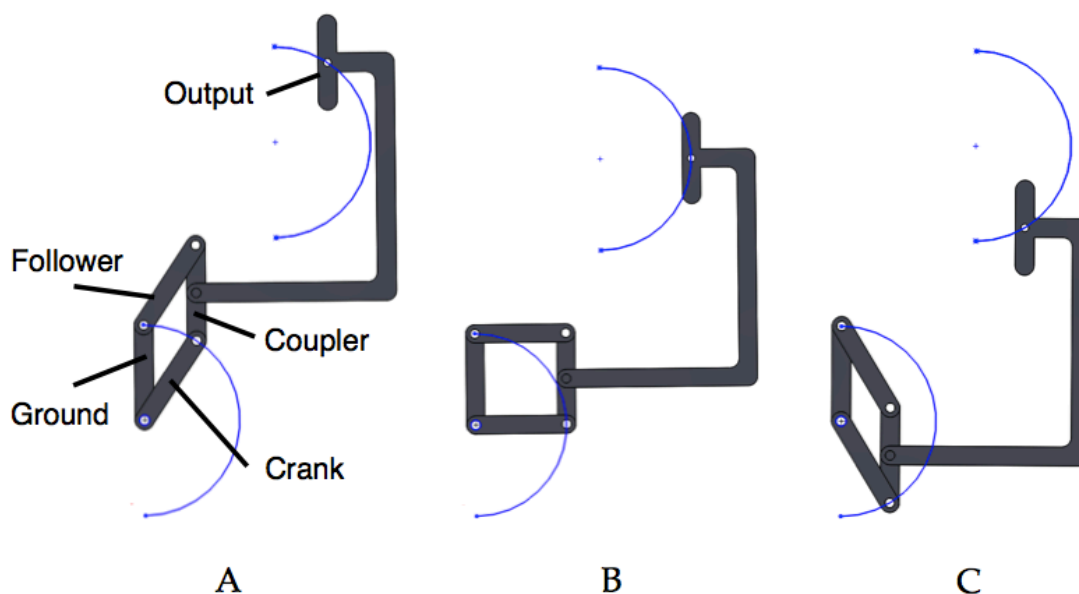


Figure 3.2. Illustration of how a parallelogram four-bar maintains parallelism during rotation. Note how the coupler link remains parallel to the ground link throughout its motion. The result is that the output maintains a parallel position relative to both the ground and coupler links. (A) Forward rotation. (B) Neutral position. (C) Reverse rotation.

Maintaining parallelism can be an extremely useful feature in the right application. In the case of BLUE SABINO, three actuated DOFs for the glenohumeral joint already exist. The relative position of these DOF in relation to the patient needs to be maintained throughout the full ROM. This is done for two reasons. First, it avoids interference between patient and robot. If the exoskeleton is allowed to move along an arc that centers about the sternoclavicular joint, its structure has the potential to collide with the user. Second, it accommodates remote placement of the scapulohumeral device. A dual parallelogram four-bar can produce vertical and horizontal rotation while maintaining a parallel output at any location, thus eliminating the need for time-consuming and difficult joint alignment.

3.1.3. Finding the Perfect Balance

Gravity compensation offers two major benefits. The first is the safety added to a system that can't collapse under its own weight should something go wrong. This is especially important when a patient is using the device. Though there are many safety precautions already being implemented such as hard stops, software stops, and emergency stops, a system that is gravity balanced lends an extra layer of protection. The second benefit is the ability to use much smaller motors to actuate balanced linkages. This results in lower actuator costs and a robot that doesn't possess more power than is required for its operation. Improperly sized motors can add unwanted stress to the system, which can lead to premature failure of components. Thus gravity compensation is beneficial to both patient safety and the overall performance of the system.

The method of gravity compensation to be used in this design is the three pulley and string arrangement described in (Sec. 2.5.3). This accommodates the use of normal springs while attaining near perfect gravity compensation. The goal is to incorporate gravity balance within the scapulohumeral device itself, thereby providing an opportunity to simultaneously balance any other mechanisms that may be attached to said device. With the freedom to place the apparatus nearly anywhere, the ability to build an enclosure for concealment of the spring is an attractive design option. This eliminates a potential pinch point while also creating a more aesthetically pleasing design. The integration of this gravity balancer will be discussed in greater detail in the following sections.

3.1.4. Bearing Selection

As discussed in (Sec. 2.4), three types of bearings were considered for this design. Ultimately, deep groove ball bearings were selected for their cost savings and beneficial attributes. Though tapered bearings are more robust, large bearings are needed in this design, as the axle diameters are oversized to accommodate combined loading. Due to this constraint, the bearings used are capable of supporting much larger loads than will be required of them in this application. Therefore the added load capacity provided by tapered bearings is inconsequential. Duplex bearings are expensive, and have to be installed in pairs. If one fails, they both must be replaced. Hence, deep groove ball bearings were selected due to their low cost and ease of maintenance.

Previously discussed (Sec. 2.4.4) was the concept of preload. Preload is not only beneficial, but is absolutely crucial to this project. The scapulohumeral device serves as the base link. It essentially supports the entire exoskeleton. As such, it is imperative that the bearings exhibit no axial endplay. Preload effectively eliminates endplay while also extending the life of the bearing. The method selected for this design is solid preload. The use of constant pressure preloading is aimed at higher speed applications where light loading conditions are present. Solid preloading provides the additional benefit of increased rigidity within a system, and is therefore suited for lower speed higher load applications. As such, solid preloading is the ideal choice for this specific design.

3.1.5. Proof of Concept: Wood Prototype

The theory behind the design of this scapulohumeral device has been developed thus far. However, early in the design process prototypes are often created to provide conceptual checks as well as physical feedback. Thus a solid model was designed in SOLIDWORKS to verify the combination of the components previously outlined. This included a dual four-bar mechanism consisting of four moving links and one stationary “ground” link (Fig. 3.3). The model developed is simple in design, with features like bearings modeled by through holes that use bolts to serve as revolute joints. The primary purpose of this early model is to verify conceptually that the combinations of components being considered for implementation are in fact sound.

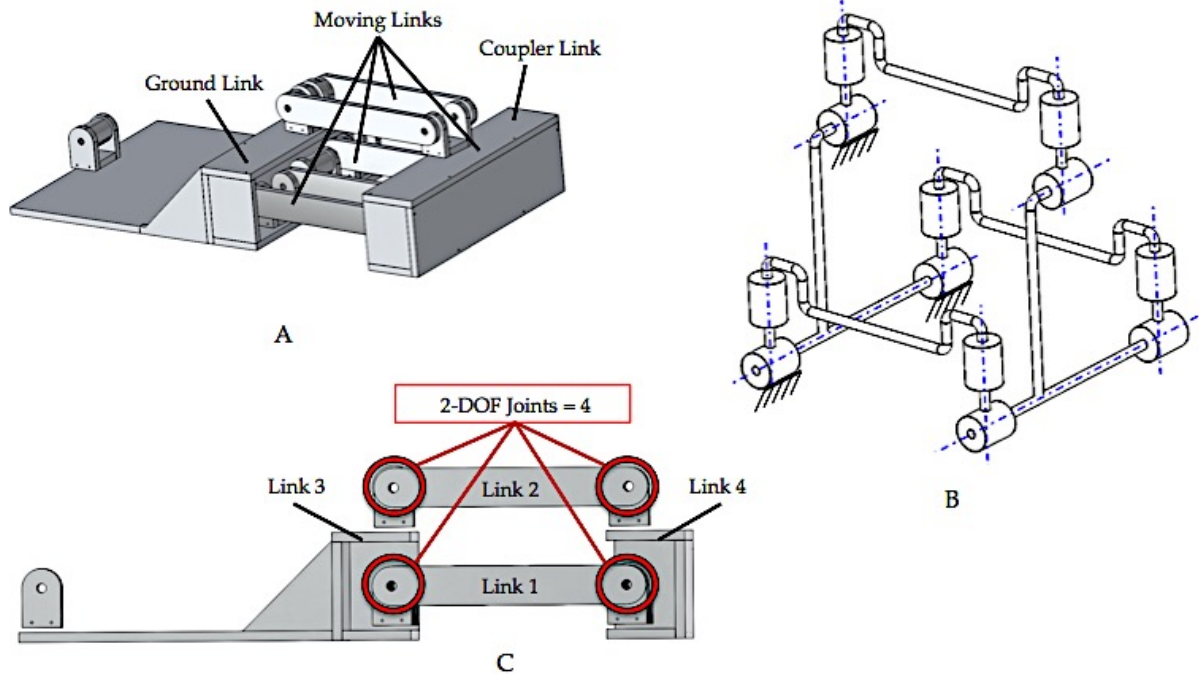


Figure 3.3. (A) Illustration of solid model with links labeled. (B) Kinematic diagram of mechanism illustrating axes of rotation and joint combinations. (C) Side section view with identification of the links and joints used to determine the mobility of the device.

A chief concern to address with this prototype is the issue of mobility. The concept of a dual four-bar mechanism is intended to not only achieve parallel motion, but also movement in two DOFs. As described earlier (Sec. 2.3.3), Gruebler's equation can identify the DOFs of a device. However, Eq. (1) accounts for planar mechanisms only. This prototype incorporates two planar four-bars, and therefore is a spatial system as a result. Because of this, the spatial Gruebler's equation (also known as the "mobility equation" or Kutzbach criterion) must be implemented:

$$F = 6(N - 1) - 5(P_5) - 4(P_4) - 3(P_3) - 2(P_2) - P_1 \quad (14)$$

where F is the mobility or DOFs of the system, N is the number of links, and P_n is the number of joints with n DOFs removed per joint. Each joint in 3D space has the capability of six DOFs. If a revolute joint is considered, its constraints allow for one DOF. Thus it removes five DOFs. For example, if three revolute joints were the objects of interest, then P_5 in Eq. (14) would be replaced with the number 3. This is synonymous with saying that there are three joints with only one DOF, or in other words, three joints that remove five DOFs. Every subsequent joint in the device is

analyzed in the same manner. Any terms that do not apply to the system being evaluated are simply omitted from the equation.

When using the spatial form of Gruebler's equation, it's important to account for redundant joints. If redundant joints in a device are not accounted for, then Gruebler's equation will incorrectly predict the mechanism's mobility. This fact is especially prevalent when considering the mobility of the aforementioned prototype. Because of the dual nature of the device, there exist several redundant joints. Therefore, after careful inspection, Gruebler's equation for the prototype in question becomes:

$$F = 6(4 - 1) - 4(4) \Rightarrow 2 \text{ DOF}$$

As shown earlier (Fig. 3.3), the total number of links in the prototype is four. The total number of two DOF joints is four as well. When these values are applied to Eq. (14), it can be seen that the prototype does in fact possess the desired mobility, two DOFs (Fig. 3.4).

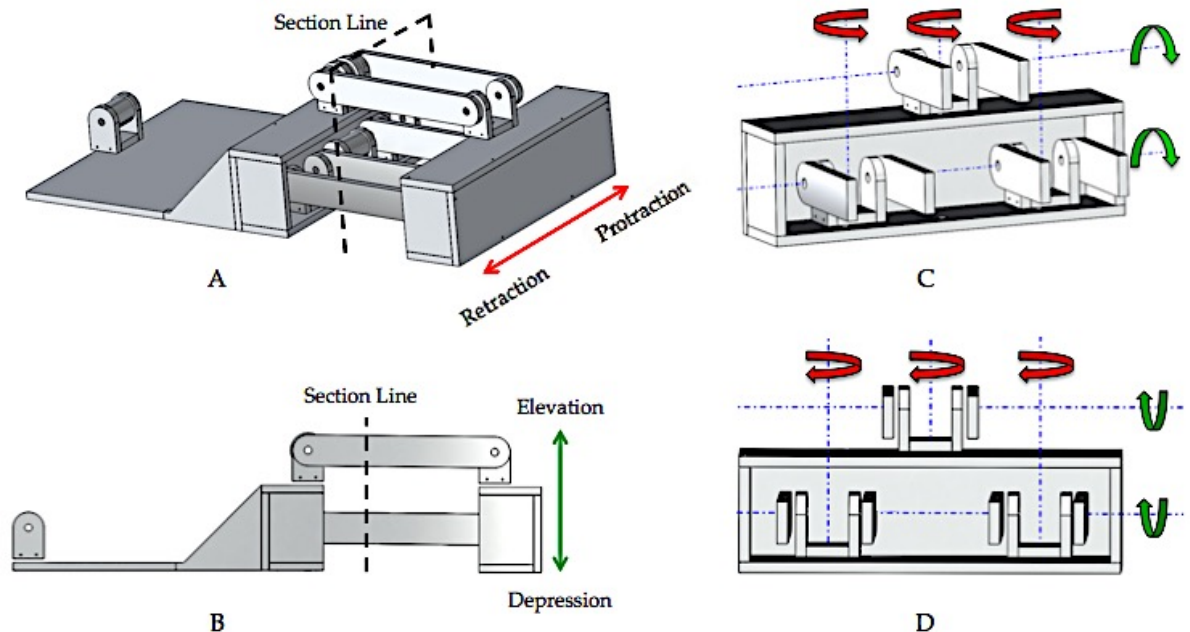


Figure 3.4. (A) Isometric view of solid model. Section line indicates plane of intersection which results in views (C) and (D). Direction of protraction and retraction are also identified for the given orientation. (B) Side view of solid model. Section line is again identified for further clarification. The direction of elevation and depression are also indicated for the given orientation. (C) Section view of prototype showing dual four-bar movement, in this view protraction and depression are being performed. (D) Front section view illustrating simultaneous retraction and elevation of the dual four-bar mechanism.

Rapid prototyping is becoming commonplace, techniques like 3D printing and laser cutting are a couple of ways to produce economical and time-efficient models. Once the function and mobility of the solid model was verified, a physical proof of concept prototype was produced (Fig. 3.5). Constructed of $\frac{1}{4}$ " Baltic birch plywood by way of a laser cutter, the entire device was assembled and evaluated in regards to ROM, mobility, and potential weak points in design.

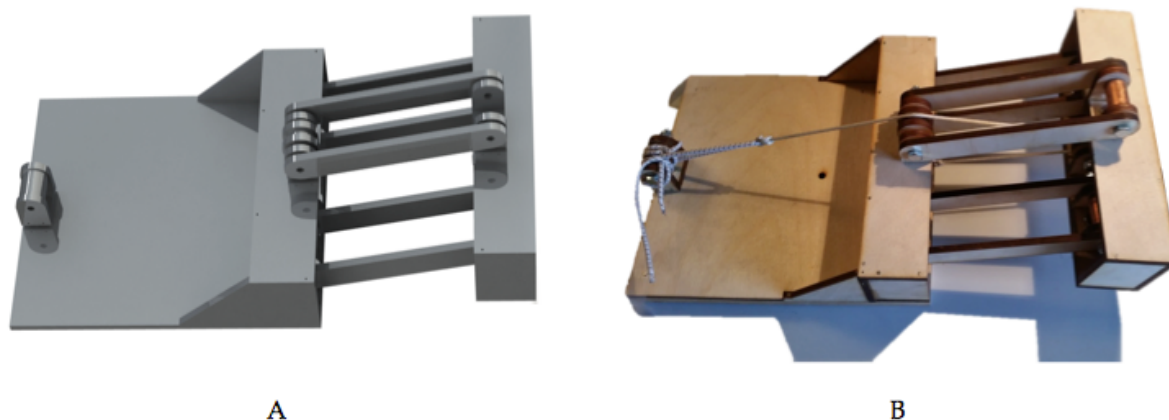


Figure 3.5. (A) SOLIDWORKS model of the proof of concept prototype. (B) Actual prototype created by use of a laser cutter. The joints are revolute with bolts serving as the potential bearings. Note the pulleys; gravity compensation was included in the prototype to demonstrate a possible method for its integration.

The physical prototype proved to be an effective evaluation tool. A rudimentary form of gravity compensation was included in the proof of concept. Though the pulley and string arrangement was not optimized, its inclusion was primarily to demonstrate a potential location for integration into the final design. However, as can be seen in (Fig. 3.5), the gravity compensation worked remarkably well, as the coupler link would remain stationary at nearly any position it was placed. The prototype demonstrated the need for an additional top link, as the system was sensitive to twist. As stated previously, this results in a redundant link and accompanying joints. This effectively increases the stability of the device when subjected to loading, but does not change the kinematic behavior. Simply put, the mobility is maintained at two DOFs even though the number of links and joints are increased. Additionally, the dual-link setup at each pivot allows for dual bearings, which simultaneously accommodate moment and axial loading, but also provide an opportunity to implement solid bearing preload. Lastly, the desired ROM was easily attained and the parallel function performed as expected. Thus the proof of concept verified the use of a dual four-bar mechanism for achieving clavicular motion.

3.2. TRANSITIONING FROM PROOF OF CONCEPT TO FINAL DESIGN

The proof of concept prototype verified that the theory behind the device was sound. However, developing a final design from a proof of concept is a monumental task. One of the first questions that needed answered was: what magnitude of forces and torques would this device have to support? The answer drives much of the design, as in sizing of components and final material selection. Unfortunately, BLUE SABINO does not exist. This makes determining the forces and torques difficult. However, the EXO-UL8 does exist and can be used to identify upper boundaries for these variables (Fig. 3.6).

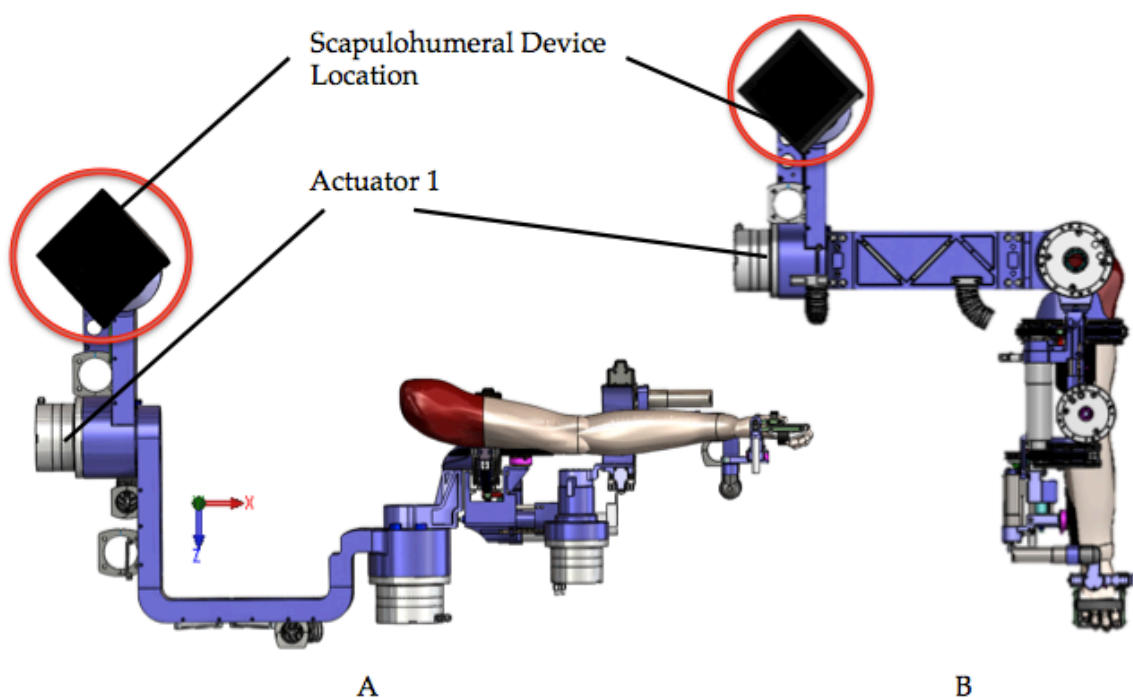


Figure 3.6. (A) First position to produce a maximum moment about the Z-axis. (B) Second position to produce a maximum moment about the X-axis. The scapulohumeral device will assume the position circled, thus actuator one will be directly mounted to the mechanism.

As can be seen in (Fig. 3.6), the moments produced are summed about actuator one. This is due to the fact that actuator one will be directly mounted to the scapulohumeral device. A direct connection eliminates the need for an additional link and affords more space behind the patient; an important feature that is discussed in more detail in (Sec. 3.2.7). To calculate the necessary moments and forces needed to determine design specifications, a classic approach was implemented. If a force is moved to a new location, it can be replaced with a force of equal magnitude and direction and an accompanying moment. The moment is

simply a product of the force multiplied by the distance it is moved. In two dimensions this is a straightforward procedure. In three dimensions this approach can become a bit cumbersome. However, with the aid of linear algebra the process can be simplified:

$$\bar{M} = \bar{r} \times \bar{f} \quad (15)$$

where \bar{M} is the moment vector, \bar{r} is the position vector from the position of interest to the position of the applied force, and \bar{f} is the force vector applied. In regards to (Fig. 3.6), the mass of the EXO-UL8 links and actuators are known. A 95th percentile male arm mass was included in the analysis, and five positions of interest were identified. These positions were then used in Eq. (15) and summed about the center (both vertically and horizontally) of the actuator mount (position denoted by the green dot) to arrive at the total moments about the X and Z-axes (Fig. 3.7).

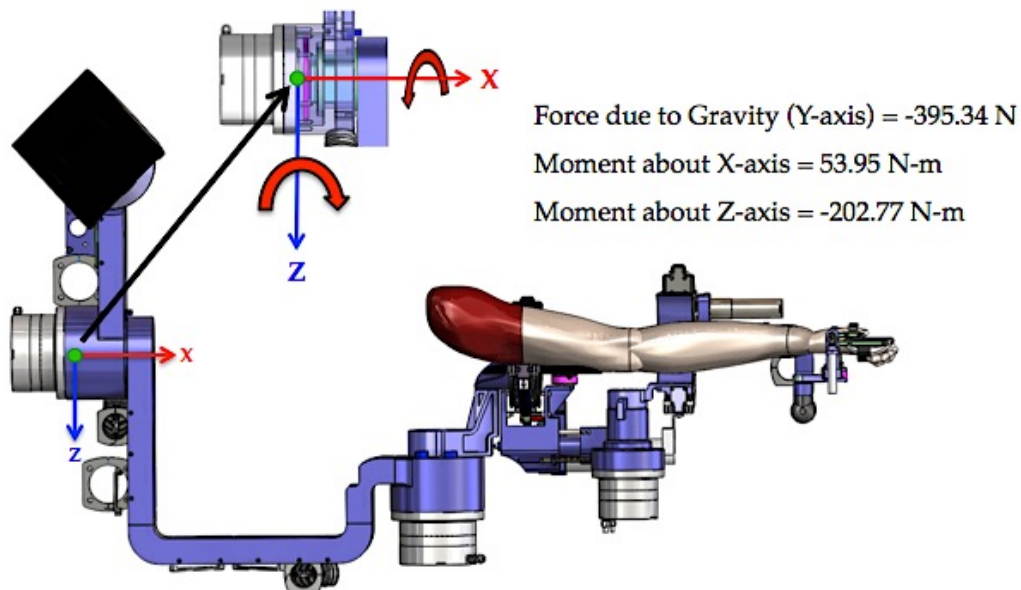


Figure 3.7. Moments and force derived from the EXO-UL8 solid model.

By quantifying the forces and torques experienced by the scapulohumeral device, the appropriate material could be selected. Previous designs (e.g. EXO-UL7, EXO-UL8) used 6061-T6 aluminum. Generally, 6061-T6 is a good all-purpose aluminum alloy. However, as outlined previously, strength, rigidity, and weight are primary concerns. The latter constraint is of little concern, as the scapulohumeral

device will be gravity balanced. Likewise, rigidity due to material properties (modulus of elasticity) are nearly identical for both materials, thus rigidity will be a function of geometry in this design. The same cannot be said of strength between materials.

Since the scapulohumeral mechanism will serve as the base link, strength is vital to its operation. In this regard, 7075-T6 aluminum is the material of choice for this particular application, as it has nearly twice the ultimate tensile and yielding strength of 6061-T6. From a stress-life point of view, this results in superior fatigue properties. Higher strength also enables the ability to create lighter parts that can bear the same stress levels as 6061-T6. The two main disadvantages are cost and increased difficulty in machinability. However, the advantages afforded by 7075-T6 far outweigh these detriments, thus its use is warranted in this design.

3.2.1. Link Design

As previously discussed, a fixed link length was determined to be appropriate. Therefore, the upper bound of clavicle length presented in (Sec. 3.1.1) established the center-to-center distance (152 mm) between bearing bores at the opposing ends of the link. Width of the link is kept to a minimum, a compromise of weight, size, and strength. The primary constraint is providing enough material to press fit the bearings at each end, and maintaining rigidity along the length of the link to resist twisting. As was discovered with the prototype, this design is sensitive to moments. However, a fourth link has been added to the design to help address this issue. Thus the moments and force shown in (Fig. 3.7) is shared between four links, each of which has two pairs of bearings.

As stated previously, paired bearings allow moments and axial loads to be accommodated. Moreover, solid preload can be implemented thereby increasing overall rigidity. Large radiuses are found at each end of the link to provide clearance during operation and to mitigate stress concentrations due to the removal of material for said clearance. Lastly, material has been removed from the center of the link to reduce the overall mass (Fig. 3.8). To this end, if it is found that greater rigidity is required, simply removing less or no material from the center can stiffen the link. The advantage of the design shown here is its minimal mass. Unfortunately this attribute also makes it more prone to deformation under combined loading.



Figure 3.8. Renders of different link views. (A) Top view. (B) Side view. (C) Isometric view.

3.2.2. Elevation/Depression Sub-Assembly

One of the key elements in this design is the ability to preload the bearings. Though this adds complexity, the resulting increase in rigidity, bearing life, and elimination of axial endplay is too beneficial to preclude. The aforementioned links (Fig. 3.8) were designed with this function in mind. The overall assembly of the links is modular in nature. Vertical posts are used to supply protraction and retraction of the system (Sec. 3.2.4). The shafts or “bearing axles” to allow elevation and depression intersect these posts, thus forming a u-joint (Fig. 3.9). A slip fit on the shaft allows for easy assembly, as the axle can be simply “slid” into place from either side of the link.

Solid preload is achieved by machined spacers placed between the inside surface of the inner race, and a machined flat on the intersecting post. Intentionally machined to be short, shims are used to adjust the spacers to their final dimension. Once proper preload is attained, nuts with nylon inserts are used to lock the bearing assembly in place. One advantage of this method is the solid connection that is established via the spacer and shims. Thus the nuts can be tightened without unintentionally applying additional preload. Although this process can be lengthy, it allows for precise preloading, and should only have to be performed upon initial assembly of the device.

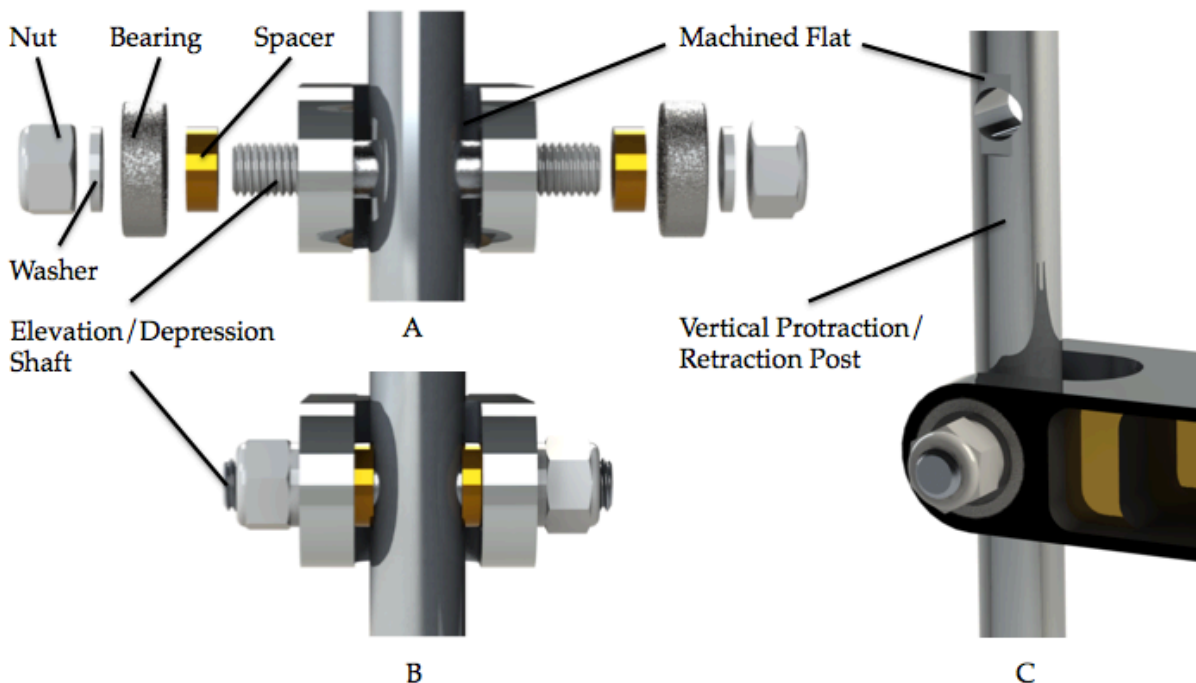


Figure 3.9. Illustration of the Elevation/Depression sub-assembly. (A) Exploded view of the assembly identifying key elements. (B) Entire constructed assembly. (C) Illustration of the assembly with top link omitted to show the machined flat of the post. The flat serves as the other seat for the spacer to be pressed against when preloaded.

3.2.3. Ground and Coupler Link Design

An interesting phenomenon occurs when dealing with dual four-bars, they share a common ground and coupler link. The ground link serves as one side of the “box” that forms the scapulohumeral device. The coupler forms the opposite side and also serves as the attachment point for the rest of the exoskeleton (Fig. 3.1). It is for this reason that both “links” must be robust in design. Because this is a dual four-bar mechanism the design allows for symmetry, which is not only helpful for machining purposes, but also lends aesthetic appeal to the apparatus.

The only structural difference between the links is the addition of a curved slot in the ground link (Fig. 3.1). This slot is a clearance hole for the wire rope used in the gravity balancer, a feature that will be further discussed in (Sec. 3.2.5). Otherwise, the ground and coupler links are identical. Essentially, these links form a box with one side removed. This structural compromise combined with the height of the links creates a potential weakness with respect to rigidity, an issue that is further explored in (Sec. 4.3). Lastly, the links are designed to house three pairs of bearings, two for the dual four-bar mechanism and one for the gravity balancer.

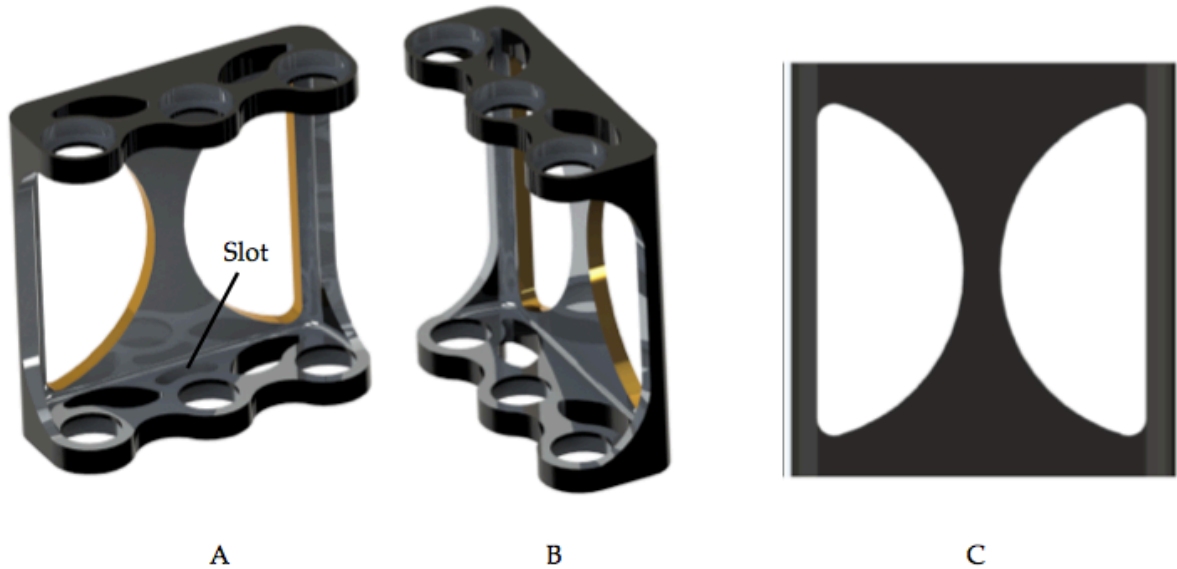


Figure 3.10. (A) Ground link, note the semicircular slot to accommodate the wire rope of the gravity balancer. (B) The coupler link. (C) Rear view.

3.2.4. Protraction/Retraction Sub-Assembly

Similar to the elevation/depression sub-assembly, a solid preload is used to set the bearings in this construction. The vertical posts present a unique challenge however. Like the shafts that intersect them, the posts are designed to simply “slip” through the inner bore of the bearings that support them. The challenge arises when considering the spacers. Unlike the elevation/depression shafts, there is no natural stop for the other side of the spacer. Consequently, while one side is captivated by the inner race of the bearing, the other end is left free to move.

Solid preloading of the vertical post bearings is achieved through the addition of two-piece shaft collars (Fig. 3.1). The shaft collars provide a stop for the free side of the bearing spacers. Their relative vertical location is dictated by a relief groove machined into the top and bottom of the posts. The collars themselves also have a machined relief. This is to ensure that the shaft collars do not interfere with the elevation/depression link assembly during operation. With the use of collars, a solid preload can be applied to the vertical post bearings. Appropriate preload is achieved in the same manner described for the elevation/depression link assembly. The convenience and utility of shaft collars make the preloading process easier to perform. Furthermore, because of their two-piece design, the collars provide an efficient means of disassembly if ever the system is in need of maintenance.

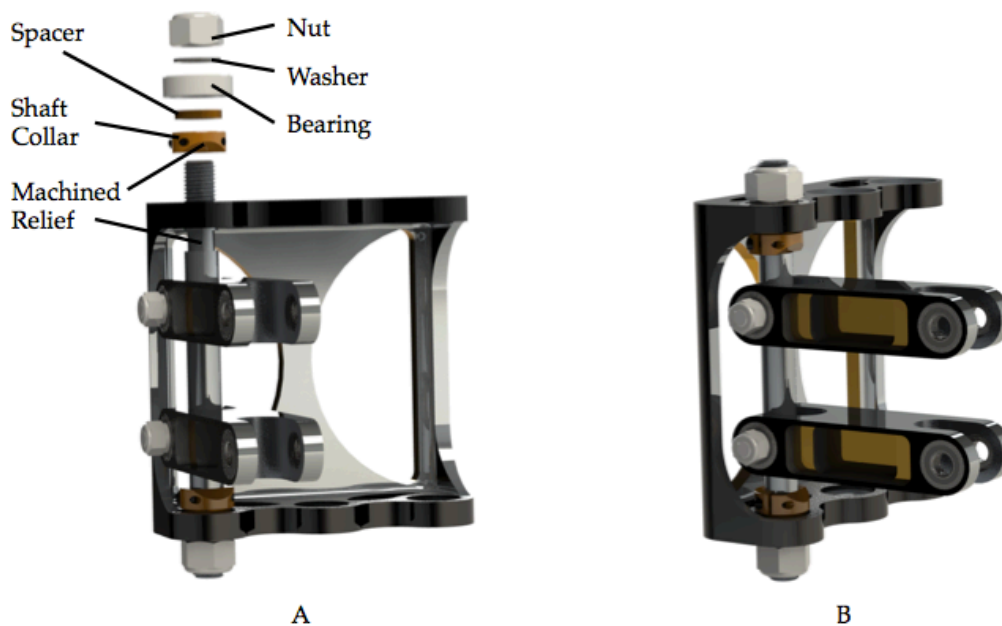


Figure 3.11. Illustration of protraction/retraction assembly. (A) Exploded view of assembly identifying chief components. Note the use of the machined relief to vertically position the collar on the post. The collars have an added relief to avoid interference with the links as they approach their maximum ROM. (B) Entire assembly fully constructed. Only one of the three post assemblies is shown. The other two are omitted for sake of clarity.

3.2.5. Pulley-Based Gravity Balancer

As shown in (Fig. 3.5), a pulley and string arrangement has been selected for integration into this design. The overall ROM of the device will be limited by mechanical stops. This allows for the minimum breaking strength of the rope to be decreased, as the rope will never “see” maximum overloads, only the links will. In the event of extreme shock loading, the spring will fail before the rope, further justifying the lowered strength restriction. The advantage of a reduced strength limit is the subsequent decrease in wire rope diameter. In this application, 7 x 49 strand rope has been selected for its flexibility and fatigue resistance. Because of its flexibility, the diameter of the pulley can be smaller than if other stranded options were implemented (e.g. 7 x 7). Therefore, a rope diameter of 1.98 mm with a minimum pulley root diameter of 29.70 mm has been designated.

The pulleys selected for this design are made of nylon, which simultaneously increase fatigue life of the wire and remove the need for “jacketing”, thereby keeping the wire diameter to a minimum. As discussed in (Sec. 2.5.4), the arrangement used here can be adjusted by the K-type method. This allows for the pulleys and links to remain in their fixed positions, while accounting for payload changes through simple manipulation of spring stiffness.

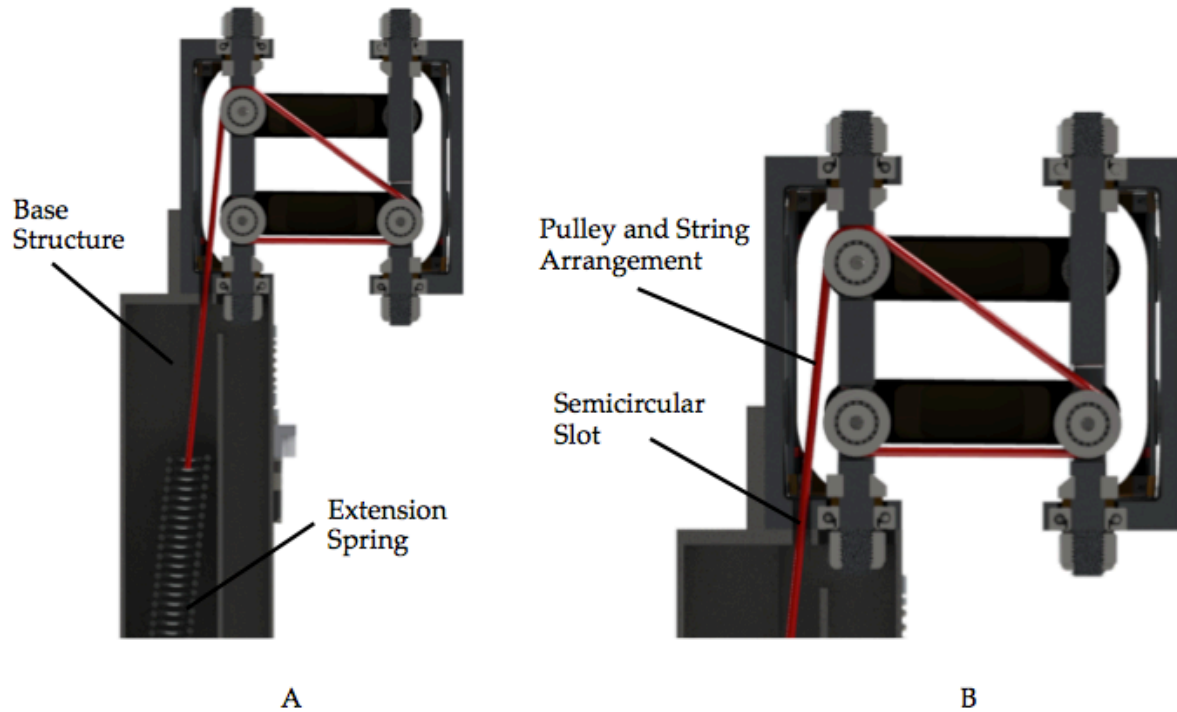


Figure 3.12. (A) Section view of entire balancing mechanism. The base structure serves as both a mounting surface for the scapulohumeral device and also to conceal the extension spring. (B) Close-up of the section view to illustrate the semicircular slot and three-pulley gravity balancing system.

3.2.6. Actuation and Flexible Shaft Coupling

Like the EXO-UL8 before it, BLUE SABINO uses harmonic drives as its main form of actuation. Though harmonic drives are expensive, the multitudes of benefits they provide (Sec. 2.2) make them a valid choice. In this design, gravity balancing results in low-torque requirements. By far, the largest contributor to torque demand is gravity, but this is effectively zero due to the gravity equilibrium system. Therefore, the only torque required for this device is due to inertia. That being said, the appropriate torque for elevation/depression and protraction/retraction may be found by:

$$T = I\alpha \quad (16)$$

where T is the torque (N-m), I is the moment of inertia ($\text{Kg}\cdot\text{m}^2$), and α is the angular acceleration (rad/sec^2). The solid model (Fig. 3.13) was used to determine the moment of inertia (including mass of the model, 95th percentile male arm, and 2.5 Kg mass grasped during ADLs). Like the values obtained earlier (Fig. 3.7), this provides

a conservative assessment, as the BLUE SABINO will have a reduced mass. The acceleration is the same value used in the EXO-UL8 design and when compared to other designs [17], [22], is of similar magnitude. The calculated torque from the solid model is compared against that of a slender rod comprised of the same overall length and mass. This is done to ensure that the torque obtained is reasonable and thus acceptable for actuator sizing (Fig. 3.13).

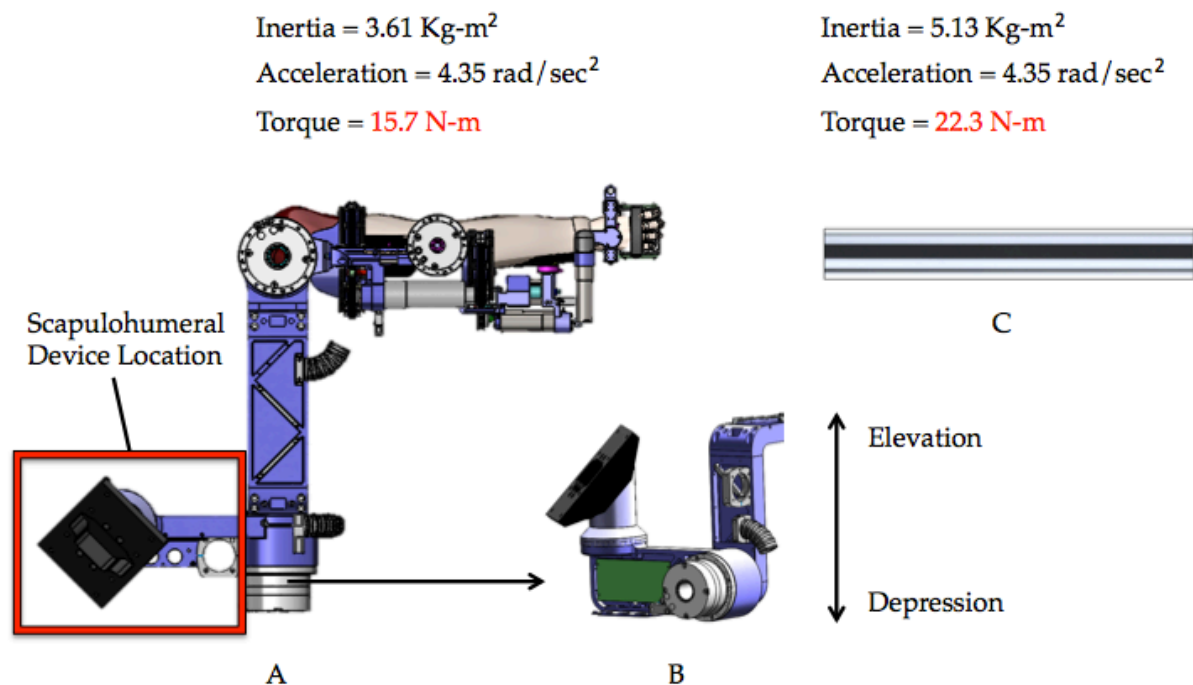


Figure 3.13. (A) Solid Model used to determine moment of inertia for the EXO-UL8. The position shown produces the largest moment due to inertia. For this device, this occurs during shoulder abduction/adduction while the scapulohumeral device is simultaneously elevating and depressing respectively. (B) Isometric view of the EXO-UL8 and scapulohumeral device junction. The relative direction of elevation and depression are shown for clarity. (C) Slender rod with same length and mass properties as EXO-UL8 used as comparison.

The calculations shown (Fig. 3.13) reveal an appropriate behavior. A slender rod assumes even distribution of mass throughout the body. However, as can be seen in (Fig. 3.13), the mass of the exoskeleton is not distributed evenly. Thus the discrepancy in torque values is a direct result of the uneven dispersion of mass, and serves as a validity check. Furthermore, the worst-case scenario was applied here, with the exoskeleton performing shoulder abduction/adduction while supporting a 95th percentile male arm and grasping a 2.5 Kg mass. Therefore the value calculated is conservative, which provides a reasonable value for use in sizing the actuator.

An additional consideration in the choice of actuator size is the expected mass reduction in the BLUE SABINO design. This determination is difficult, as it is early in the design process. However, a few decisions have been made that can be used to more closely approximate actuator needs. For example, the two large actuators on the EXO-UL8 are SHA-32 series. They have a combined mass of 12.4 Kg [38]. The SHA-32 actuators are being replaced by smaller SHA-25 series that collectively have a mass of 6.2 Kg. Furthermore, the current actuator for elbow flexion/extension is also being down-sized from a SHA-25 to a SHA-20 series actuator resulting in an additional 1 Kg mass reduction. Overall, a mass decrease of 7.2 Kg is achieved due to actuators alone.

With a conservative torque calculated and a known mass reduction, a determination can be made in regards to actuator size. If the 7.2 Kg corrections are made to the original model, the result is a required torque of 13.85 N-m. Therefore, the SHA-20 with a 51:1 gear reduction is the actuator of choice [38]. With a continuous operating torque of 21 N-m and a peak torque of 73 N-m, the SHA-20 is ideal for this design. Not only will the motor be primarily operating in its optimum range, but the peak torque will accommodate temporary moments of shock loading as well. However, care must be taken in establishing the proper method of transmitting torque from the motor to the device.

Transmission of torque between the motor output shaft and the shaft that is driven is not a trivial decision. Alignment of the shafts is one of the chief concerns during and after assembly. Three primary forms of misalignment can occur: parallel, axial, and angular (Fig.). Even small misalignments on the order of 0.02 mm or 0.5° angularly can result in excessive stresses on bearings. Rigid shaft couplings provide the best overall transmission of torque, however they are intolerant of misalignment. Thus proper setup often requires laser guidance and complex bracketing. Neither of these options is suitable for this application, as funding is finite and space for bracketing is limited.

Flexible shaft couplings present another viable solution to the problem of torque transmission. Unlike rigid couplings, flexible couplings are tolerant of misalignment, with some versions capable of handling all three forms discussed previously. However, with flexibility comes compromise. Namely, lower torsional rigidity, lower connection strength, and windup. Windup refers to the coupler

acting like a spring. If a torque is applied to one end of the coupler, it begins to turn. However, there may be a delay in this motion at the opposite end of the coupler. Thus in an exaggerated example, one end may rotate 3° before the other end begins to move at all. This phenomenon is known as windup, which basically describes the elastic deformation of material due to torque. Even solid shafts experience this effect, however, it usually goes unnoticed due to their high torsional stiffness. In the case of flexible couplers, not only can windup be noticeable, it can be excessive and ultimately unsuitable in some cases. Thus care must be taken in selecting the appropriate coupler for the given application.

Though many types of flexible couplers exist, only one fulfills the required design constraints for this mechanism. Positional accuracy is paramount. Small deviations in this device translate to large deviations at the end effector. Not only this, but harmonic drive actuators are known for their accuracy, precision, and repeatability (Sec 2.2). A poor choice in coupling has the potential to mitigate these attributes and therefore the effectiveness of the entire design.

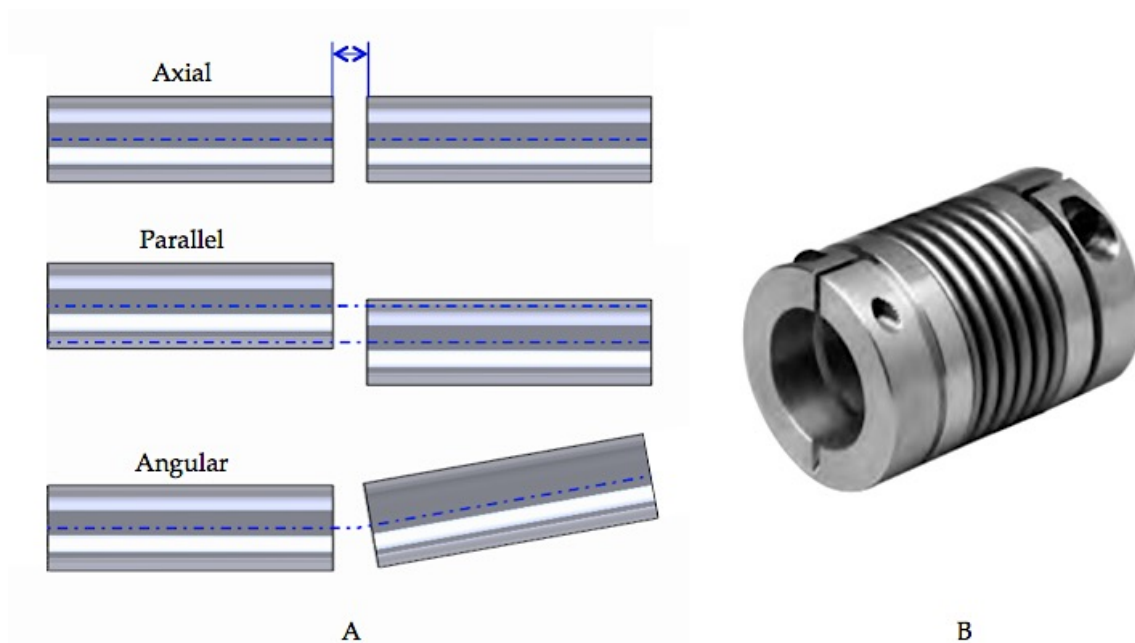


Figure 3.14. (A) Illustration of the three types of misalignment: axial, parallel, and angular. (B) BWLC 78 bellows coupler selected for torque transmission.

The only coupler to sufficiently address the aforementioned needs is a bellows coupler (Fig.). Capable of accommodating all three types of misalignment, bellows couplers are known for their high positional accuracy. They are used in

many forms of motion control due to this feature. Furthermore, in terms of torsional stiffness, they approach values near that of rigid couplers. Thus windup is minimal. Finally, they are maintenance free and can handle large torque transmission in regards to their size. The BWLC 78 bellows coupler by LoveJoy Inc. was selected for this application [67]. With a nominal torque rating of 60 N-m, the BWLC 78 is an ideal mate to the SHA-20, and is capable of withstanding potential shock loading that the system may experience.

3.2.7. The Final Design: PANDORA

The previous sections revealed the individual components and subassemblies that together comprise the scapulohumeral device. As with all designs, an appropriate moniker is needed. PANDORA is the title selected for this mechanism. Although it is a tongue-and-cheek homage to the classic Greek myth, it also forms the acronym that describes its function: Parallel Positioning Dual Four-Bar Mechanism (Fig. 3.15) and (Fig. 3.16).

One of the primary goals discussed in (Sec. 1.3.3) was for the inclusion of scapulohumeral rhythm into BLUE SABINO. Based on its predecessors' designs, the most logical location for PANDORA is as the base link. This is due in part to the other link and joint locations being established by the aforementioned versions. However, as mentioned in (Sec. 3.1.2) the unique capabilities of PANDORA allow it to be placed anywhere relative to the patient, thus the second qualifier for its use as a base link. Finally, as shown in (Sec. 3.1.3), gravity compensation only adds to the utility of this device and further justifies its location as the base link.

The last design concern in regards to PANDORA is its integration into the existing EXO-UL8 model. Much of BLUE SABINO will mirror this design, as such, positioning of PANDORA can be determined now rather than having to wait until future concepts are developed (Fig. 3.18) and (Fig. 3.19). A key secondary function of PANDORA is the potential concealment of electrical wires, and adjustment capabilities to accommodate patients of differing shoulder widths. The base tower that PANDORA attaches to serves both of these functions. As previously described, the tower conceals the spring used for gravity compensation in one compartment, while a second compartment serves to simultaneously partition and house electrical wires (Fig. 3.17).

The base towers also possess the capability to accommodate patients of different shoulder widths. Though not currently designed, one proposed concept involves linear tracks. The base towers could then move toward and away from one another in a designated plane, thereby permitting use of BLUE SABINO by different sized patients. The other reason for this adjustment capability is due to posterior entry and exit of the device. Most likely an interactive environment involving virtual reality or tasks simulated by additional robots will prohibit anterior entry. A potential application of this concept is illustrated in (Fig. 3.17).

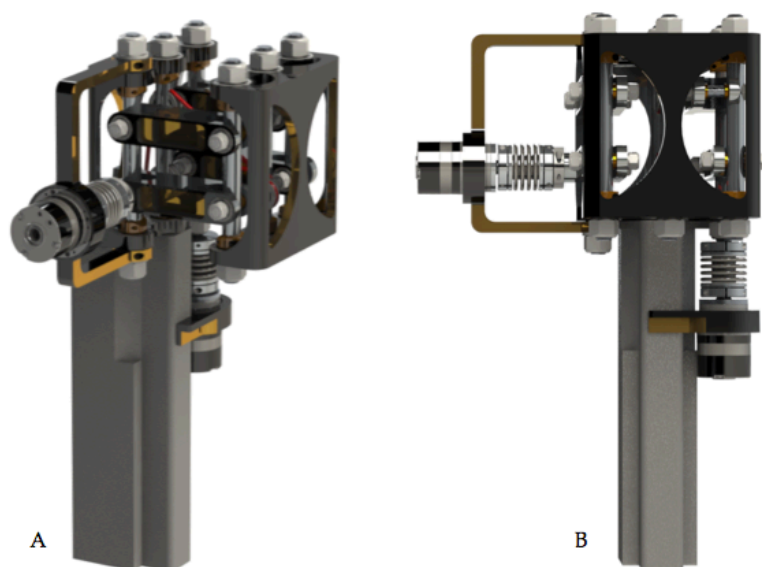


Figure 3.15. (A) Isometric view of PANDORA. (B) Front View of the full assembly.

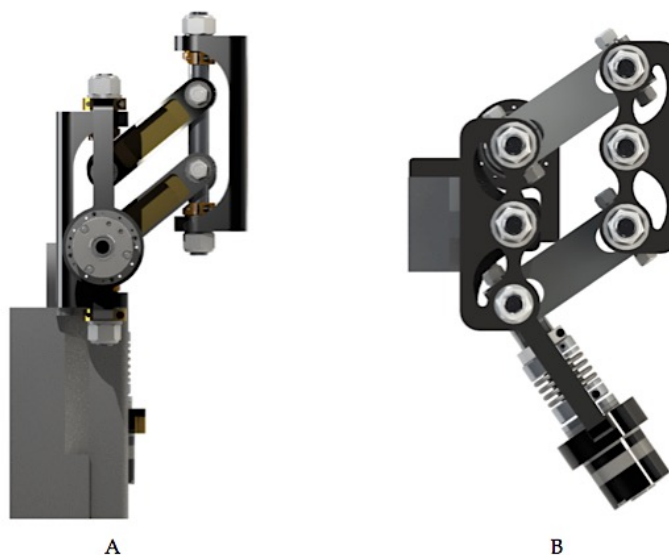


Figure 3.16. (A) Side view of PANDORA illustrating parallel movement for elevation and depression. (B) Top view showing parallel movement of shoulder protraction and retraction.

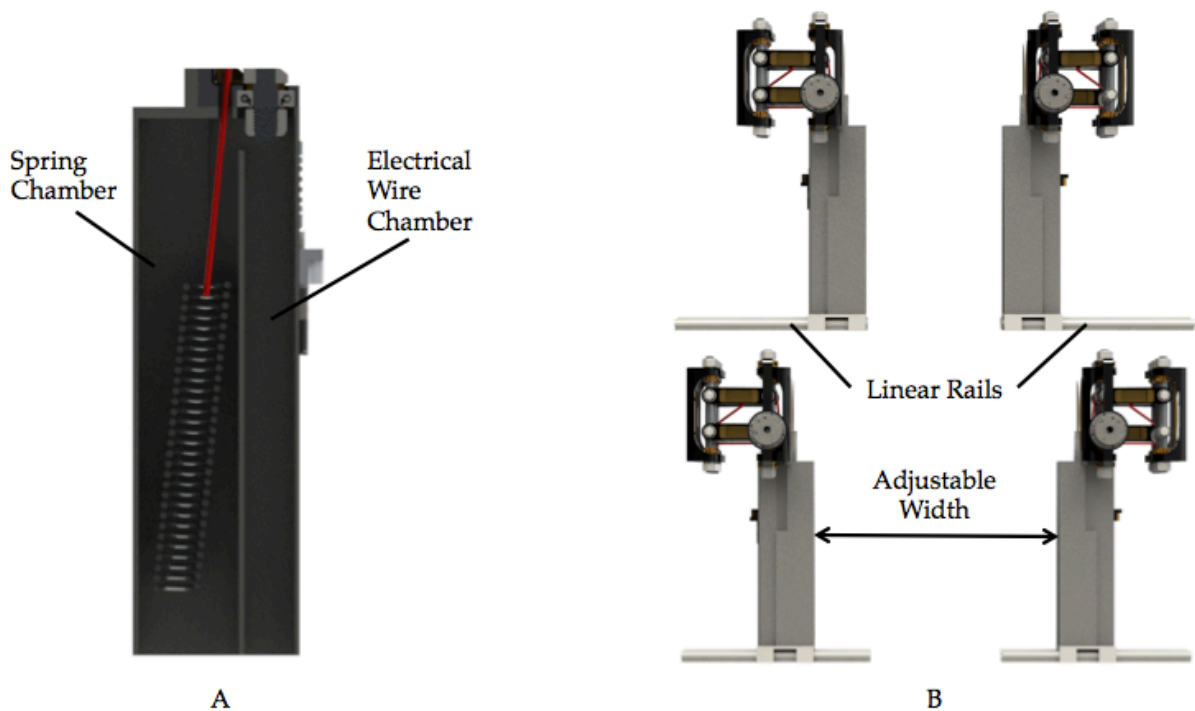


Figure 3.17. (A) The base towers of PANDORA provide concealment for the gravity balancer springs and electrical wires that power the actuators. (B) Proposed concept for width adjustment. Linear rails are an economical and practical solution. The carriages can be locked in place when the desired location is reached.

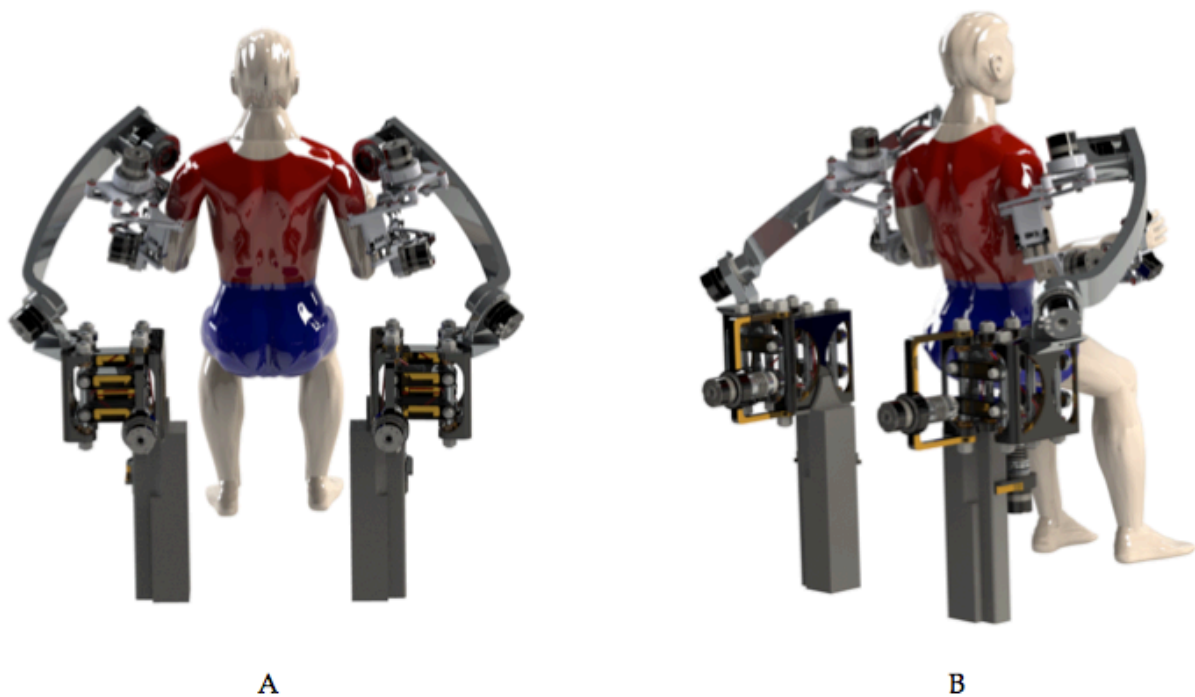


Figure 3.18. (A) Rear view highlighting the importance of width adjustment and the suggested positioning of PANDORA. As the base link, PANDORA can be used to gravity balance the entirety of the exoskeleton. All subsequent links and actuators shown are potential design concepts for BLUE SABINO. (B) Rear isometric view intended to provide a better spatial representation. Linear rails are omitted to provide clarity.

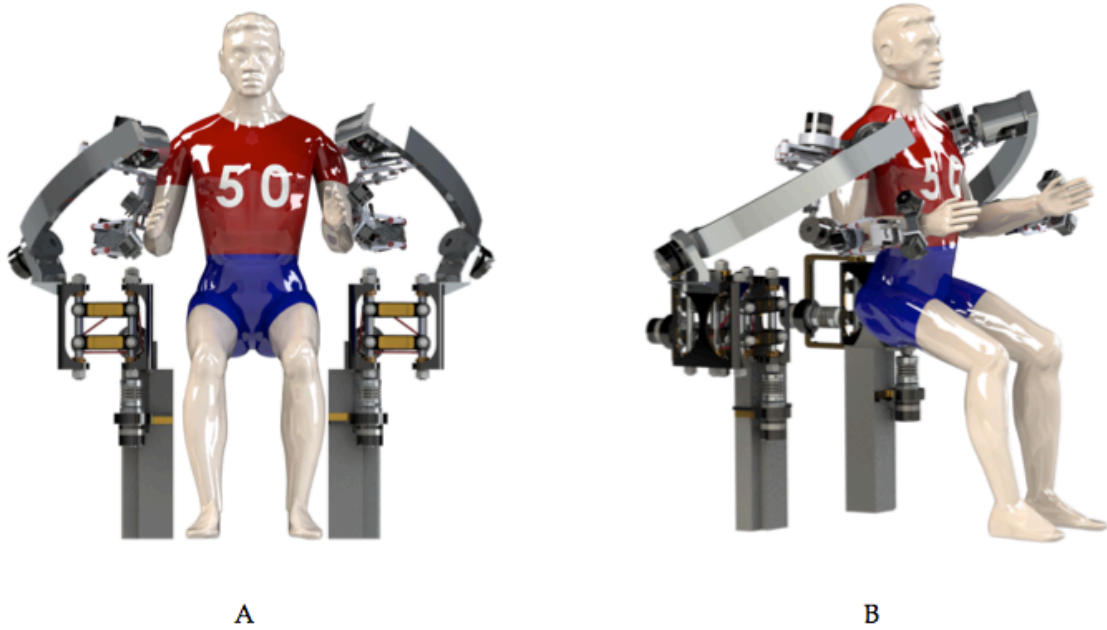


Figure 3.19. (A) Front view. (B) Front isometric view. Note the distance from PANDORA to the subject. To provide full ROM, PANDORA must be positioned far enough posterior to the patient as to not interfere with their movement. Though the linear rails have been omitted in this figure for sake of clarity, it can be seen that their proposed placement is favorable to the overall design presented here.

4. RESULTS

The theory and design behind the development of PANDORA has been presented thus far. However, the results of the decisions made and consequent design implementations must be validated and verified. Unfortunately, validation can only be performed once the device has been fabricated and thoroughly verified. Validation in this scope is defined as whether the device meets the needs of the patients and stakeholders of the present work (e.g. University of Idaho, St. Luke's Rehabilitation Institute, etc.). Therefore, this chapter focuses on the verification of PANDORA. Evaluating whether it meets the design needs that were specified earlier (Sec. 3.1).

4.1. MATERIAL SELECTION AND LINK DESIGN

It was mentioned earlier that unlike its predecessor, BLUE SABINO is to be constructed of 7075-T6 aluminum rather than 6061-T6 aluminum. Several reasons were stated as to why this determination was made. As a brief reminder, strength was the primary driving force behind the selection. The result of this decision is illustrated in (Fig. 4.1). The EXO-UL8 used a minimum factor of safety (FOS) of 1.2. Likewise, every individual component and sub-assembly tested hereafter must exceed this minimum value.

As previously discussed (Sec. 3.1), rigidity is determined for each sub-assembly as a function of overall deflection at the end effector. The maximum deflections of which were determined by the data presented in (Fig. 3.7) and (Fig. 3.13). These values are presented in the sections that follow. SOLIDWORKS was used exclusively to perform Finite Element Analysis (FEA) simulations. Because PANDORA is still in the design phase, experimental data cannot be obtained. Thus the results described in this chapter are analytical only.

The first FEA simulation was performed on the link design (Sec. 3.2.1). This simulation also afforded the opportunity to evaluate the material choice of 7075-T6. The tensile strength of 7075-T6 is reflected in the factor of safety calculation shown in (Fig. 4.1). Both materials provide a FOS above the minimum instituted earlier. The analysis also shows that the stress concentrations are highest where the bearings are press fit, an expected result.

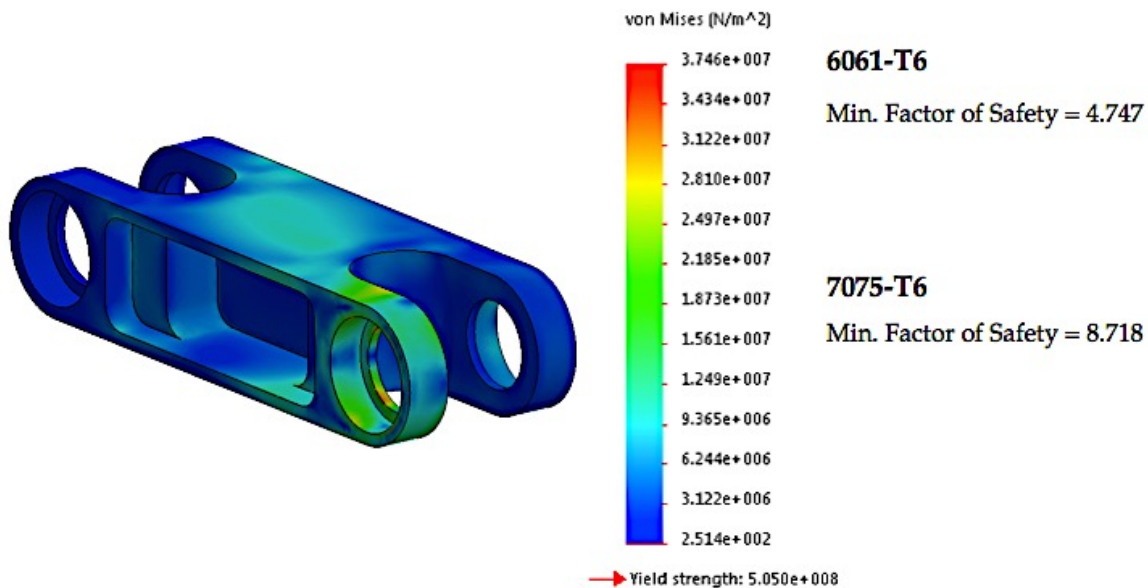


Figure 4.1. FEA analysis of the link design. As reported, both 6061-T6 and 7075-T6 aluminum were used in the analysis. Fixtures and loading remained unchanged between tests; only the material was altered to allow for direct comparison.

4.2. ELEVATION/DEPRESSION SUB-ASSEMBLY VERIFICATION

Another key area of concern due to torque loading is the elevation and depression sub-assembly. Though the load is shared by three other links, the spacing between bearings is relatively narrow; therefore the force induced by an external moment is larger than if the bearings were placed farther apart.

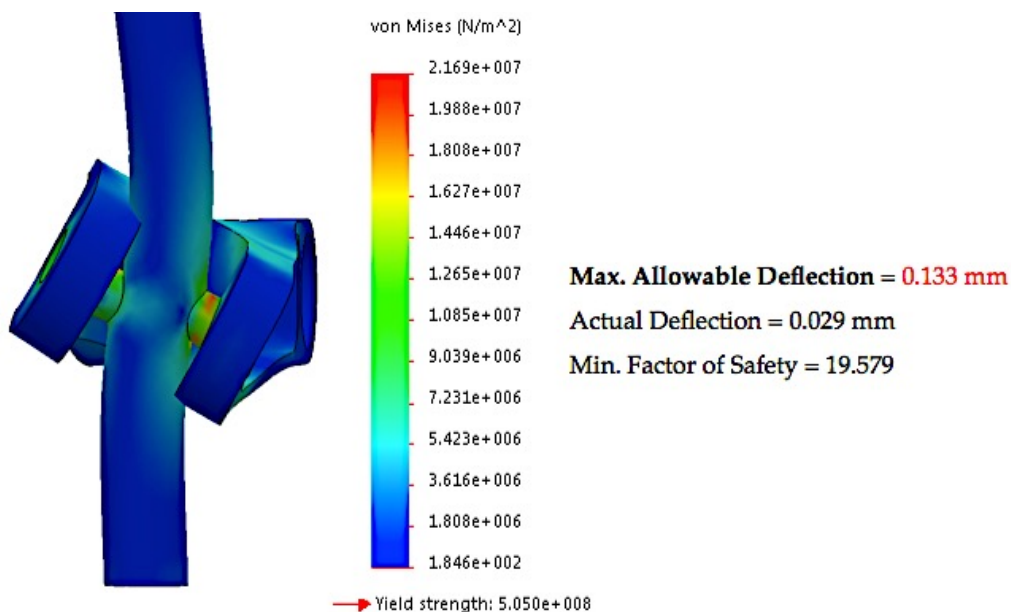


Figure 4.2. Elevation/Depression subassembly analysis. FEA shows that the highest levels of stress occur at the junction of the bearing axle and the vertical post.

An interesting result can be seen in (Fig.). The minimum FOS of the entire subassembly is significantly higher than the FOS exhibited by the link tested in (Fig. 4.1). FEA simulation also shows that the overall deflection falls beneath the maximum allowable limit. Finally, the stress concentration is highest at the intersection of the bearing axle and vertical post. As previously described, this behavior was expected, due to the combination of the moment applied and the limited spacing of the bearings.

4.3. FEA OF GROUND AND COUPLER LINK

The ground and coupler links are of particular concern in this design. Due to the unique motion of PANDORA and the ROM required, these links were designed with the expectation of higher stresses due to their lack of overall mass and structure.

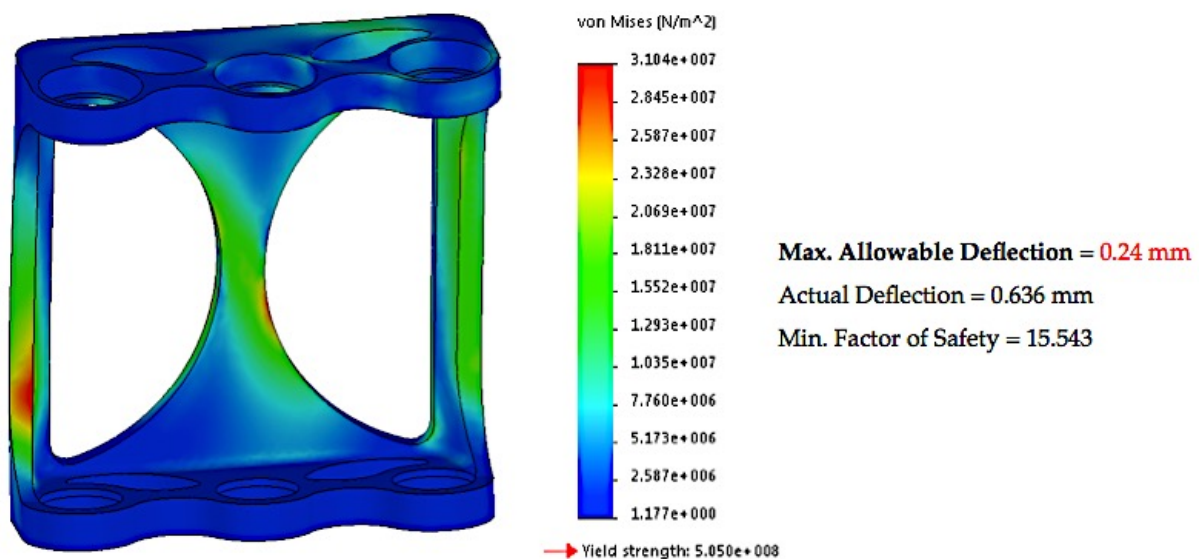


Figure 4.3. Results of FEA analysis on the coupler link. The highest concentrations of stress are shown in red.

It can be seen that for this individual component, the deflection criteria is violated by a factor of 2.65. Two areas, the web and pillar of the link, are exposed to the highest concentrations of stress. However, these links were designed with the assumption that they will become substantially stiffer when assembled with their corresponding vertical posts and bearing preloads.

4.4. GROUND AND COUPLER LINK SUB-ASSEMBLY SIMULATION

Expanding upon previous remarks, the results of FEA for this sub-assembly are of particular interest. This is because the legitimacy of assuming increased rigidity by providing a fourth “side” to the box can now be verified.

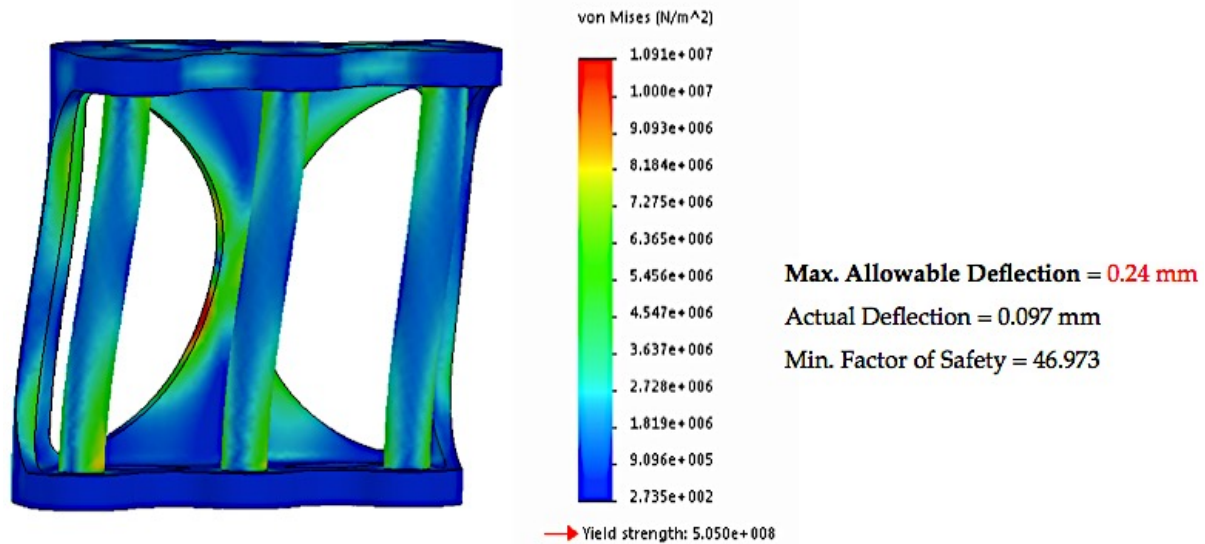


Figure 4.4. FEA simulation of the ground/coupler link assembly. The addition of the vertical posts results in lower stress concentrations.

As can be seen in (Fig. 4.4), with the posts incorporated, the result is lower overall stress concentrations than witnessed in the unassembled link. This result is especially prevalent in the left pillar. As an individual component, this was an area subjected to high-localized stress. However, in this simulation it can be seen that the stress concentration has been mitigated. Thus, the lower stresses result in the highest FOS found during analysis. Moreover, the maximum deflection has been reduced by a factor of 6.6.

4.5. MOTOR MOUNT, DRIVEN LINK, AND DRIVEN SHAFT ANALYSIS

Although the focus of this chapter has been on the components and assemblies discussed in (Sec. 3.2), there are three additional components that need verification. The motor mount that houses the actuator responsible for elevation and depression is positioned at a significant distance from the link it drives. Thus it is important to ensure that it won't fail the FOS criteria while delivering peak torque (73 N-m). The second component is the link that is driven by said actuator.

Ultimately it is a thin-walled tube attached to the drive shaft by a collar. Therefore it must be tested for stress at its connection point. The last component is the drive shaft responsible for protraction and retraction. The results for all three components are shown in (Fig. 4.5). Their respective locations in the overall assembly are shown in (Fig. 4.6) for reference.

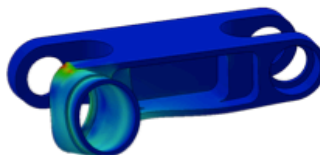
Min. Factor of Safety = 7.279

Min. Factor of Safety = 5.177



A

Min. Factor of Safety = 7.021



B



C

Figure 4.5. (A) Motor Mount. (B) Driven link. (C) Drive shaft for protraction/retraction.

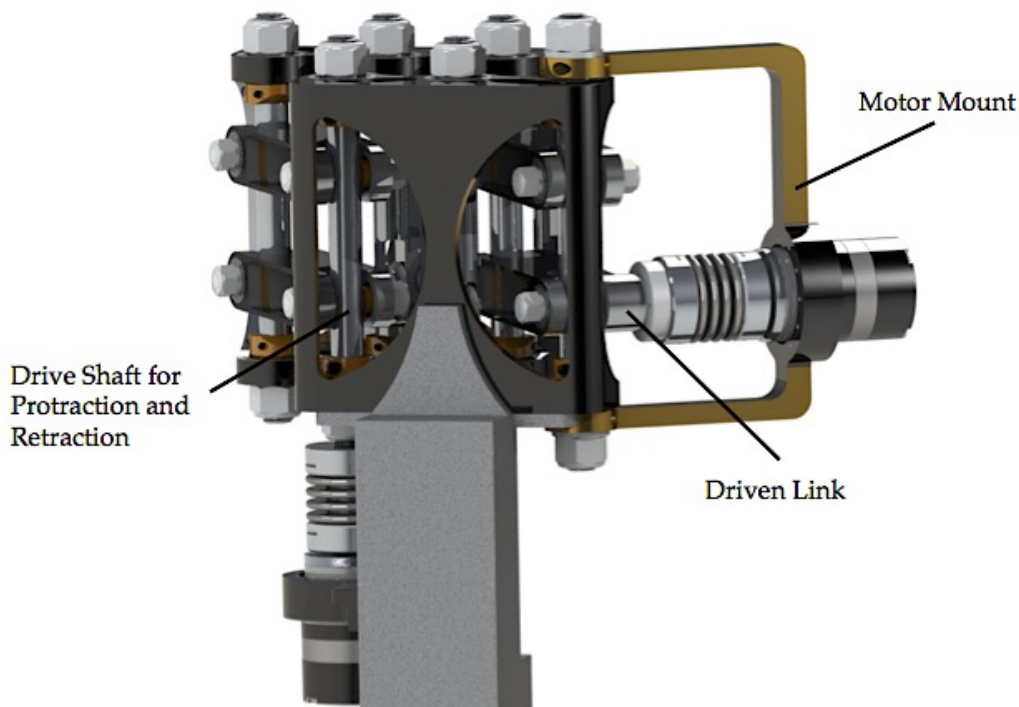


Figure 4.6. Locations of the three components analyzed in (Fig. 4.5).

It is apparent from the results shown in (Fig. 4.5) that the minimum FOS constraint is not violated for any of the components. The driven shaft reported the lowest factor of safety. This was unexpected, as the motor mount was predicted to be the component most susceptible to high stress concentrations due to its distance from the driven link. Lastly, the driven link reported the lowest deflection of the three components tested.

5. DISCUSSION

The design and development of a novel two-DOF scapulohumeral device has been presented in this document. Termed PANDORA, this device operates on the principle of clavicular motion. By capitalizing on the small ROM the clavicle experiences during shoulder movement, a fixed length link can be used to accommodate both large and small patients (Sec. 3.1.1). Furthermore, the complex motion of the scapulothoracic joint is allowed to occur naturally. This results in full shoulder mobility while simultaneously simplifying the biomechanical process.

Other systems exist that have also incorporated these additional DOFs (Sec. 1.3.2), however all of them must be aligned properly with the center of rotation of the sternoclavicular joint. This can be a time-consuming procedure with inherent inaccuracies. The design presented here overcomes this limitation. Through the use of a dual four-bar mechanism, clavicular motion can be emulated remotely. This allows the device to be placed anywhere relative to the patient, offering freedom in the design of additional subsystems.

A proof of concept was designed and tested. First, verification of ROM and mobility were performed through analysis of a solid model designed in SOLIDWORKS. Once verified, a wood prototype was constructed. The prototype proved the validity of parallel motion and combining both DOFs into a single mechanism. Valuable insight was gained as to the effects of moment loading on the linkages. Thus an informed approach was applied to the design of an eventual full-scale model.

One particular challenge in this endeavor was the determination of loading requirements. BLUE SABINO does not exist; therefore values for torque and force were not readily available. However, BLUE SABINO is the successor to the EXO-UL8. Through collaboration with UCLA, data was provided to overcome these unknowns. PANDORA was designed according to this data and as such is conservative in nature. A chief goal in the development of BLUE SABINO is a substantial reduction in mass over that of its predecessor. A known reduction of 7.2 Kg is attributed to resizing of actuators alone. When combined with the use of 7075-T6, the opportunity for further mass reduction is significant. Therefore the figures used to define PANDORA's constraints automatically institute a

considerable factor of safety, resulting in additional confidence in its design and subsequent performance capabilities.

Material selection and the careful consideration of geometry are paramount in this design. Firstly, as mentioned above, 7075-T6 aluminum is the material implemented. The ultimate tensile and yielding strength are nearly double that of 6061-T6, which is proportional to the increase in the factor of safety when directly compared. This is verified in (Fig. 4.1). By changing only the material and holding all other variables constant, the factor of safety for 7075-T6 is 1.85 times higher than 6061-T6. This fact is echoed in the comparison of tensile strength between the two materials. At 570 MPa (7075-T6) and 310 MPa (6061-T6), the same ratio is obtained. This characteristic affords the opportunity to reduce mass in the overall design while remaining in the elastic portion of the stress-strain curve. Lastly geometry in design plays an important part, as rigidity is a function of the modulus of elasticity, area, and length (Sec. 3.1).

Rigidity is a key focus throughout the development of PANDORA. The combination of serving as a base link and being subjected to combined loading, rigidity is vital. The role as a base link demands that displacements be minimal. Small displacements experienced by PANDORA translate to large displacements at the end effector. Therefore, a maximum displacement of two millimeters has been deemed the upper limit that may be exhibited at the end effector (Sec. 3.1). Due to this constraint, FEA was conducted on key components (Ch. 4).

FEA simulations were used exclusively to verify individual components and subsequent sub-assemblies. This is due to PANDORA existing in design form only. Therefore experimental data is unable to be obtained currently. However, FEA is an industry standard that can provide critical insights and highlight problematic design features. When applied to PANDORA, it was found that all components and sub-assemblies did not exceed the required displacement criteria. The lowest factor of safety found was 5.177, which occurred at the protraction/retraction drive shaft. It should be noted that this was a result of a peak torque applied (73 N-m). The average magnitude of torque expected for this component is below (14 N-m). For comparison, this produces a minimum factor of safety of 20.708. Therefore, while this component had the lowest value tested, it is well within safe operating conditions.

As previously described, not only were individual components verified, but their consequent sub-assemblies were as well. Some components (e.g. the ground and coupler links) were designed specifically with the sub-assembly in mind, capitalizing on the notion of synergy. That is to say that optimal performance is not achieved individually, but as a whole. This was an intentional feature, as it allowed for a streamlined design that could simultaneously accommodate the required ROM while minimizing mass and maximizing rigidity. This concept is exemplified in the comparison of the ground and coupler links to their respective assemblies. Individually, the links performed the worst of any individual component with respect to rigidity (0.636 mm deflection). However, when placed in their assembly, the overall deflection was reduced to 0.097 mm. This is a reduction of 85%, thus emphasizing the significant effects that synergy can impart.

Overall, the results of the FEA simulations effectively verified the deflection constraint imposed on the design. This constraint is based upon the load specifications presented in (Fig. 3.7) and (Fig. 3.13), which are presumably higher than the actual loading will be in the final BLUE SABINO design. Thus it can be concluded that, from a structural design viewpoint, PANDORA is more than suitable for this application. Considering the other advantages PANDORA provides (e.g. remote location, scapulohumeral motion, etc.), this device is not only novel in its design, but also in the function for which it was created.

5.1. FUTURE WORK

Although the results presented in (Ch. 4) are favorable, and the prototype discussed in (Sec. 3.1.5) verified the theory behind PANDORA, the journey is far from over. From a global perspective, the BLUE SABINO project is still in its infancy. PANDORA literally represents the first link in the chain. From a local perspective, there is still much to do in regards to PANDORA. As previously discussed, a physical model of PANDORA has yet to be produced. Although FEA has verified the solid model, there is no substitute for actual experimental data. One of the key areas still needing exploration is the effective application of bearing preload. The theory and modeling used in the design of PANDORA though valid, needs to be verified experimentally. A proper preload can dramatically improve rigidity, performance, and life of the bearings. However, improper preloading can

induce the opposite effects. Therefore this is one of the most immediate concerns needing addressed.

Another aspect that often gets overlooked in a research setting is machinability. Because the research community tends to create “one-off” designs, machinability in design is sometimes neglected. Though great care has been taken to include this concern while designing PANDORA, further evaluation should be performed. There may still exist design elements that could be improved upon in this regard.

Gravity compensation is another design feature that bears further verification. Though the theory and application presented here is sound, there is no way to test the effectiveness of the design until the physical device is created. Factors such as spring stiffness are dependent upon final design specifications, as is the appropriate string length for the pulley and cable mechanism. Lastly, the adjustment method (K-type) proposed needs to be properly examined. The principle is straightforward, but the application may not be, thus further work is required here to determine this unknown.

Lastly, there are a few loose ends within the design that still need properly addressed. Namely, these include wire routing, and adjustability. The latter item appears in two forms, adjustment of tower width and adjustment of ROM. A potential solution has been proposed for tower width adjustment (Sec. 3.2.7), however other options should also be explored in this matter. Adjustment of ROM involves the integration of mechanical stops. This is needed to accommodate patients with varying degrees of disability, which directly affects the limits of their workspace. To avoid discomfort to the patient or even injury, mechanical stops are needed to effectively safeguard against excessive ROM.

Wire routing is a concern that often gets neglected until the last phase of design, resulting in less than satisfactory integration. A cursory look at current exoskeleton designs will reveal the truth behind this observation. Therefore, PANDORA is designed with a chamber in the base tower to help stimulate this contemplation early in the process. The concept is that the chamber will provide a natural “wire-loom” in which to bundle but also conceal the wires as they are routed to their external power supplies. However, this is just a preliminary step, as the actual size of the chamber and subsequent wire routing still needs attention.

5.2. CONCLUDING REMARKS

This document explores the conception and design of a device aimed at emulating scapulohumeral rhythm. A movement that through careful study was deemed reproducible by other means, namely, clavicular motion. This realization is what led to the development of PANDORA, a dual four-bar mechanism capable of producing parallel motion about an arc from a remote location. The implications of which provide numerous benefits to the project to which it is attached, BLUE SABINO.

Ambitious in purpose, PANDORA is unlike any device currently seen in exoskeleton design. Its unique function coupled with its ability to compensate for gravity makes it ideal as a base link. Although further work is needed to see PANDORA to completion, the results of FEA simulations are promising. Through rigorous design and carefully monitored constraints, PANDORA exceeds the initial expectations assigned to it. What remains is verification and validation through experimental analysis. The hope of this author is that the actual version of PANDORA performs as well as the model presented in this work.

REFERENCES

- [1] M. J. Matarić, *The robotics primer*. Cambridge, Mass: The MIT Press, 2007.
- [2] V. Graefe and R. Bischoff, "From ancient machines to intelligent robots—A technical evolution—," in *Electronic Measurement & Instruments, 2009. ICEMI'09. 9th International Conference on*, 2009, pp. 3–418.
- [3] T. R. Kurfess, Ed., *Robotics and automation handbook*. Boca Raton: CRC Press, 2005.
- [4] N. G. Hockstein, C. G. Gourin, R. A. Faust, and D. J. Terris, "A history of robots: from science fiction to surgical robotics," *J. Robot. Surg.*, vol. 1, no. 2, pp. 113–118, Jun. 2007.
- [5] J. Eriksson, M. J. Mataric, and C. Winstein, "Hands-off assistive robotics for post-stroke arm rehabilitation," in *Proc. IEEE International Conference on Rehabilitation Robotics (ICORR'05)*, 2005, pp. 21–24.
- [6] H. Krebs *et al.*, "A paradigm shift for rehabilitation robotics," *IEEE Eng. Med. Biol. Mag.*, vol. 27, no. 4, pp. 61–70, Jul. 2008.
- [7] "Stroke Facts | cdc.gov." [Online]. Available: <http://www.cdc.gov/stroke/facts.htm>. [Accessed: 10-Nov-2016].
- [8] Shute, "How Robots Are Aiding Stroke Rehabilitation | Heart Health | US News." [Online]. Available: <http://health.usnews.com/health-news/managing-your-healthcare/heart/articles/2008/09/19/how-robots-are-aiding-stroke-rehabilitation>. [Accessed: 10-Nov-2016].
- [9] S. Mazzoleni, G. Turchetti, I. Palla, F. Posteraro, and P. Dario, "Acceptability of robotic technology in neuro-rehabilitation: Preliminary results on chronic stroke patients," *Comput. Methods Programs Biomed.*, vol. 116, no. 2, pp. 116–122, Sep. 2014.
- [10] R. A. R. C. Gopura, D. S. V. Bandara, K. Kiguchi, and G. K. I. Mann, "Developments in hardware systems of active upper-limb exoskeleton robots: A review," *Robot. Auton. Syst.*, vol. 75, pp. 203–220, Jan. 2016.
- [11] W. S. Harwin, T. Rahman, and R. A. Foulds, "A review of design issues in rehabilitation robotics with reference to North American research," *IEEE Trans. Rehabil. Eng.*, vol. 3, no. 1, pp. 3–13, 1995.

- [12] H. M. Van der Loos and D. J. Reinkensmeyer, "Rehabilitation and health care robotics," in *Springer Handbook of Robotics*, Springer, 2008, pp. 1223–1251.
- [13] H. I. Krebs and B. T. Volpe, "Rehabilitation Robotics," in *Handbook of Clinical Neurology*, vol. 110, Elsevier, 2013, pp. 283–294.
- [14] H. S. Lo and S. Q. Xie, "Exoskeleton robots for upper-limb rehabilitation: State of the art and future prospects," *Med. Eng. Phys.*, vol. 34, no. 3, pp. 261–268, Apr. 2012.
- [15] J. Rosen, "UCLA | Bionics Lab > Wearable Robotics > Exoskeleton Prototype 1." [Online]. Available: http://bionics.seas.ucla.edu/research/exoskeleton_device_1.html. [Accessed: 08-Nov-2016].
- [16] J. Rosen, M. Brand, M. B. Fuchs, and M. Arcan, "A myosignal-based powered exoskeleton system," *IEEE Trans. Syst. Man Cybern.-Part Syst. Hum.*, vol. 31, no. 3, pp. 210–222, 2001.
- [17] J. C. Perry, J. Rosen, and S. Burns, "Upper-Limb Powered Exoskeleton Design," *IEEEASME Trans. Mechatron.*, vol. 12, no. 4, pp. 408–417, Aug. 2007.
- [18] B. Sheng, Y. Zhang, W. Meng, C. Deng, and S. Xie, "Bilateral robots for upper-limb stroke rehabilitation: State of the art and future prospects," *Med. Eng. Phys.*, vol. 38, no. 7, pp. 587–606, Jul. 2016.
- [19] Yupeng Ren, Sang Hoon Kang, Hyung-Soon Park, Yi-Ning Wu, and Li-Qun Zhang, "Developing a Multi-Joint Upper Limb Exoskeleton Robot for Diagnosis, Therapy, and Outcome Evaluation in Neurorehabilitation," *IEEE Trans. Neural Syst. Rehabil. Eng.*, vol. 21, no. 3, pp. 490–499, May 2013.
- [20] C. Carignan, J. Tang, and S. Roderick, "Development of an exoskeleton haptic interface for virtual task training," in *2009 IEEE/RSJ International Conference on Intelligent Robots and Systems*, 2009, pp. 3697–3702.
- [21] D. Koo, P. H. Chang, M. K. Sohn, and J. Shin, "Shoulder mechanism design of an exoskeleton robot for stroke patient rehabilitation," in *2011 IEEE International Conference on Rehabilitation Robotics*, 2011, pp. 1–6.
- [22] T. Nef, M. Guidali, and R. Riener, "ARMin III – arm therapy exoskeleton with an ergonomic shoulder actuation," *Appl. Bionics Biomech.*, vol. 6, no. 2, pp. 127–142, Jul. 2009.

- [23] T. Nef, M. Guidali, V. Klamroth-Marganska, and R. Riener, "ARMin - Exoskeleton Robot for Stroke Rehabilitation," in *World Congress on Medical Physics and Biomedical Engineering, September 7 - 12, 2009, Munich, Germany: Vol. 25/9 Neuroengineering, Neural Systems, Rehabilitation and Prosthetics*, O. Dössel and W. C. Schlegel, Eds. Berlin, Heidelberg: Springer Berlin Heidelberg, 2009, pp. 127–130.
- [24] S. J. Ball, I. E. Brown, and S. H. Scott, "MEDARM: a rehabilitation robot with 5DOF at the shoulder complex," in *2007 IEEE/ASME international conference on Advanced intelligent mechatronics*, 2007, pp. 1–6.
- [25] M. Dežman, "DESIGN AND CONTROL OF COMPLIANT WEARABLE ROBOT MECHANISMS."
- [26] B. Kim and A. D. Deshpande, "Controls for the shoulder mechanism of an upper-body exoskeleton for promoting scapulohumeral rhythm," in *2015 IEEE International Conference on Rehabilitation Robotics (ICORR)*, 2015, pp. 538–542.
- [27] "Shoulder Complex | Clinical Gate." .
- [28] L. Lippert and L. Lippert, *Clinical kinesiology and anatomy*, 4th ed. Philadelphia: F.A. Davis, 2006.
- [29] M. Peat, "Functional anatomy of the shoulder complex," *Phys. Ther.*, vol. 66, no. 12, pp. 1855–1865, 1986.
- [30] V. T. Inman, J. B. deC M. Saunders, and L. C. Abbott, "Observations on the Function of the Shoulder Joint," *J Bone Jt. Surg Am*, vol. 26, no. 1, pp. 1–30, Jan. 1944.
- [31] N. K. Poppen and P. S. Walker, "Normal and abnormal motion of the shoulder," *J Bone Jt. Surg Am*, vol. 58, no. 2, pp. 195–201, 1976.
- [32] J. J. Bray, *Prosthetic Principles, Upper Extremity Amputations: Fabrication and Fitting Principles*. Prosthetics-Orthotics Education Program, Division of Orthopedic Surgery, University of California, Los Angeles, 1970.
- [33] P. M. Ludewig, S. A. Behrens, S. M. Meyer, S. M. Spoden, and L. A. Wilson, "Three-dimensional clavicular motion during arm elevation: reliability and descriptive data," *J. Orthop. Sports Phys. Ther.*, vol. 34, no. 3, pp. 140–149, 2004.
- [34] K. Nagarchi et. al, "Morphometry of Clavicle," *Journal of Pharmaceutical Science and Research*. [Online]. Available: <http://www.jpsr.pharmainfo.in/issue.php?page=54>. [Accessed: 11-Nov-2016].

- [35] P. M. Ludewig, V. Phadke, J. P. Braman, D. R. Hassett, C. J. Cieminski, and R. F. LaPrade, "Motion of the Shoulder Complex During Multiplanar Humeral Elevation," *J. Bone Jt. Surg.-Am. Vol.*, vol. 91, no. 2, pp. 378–389, Feb. 2009.
- [36] R. L. Norton, *Machine design: an integrated approach*, 3rd ed. Upper Saddle River, N.J: Pearson Prentice Hall, 2006.
- [37] K. Ueura and R. Slatter, "Development of the harmonic drive gear for space applications," *Eur. Space Agency-Publ.-ESA SP*, vol. 438, pp. 259–264, 1999.
- [38] " | Harmonic Drive | Harmonic Drive." [Online]. Available: <http://www.harmonicdrive.net/technology>. [Accessed: 24-Oct-2016].
- [39] N. Repčić, N. Pervan, and I. Šarić, *Application of Harmonic Drive Gears in Machine Tools*. TMT, 2010.
- [40] A. Slocum, "FUNdaMENTALS of Design." [Online]. Available: <http://pergatory.mit.edu/resources/FUNdaMENTALS.html>. [Accessed: 24-Oct-2016].
- [41] A. G. Erdman and G. N. Sandor, *Mechanism Design: Analysis and Synthesis*. Prentice-Hall International, 1997.
- [42] J. S. Rao and R. V. Dukkupati, *Mechanism and Machine Theory*. Wiley, 1989.
- [43] A. K. Natesan, "Kinematic analysis and synthesis of four-bar mechanisms for straight line coupler curves," 1994.
- [44] N. Sclater and N. P. Chironis, *Mechanisms and mechanical devices sourcebook*, 4th ed. New York: McGraw-Hill, 2007.
- [45] C. S. SHARMA and K. PUROHIT, *THEORY OF MECHANISMS AND MACHINES*. PHI Learning, 2006.
- [46] D. Reuther, "Four-bar Three-position Mechanism Synthesis Using the Principles of Fuzzy Logic Mathematics," 2014.
- [47] V. Zamfir and H. Vîrgolici, "SYNTHESIS OF FOUR-BAR LINKAGE USING DISPLACEMENT EQUATIONS," *Ann. Univ. Petrosani Mech. Eng.*, 2010.
- [48] D. Dowson and B. J. Hamrock, "History of ball bearings," 1981.
- [49] "Introduction to Bearings | NSK Global." [Online]. Available: <http://www.nsk.com/services/basicknowledge/introduction.html>. [Accessed: 29-Oct-2016].

- [50] "Bearing Timeline - American Bearing Manufacturers Association." [Online]. Available: http://www.americanbearings.org/?page=bearing_timeline. [Accessed: 29-Oct-2016].
- [51] C. P. Chaudhari, B. B. Thakare, S. R. Patil, and S. U. Gunjal, "A STUDY OF BEARING AND ITS TYPES."
- [52] "Bearing types and designs." [Online]. Available: <http://www.skf.com/us/products/bearings-units-housings/super-precision-bearings/principles/selecting-super-precision-bearings/bearing-types-and-designs/index.html>. [Accessed: 30-Oct-2016].
- [53] "Types of Bearings – Ball Bearing Engineering – NMB." [Online]. Available: <http://www.nmbtc.com/bearings/engineering/bearing-types/>. [Accessed: 30-Oct-2016].
- [54] "Single Row Deep Groove - Single Row Ball Bearings | AST Bearings." [Online]. Available: <http://www.astbearings.com/single-row-deep-groove.html>. [Accessed: 29-Oct-2016].
- [55] ": Deep-groove ball bearings | GRW High Precision Bearings." [Online]. Available: <http://www.grwbearing.com/products/high-precision-ball-bearings/radial-deep-groove-ball-bearings.html>. [Accessed: 30-Oct-2016].
- [56] "TS." [Online]. Available: <http://www.timken.com/en-us/products/bearings/productlist/roller/Tapered/SingleRow/Pages/TS.aspx>. [Accessed: 30-Oct-2016].
- [57] "Bearings | JTEKT Corporation." [Online]. Available: <http://www.jtekt-na.com/products/bearings>. [Accessed: 30-Oct-2016].
- [58] J. L. Herder, *Energy-free Systems: Theory, Conception and Design of Statically Balanced Spring Mechanisms*. 2001.
- [59] R. D. Clark, "Lucien LaCoste," *Lead. Edge*, vol. 3, no. 12, pp. 24–29, 1984.
- [60] M. Schenk and S. D. Guest, "On zero stiffness," *Proc. Inst. Mech. Eng. Part C J. Mech. Eng. Sci.*, p. 954406213511903, 2013.
- [61] W. D. van Dorsser, R. Barents, B. M. Wisse, M. Schenk, and J. L. Herder, "Energy-free adjustment of gravity equilibrators by adjusting the spring stiffness," *Proc. Inst. Mech. Eng. Part C J. Mech. Eng. Sci.*, vol. 222, no. 9, pp. 1839–1846, Sep. 2008.

- [62] P.-Y. Lin, W.-B. Shieh, and D.-Z. Chen, "A theoretical study of weight-balanced mechanisms for design of spring assistive mobile arm support (MAS)," *Mech. Mach. Theory*, vol. 61, pp. 156–167, Mar. 2013.
- [63] W. D. van Dorsser, R. Barents, B. M. Wisse, and J. L. Herder, "Gravity-Balanced Arm Support With Energy-Free Adjustment," *J. Med. Devices*, vol. 1, no. 2, p. 151, 2007.
- [64] E. A. Dijkman, *Motion geometry of mechanisms*. Cambridge ; New York: Cambridge University Press, 1976.
- [65] R. Barents, M. Schenk, W. D. van Dorsser, B. M. Wisse, and J. L. Herder, "Spring-to-spring balancing as energy-free adjustment method in gravity equilibrators," *J. Mech. Des.*, vol. 133, no. 6, p. 61010, 2011.
- [66] D. B. Chaffin, G. Andersson, B. J. Martin, and others, *Occupational biomechanics*. Wiley New York, 1999.
- [67] "Lovejoy, Inc. : Products : Motion Control Couplings : Bellows Style (BWC and BWLC Series)." [Online]. Available: <http://www.lovejoy-inc.com/products/motion-control-couplings/bellows.aspx>. [Accessed: 17-Nov-2016].